

Determining the influence of population variation on compliance with radiofrequency exposure limits

A thesis submitted in fulfilment of the requirements for the degree of Doctor of Philosophy by

Maia Sauren

BEng Electrical Engineering

Electrical and Computer Engineering
College of Science, Engineering and Health
RMIT University
June 2011

Declaration

I certify that except where due acknowledgement has been made, the work is that of the author alone; the work has not been submitted previously, in whole or in part, to qualify for any other academic award; the content of the thesis is the result of work which has been carried out since the official commencement date of the approved research program; and, any editorial work, paid or unpaid, carried out by a third party is acknowledged.

Maia Sauren

Date

Acknowledgements

This work owes thanks to many people for guidance and support. I am grateful to the opportunities I've had to learn much more than science or engineering during the course of this project, from many people, not least of all my PhD supervisors. I would like to offer my warmest thank you to Ray McKenzie, who has been a fount of knowledge about a variety of topics and suggested many of the ideas behind this work; and to Dr. Elena Pirogova, who has offered patient support and ongoing help in navigating administrative systems. I would also like to acknowledge the encouragement and opportunities offered to me by Prof. Irena Cosic, particularly through the early stages, and for giving me with the chance to undertake a PhD.

I received financial technical assistance from a number of people at the Telstra Research Laboratories, now sadly defunct; the Australian Centre for Radiofrequency Bioeffects Research; and Ericsson Research Laboratories, Sweden. I thank all inhabitants of the infamous TRL Tea Room, for a one of a kind education; Steve Iskra and Vitas Anderson, for technical guidance; Robert McIntosh, for answering all kinds of questions over the years and helping me shape the final draft. I am indebted to Mike Wood and Geoff Bail for logistics and sponsorship for my collaboration with Ericsson Research Laboratories; Prof. Rodney Croft for kindness, generosity and helpful advice; the RF research team at Ericsson, in particular Christer Törnevik and Björn Hansson for training, assistance, and an amazing opportunity; and Anders Westermark at the Karolinska Institute, for lending me a human skull.

Invaluable technical assistance came from many and unexpected places. Daniel Smith provided endless evenings of Unix and data wrangling, without which this work would not have been possible. Mel Van Rooyen of EMSS helped solve modelling issues. The Ericsson Race Yacht building team advised me on working with fibreglass. Chris Zombolas and Peter Jakubiec provided time and expertise at EMC Technologies for SAR testing and analysis. I am also grateful for advice I received from Dr. Morris Odell, Victorian Institute of Forensic Medicine, and Prof. John Clement, Melbourne University, regarding facial reconstruction.

Closer to home, I'd like to thank fellow sufferers at Brain Sciences Institute, all now moved on: Sumie Leung, Vanessa Cropley, Sarah Loughran, and Nicholas Perentos. Bonnie Alexander and Nadia Niaz provided tea, chocolate, moral support, and stickers. A special thank you to Bonnie for proof reading several chapters and assisting with figures. I reserve a heartfelt thank you to Daniel Narbett for formatting and editing, and helping me bring this thing to an end; to the inimitable Halo Jones, for study company, proofreading and other errands; and Ms. Georgia Boyce, for multi-faceted support and surprises in the mail. Countless friends, close ones and family – far too many to mention, by name or contributions - thank you for supporting me through this process.

This study was partly funded by the National Health and Medical Research Council (NHMRC), Australia; Telstra; and Ericsson Research Laboratories, Sweden.

Abstract

The rise in ubiquity of radiofrequency (RF) wireless communication technologies has been accompanied by public concern regarding safety of their use.

Guidelines provided by expert bodies agree that limiting thermal rise in humans and other animals due to RF exposure provides protection from negative health effects. Measuring localised temperature changes in living bodies, however, especially in sensitive tissues such as brains and eyes, is difficult and dangerous to life.

Physical or numerical models of humans are used instead. Compliance with safety standards for RF emitting devices is measured in a metric known as SAR (Specific Energy Absorption Rate) which describes energy absorption in tissue; this in turn may be quantified as thermal effect.

How best to model humans for accurate SAR estimates remains an open question. Much work has been done over the years, attempting to quantify which and how anatomic parameters such as tissue morphology, size, dielectric properties and relative location, affect energy absorption; and how to incorporate those parameters into models that provide conservative SAR estimates protecting all individuals.

Since the available models are either highly representative and complex or simple single tissue models, this issue is not easily explored, since the identified parameters are not easily varied within the models. Limitations of current methods include: the insufficiently-tested assumption that Caucasian adult male models provide conservative SAR estimates for all populations; wide disparity in modelling and measurement techniques when testing effect of anatomic variations on SAR; and the use of a handful of morphologically accurate models to examine effect of anatomic variations on energy distribution, with the implication that a randomly chosen individual will provide sufficient information regarding the spread of human anatomical variation.

Taking advantage of the maturity of current computational tools, attempts have been made here to overcome these limitations by:

- creating a unique alternative model of the human head, incorporating a reduced set of tissues in a semi-homogeneous, simplified geometry for which the key parameters may be varied parametrically
- validating the computational model using simplified physical models of human heads, custom made for this purpose
- gathering data from literature regarding what variations exist in human populations for two tissue parameters
- systematically testing what relationships exist between several anatomic variations in adult humans and consequent energy absorption due to RF exposure at 900 MHz, namely: cranial thickness; skin thickness; head size; and dielectric properties of tissues.

Some of the assumptions behind current compliance methodologies have been tested for appropriateness. Results indicate that at the range of normal human variation, cranial thickness and skin thickness of the head do not significantly affect magnitude or distribution of energy absorption, but that their inclusion in models is vital for accurate SAR estimation; that dielectric properties of certain tissues affect magnitude and distribution of SAR more than others; and that smaller head sizes increase SAR in this model.

Overall, results suggest that SAR predictions could not have been anticipated using *a priori* reasoning, as location and magnitude of SAR maxima were seen to alter in unexpected and irregular ways with variations in tissue parameters. A compromise model like the one proposed here, which provides a point of diminishing returns between the high complexity of the multi-tissue models and the single-tissue homogeneous model, allows increased granularity for determination of SAR maxima in sensitive tissues.

Results of this work provide some inroads into establishing the level of complexity necessary for simulating human heads for radiofrequency exposure compliance calculations. Relationships between magnitude and location of regions of high SAR in the head and variables listed above have been quantified and qualified in this thesis.

The model proposed here is available for public use upon request. It can easily be amended to incorporate more or fewer tissues with varying levels of complexity; augmented to better resemble anatomy of children's heads; or used in its current state to further explore relationships between anatomic variations and absorption at the same frequency used here, or other RF frequencies.

List of figures

Figure 1: Examples of (a) planar model of human tissue (from (Abdalla and Teoh 2005)) and (b) layered sphere (from (Nikita, Stamatakos et al. 2000))	21
Figure 2: (a) Visible Human and (b) Specific Anthropometric Phantom, two extremes of tissue granularity	22
Figure 3: Virtual Family (from (Christ, Kainz et al. 2010))	23
Figure 4: Non-uniform scaling of an adult heterogeneous head to derive children's heads (from (Wang and Fujiwara 2003))	24
Figure 5: Geometry Head model, shown with various cutplanes.....	26
Figure 6: The electromagnetic spectrum (adapted from Telstra Research Laboratories training materials)	30
Figure 7: Propagation of an electromagnetic wave (adapted from http://www.mike-willis.com/Tutorial/PF3.htm)	33
Figure 8: Effect of frequency on whole body average SAR (in far field). For E-polarization the SAR will increase with increasing frequency as a function of f^2 , up to the resonance frequency for the object, and then decrease as a function of $1/f$ (adapted from Telstra Research Laboratories RF training materials)	42
Figure 9: Planes and directions of the human body (adapted from http://staff.ucc.edu/alc-paez/biology/anat_planes/planes.htm)	50
Figure 10: The human skull.....	51
Figure 11: Anthropometric measures of the head and face (from (Churchill 1976))	52
Figure 12: The Geometry Head model. Parentheses provide the dimensions used in the base-level model, based on anatomic measurements taken from a large sample of adult Caucasian males (Farkas 1994).....	55
Figure 13: DASy4 exposure system and schematic of components	63
Figure 14: Initial tests using adult skull in flat part of SAM phantom at EMC Technologies, Melbourne, Australia	64
Figure 15: Shell phantoms with wooden support frame holding a skull, (a) top and (b) side (right) views.	65
Figure 16: High concentration of gelling agent makes for a grainy texture; dielectric properties are difficult to measure. Food dye was added to differentiate tissues.	68
Figure 17: Exposure setup for SAR tests used in this study. $P_{\text{reflected}} = P_A$ (coupling factor) + P_B (measured reflection coefficient) + P_C (reflection coefficient through cable).	70
Figure 18: 'cheek' (above) and 'tilt 'positions as shown on SAM phantom (image adapted from (IEEE 2003)).....	71
Figure 19: (a) establishing the Ear Canal Reference Point (ERP) on the skull; (b) Dipole was positioned with antenna feed point flush against the ERP, marked on the shell phantoms (c) 1 mm and 2 mm spacers between the skull and phantom; (d) skull is attached to shell using plastic screws to minimise electromagnetic interference.....	71
Figure 20: Defining measurement regions within (a) adult phantom and (b) child phantom. Measurement planes are marked and numbered. The three red crosses on each image identify the reference points used to 'teach' the robot the location of the measurement space. The blue cross in each image denotes position of the Ear Reference Point, the ERP was marked on the outside of the shell and the dipole was positioned against it. The blue rectangle in the brain area represents the point of comparison for physical and computational models, see Section 3.1.5.....	73

Figure 21: Measurement points used by the probe for a volume scan within adult skull. The skull surface was 'learned' by the robot for a plane, then extended contralateral to the dipole for 30 mm to obtain volume scan area.....	73
Figure 22: Comparison point used in computational models, shown in side and top view of the adult model.....	79
Figure 23: Single point SAR comparison in the physical and computational models.....	79
Figure 24: 1g peak spatial SARs in the physical and computational models.....	82
Figure 25: 10g peak spatial SARs in the physical and computational models.....	82
Figure 26: Location of 1g and 10g SAR cubes (10g SAR shown here) in the brain of computational models.....	84
Figure 27: Area and volume SAR scans of physical models. Locations of measured areas are shown in Figure 20.....	85
Figure 29: SAR plots of Geometry Head with (a) 4 mm (b) 6 mm and (c) 11 mm cranial thicknesses. .	103
Figure 30: Relationship between cranial thickness and SAR.....	104
Figure 31: Skin thickness and SAR.....	114
Figure 32: SAR in each tissue as skin thickness is varied.....	114
Figure 33: Relationship between head size and (a) WHA, 1g and 10g SAR as raw SAR values (b) WHA, 1g and 10g SAR as percentage variation (c) SAR in each tissue	120
Figure 34: SAR plots inside Geometry Head as head size is varied	121
Figure 35: Geometry Head model created in FEKO software package, shown here with a cutplane. Different colours denote different tissues, and therefore regions of different dielectric properties. The yellow circle denotes the artefact point, explained above in Section 3.5.	131
Figure 36: Dielectric properties used in this study. Conductivity and permittivity as described by Gabriel were used varied to ± 10 , ± 20 and ± 30 per cent with all other variables kept constant for each test.....	132
Figure 37: 1g peak spatial SAR variation with dielectric properties of all tissues	137
Figure 38: 10g peak spatial SAR variation with dielectric properties of all tissues.....	138
Figure 39: WHA SAR variation with dielectric properties in all tissues.....	139
Figure 40: SAR variations in the brain tissue with dielectric properties in all tissues.....	141
Figure 41: SAR variations in the eye tissue with dielectric properties in all tissues	144
Figure 42: SAR variations in the fat tissue with dielectric properties in all tissues	147
Figure 43: SAR variations in the filler (average head) tissue with dielectric properties in all tissues.....	150
Figure 44: SAR variations in the skin tissue with dielectric properties in all tissues	153
Figure 45: SAR variations in the skull tissue with dielectric properties in all tissues	156
Figure 46: SAR changes in each tissue as the conductivity and permeability of one tissue are altered; values are detailed in Table 27	161
Figure 47: Artist's clay rolled into 2 mm thicknesses using a pasta roller was used for creating head casts for fibreglass shell phantoms.....	197
Figure 48: (a) side and (b) top view of the process of making a negative impression of the 'face' using fast set liquid silicon and a 'shelf' of artist's clay.....	198
Figure 49: (a) completed silicon mould and (b) fibreglass sheets pressed into a latex mould and painted with resin.....	199
Figure 50: (a) the flexible latex mould was carefully loosened from the fibreglass shell (b) underside view of a fibreglass shell	199

Figure 51: shell phantoms inside board supports, (a) top view with skull inside phantom and (b) side view 200

Figure 52: phantom and wooden frame with DAS4 system 200

List of tables

Table 1: Maxwell's electromagnetic field equations, in differential and integral forms	33
Table 2: SAR Basic restrictions and fundamental limits (adapted from Telstra Research Laboratories RF training course)	44
Table 3: Seven of the most well-known commercial EM simulators and their adopted numerical methods	48
Table 4: Single point SAR comparisons between physical and computational models	79
Table 5: 1g peak SAR in physical and computational models	82
Table 6: 10g peak SAR in physical and computational models	82
Table 7: Overview of adult cranial thickness in literature (for full information see Table 8). n refers to the number of specimen – often multiple measurements are included of the same skull.	91
Table 8 Adult cranial thickness in literature (detail)	92
Table 9: Cranial thickness and SAR	104
Table 10: Adult skin thickness in literature (summary). For full detail see Table 11. All measurements in millimetres, and include dermis and epidermis. Note that n denotes the number of measurements taken, not the number of cadavers or live volunteers	109
Table 11 Adult skin thickness in literature (detail)	110
Table 12: Skin thickness and SAR	113
Table 13: Geometry Head size variation relative to wavelength	119
Table 14: SAR and percentage SAR variation in each tissue as the head size is altered	120
Table 15: Relationship between head size and 1g and 10g SARs	120
Table 16: initial values of tissue dielectric properties and densities used in the Geometry Head model.	131
Table 17: Dielectric properties used in this study. Conductivity and permittivity as described by Gabriel were used varied to ± 10 , ± 20 and ± 30 per cent with all other variables kept constant for each test.	132
Table 18: 1g peak spatial SAR variation with dielectric properties of all tissues	137
Table 19: 10g peak spatial SAR variation with dielectric properties of all tissues	138
Table 20: WHA SAR variation with dielectric properties in all tissues	139
Table 21: SAR variations in the brain tissue with dielectric properties in all tissues	141
Table 22: SAR variations in the eye tissue with dielectric properties in all tissues	144
Table 23: SAR variations in the fat tissue with dielectric properties in all tissues	147
Table 24: SAR variations in the filler (average head) tissue with dielectric properties in all tissues	150
Table 25: SAR variations in the skin tissue with dielectric properties in all tissues	153
Table 26: SAR variations in the skull tissue with dielectric properties in all tissues	156
Table 27: Location of 1g and 10g peak spatial SARs. Images show examples of 1g and 10g locations as described in the table; exact location vary	159
Table 28: SAR changes in each tissue as the conductivity and permeability of one tissue are altered; these results are graphed in Figure 46	162
Table 29: minimum, maximum and range of SAR in each tissue, as the σ and ϵ of individual tissues is altered to $\pm 30\%$	162
Table 30: Cranial thickness results and consequent SAR results in GH versus other models	170

Table 31: Skin thickness and consequent SAR results in GH versus other models.....	170
Table 32: Dimensions of GH and commonly used models (heads only)	171
Table XXXIII: Recipes for ingredients used in heterogeneous models	201
Table XXXIV: Suggested recipes for achieving target dielectric parameters (adapted from Appendix C, P1528-2003: IEEE Recommended Practice for Determining the Peak Spatial-Average Specific Absorption Rate (SAR) in the Human Head from Wireless Communications Devices: Measurement Techniques).....	202
Table XXXV: DASY4 worst-case uncertainty budget for DASY4 assessed according to IEEE 1528. The budget is valid for the frequency range 300 MHz - 3 GHz and represents a worst-case analysis. For specific tests and configurations, the uncertainty could be considerable smaller (adapted from DASY4 User Manual).....	203

Table of Contents

ACKNOWLEDGEMENTS	3
ABSTRACT	5
LIST OF FIGURES	8
LIST OF TABLES	11
TABLE OF CONTENTS	13
CHAPTER 1: INTRODUCTION AND LITERATURE REVIEW	18
1.1 MODELLING HUMANS FOR RADIOFREQUENCY SAFETY COMPLIANCE	19
1.1.1 History of modelling humans for RF compliance	20
1.1.2 Geometry Head	25
1.2 ORIGINAL CONTRIBUTIONS	27
1.3 RESEARCH QUESTIONS	28
CHAPTER 2: BACKGROUND CONCEPTS	29
2.1 ELECTROMAGNETICS, MOBILE PHONES AND SAFETY STANDARDS	30
2.1.1 Radiofrequency	30
2.1.2 Radiofrequency and mobile telephony	31
2.1.3 Propagation of EM fields	31
2.1.3.1 Plane waves.....	32
2.1.4 Maxwell's equations.....	33
2.1.5 Near field and far field	34
2.1.6 Dielectrics	34
2.1.6.1 Conductivity.....	35
2.1.6.2 Permittivity: an electric characteristic.....	35
2.1.6.3 Permeability: a magnetic characteristic.....	36
2.1.6.4 Skin effect.....	36
2.1.6.5 Intrinsic impedance of a medium.....	37
2.1.7 Speed of EMF propagation	37
2.1.8 Refraction of EM waves in dielectrics	37
2.1.9 RF safety standards.....	38
2.1.10 Dosimetry and SAR	39
2.1.11 Field Strength	42
2.1.11.1 Power of phones.....	42
2.1.12 Location of max SARs.....	42
2.1.13 Basic restrictions and reference levels.....	43
2.1.14 Section summary.....	44

2.2	COMPUTATIONAL TECHNIQUES	45
2.2.1	MoM	45
2.2.2	FEM	46
2.2.3	FDTD	47
2.2.4	FIT.....	47
2.2.5	Choosing a modelling package	48
2.3	MEASUREMENT TECHNIQUES	49
2.4	ANATOMY.....	50
2.4.1	Planes and directions of the human body.....	50
2.4.2	Anatomy of the human skull.....	51
2.4.3	Anthropometric measurements of the human head.....	51
CHAPTER 3:	EXPERIMENTAL METHODS, RESULTS AND ANALYSIS.....	53
3.1	METHODOLOGY: THE GEOMETRY HEAD MODEL.....	54
3.1.1	Features	56
3.1.2	Parameters that may be varied	57
3.1.3	Exposure	57
3.1.4	Validation.....	58
3.1.5	Parameter testing	58
3.1.6	Metrics examined.....	59
3.1.7	Section summary	60
3.2	VALIDATION STUDY	61
3.2.1	Rationale	61
3.2.2	Methodology.....	61
3.2.2.1	<i>Physical models.....</i>	<i>61</i>
3.2.2.2	<i>Skulls.....</i>	<i>63</i>
3.2.2.3	<i>Trial run at EMCT.....</i>	<i>64</i>
3.2.2.4	<i>Phantoms.....</i>	<i>65</i>
3.2.2.5	<i>Tissue simulating Liquids</i>	<i>66</i>
3.2.2.6	<i>Measuring dielectric properties.....</i>	<i>68</i>
3.2.2.7	<i>Exposure source.....</i>	<i>69</i>
3.2.2.8	<i>Dipole positioning.....</i>	<i>70</i>
3.2.2.9	<i>Constructing the physical models</i>	<i>72</i>
3.2.2.10	<i>Defining the measurement space.....</i>	<i>72</i>
3.2.2.11	<i>1g and 10g volume cubes.....</i>	<i>74</i>
3.2.3	Analogous models	74
3.2.4	Details of physical and computational models	75
3.2.5	Results and discussion.....	78
3.2.5.1	<i>Single point SAR comparison.....</i>	<i>78</i>

3.2.5.2	<i>Averaged SAR</i>	80
3.2.5.3	<i>Uncertainty of validation study</i>	86
3.2.6	Section summary	86
3.3	CRANIAL THICKNESS.....	87
3.3.1	Why this variable is important	87
3.3.2	Literature review	87
3.3.2.1	<i>Cranial thickness in human adults</i>	87
3.3.2.2	<i>Effect of cranial thickness on RF absorption</i>	88
3.3.3	What do we expect to see?	88
3.3.4	Methodology, results and discussion	89
3.3.4.1	<i>Variation of human cranial thickness</i>	89
3.3.4.2	<i>Modelling the variable</i>	103
3.3.4.3	<i>Effect of cranial thickness on SAR</i>	103
3.3.5	Section summary	104
3.4	ADULT SKIN THICKNESS	106
3.4.1	Why this variable is important	106
3.4.2	Literature review	106
3.4.2.1	<i>Skin thickness in adult humans</i>	106
3.4.2.2	<i>Effect of skin thickness on SAR</i>	106
3.4.3	What do we expect to see?	107
3.4.4	Methodology, results and discussion	107
3.4.4.1	<i>Range of skin thickness in humans</i>	107
3.4.5	Modelling the variable.....	113
3.4.6	Relationship between SAR and human skin thickness	113
3.4.7	Section summary	116
3.5	HEAD SIZE.....	117
3.5.1	Why is this variable important?	117
3.5.2	Literature review	117
3.5.2.1	<i>Head size in human anatomy</i>	117
3.5.2.2	<i>Effect of head size on RF compliance</i>	117
3.5.3	What do we expect to see?	118
3.5.4	Methodology	118
3.5.5	Results and analysis.....	122
3.5.5.1	<i>Artefact point</i>	122
3.5.5.2	<i>SAR results</i>	122
3.5.6	Section summary	123
3.6	DIELECTRIC PROPERTIES OF TISSUES	124
3.6.1	Why this variable is important	124
3.6.2	Literature review	124

3.6.2.1	<i>Dielectric properties of human tissues in literature</i>	124
3.6.2.2	<i>Effect of dielectric properties on SAR</i>	127
3.6.2.3	<i>Literature review summary</i>	129
3.6.3	What do we expect to see?.....	129
3.6.4	Methodology.....	130
3.6.5	Modelling the variable.....	130
3.6.6	Results and analysis.....	133
3.6.6.1	<i>Artefact</i>	134
3.6.6.2	<i>1g and 10g SAR</i>	134
3.6.7	What tissue dielectric properties affect WHA, 1g and 10 SAR?.....	134
3.6.8	What tissues' dielectric properties affect SAR in the brain?.....	140
3.6.9	What tissues' dielectric properties affect SAR in the eye?	142
3.6.10	What tissues' dielectric properties affect SAR in fat?	145
3.6.11	What tissues' dielectric properties affect SAR in the filler tissue?.....	148
3.6.12	What tissues' dielectric properties affect SAR in the skin?.....	151
3.6.13	What tissues' dielectric properties affect SAR in the skull?	154
3.6.14	General trends.....	157
3.6.15	When the dielectric properties of a single tissue vary, what happens to the rest of the tissues in the GH model?	160
3.6.16	Summary.....	163
3.6.17	SAR in the brain.....	163
3.6.18	SAR in the eye	163
3.6.19	SAR in the fat.....	163
3.6.20	SAR in the filler.....	164
3.6.21	SAR in the skin	164
3.6.22	SAR in the skull	164
3.6.23	Overall re-distribution of SAR with dielectric property variation	164
CHAPTER 4:	FURTHER DISCUSSION	166
4.1	SUMMARY AND FURTHER DISCUSSION OF RESULTS	167
4.1.1	What anatomic variations affect SAR?	167
4.1.2	What tested variables do not significantly affect SAR?.....	167
4.1.3	Where does high SAR occur?.....	168
4.1.4	What anatomic variations create the worst case SAR scenario?	168
4.2	RESULTS IN CONTEXT	170
4.3	VALIDITY OF RESULTS.....	172
4.3.1	What other factors could be included in the model?.....	172
4.3.2	Uncertainty.....	173
4.3.2.1	<i>Computational modelling</i>	173
4.3.2.2	<i>Physical modelling</i>	173

4.3.3	Limitations of the model	175
4.3.3.1	<i>Limited tissue set</i>	175
4.3.3.2	<i>Artefact</i>	176
4.3.3.3	<i>Thermoregulation</i>	176
4.4	CRITICAL ANALYSIS OF METHODS	177
4.4.1	Computational modelling.....	177
4.4.1.1	<i>Modelling package</i>	177
4.4.1.2	<i>Model construction</i>	177
4.4.1.3	<i>Parameters incorporated into the model</i>	177
4.4.2	Physical modelling.....	177
4.4.2.1	<i>Model construction</i>	177
4.4.2.2	<i>Model testing</i>	178
4.5	BENEFITS AND USES OF THIS WORK.....	179
4.5.1	Parametric model.....	179
4.5.2	Ethnic populations.....	179
4.5.3	Other frequencies.....	179
4.5.4	Implications for safety standards.....	179
CHAPTER 5: CONCLUSIONS		181
5.1.1	What parameters of human anatomy contribute to absorption of energy due to RF exposure?	181
5.1.2	What variability exists in the relevant anatomic variations?	182
5.1.3	What is the relationship between these anatomic parameters and SAR?.....	182
5.1.4	What do these results imply for the safety standards for RF exposure?.....	183
5.1.5	Given that existing models do not allow easy exploration of effect of anatomic parameters on SAR, can a new model be created without this limitation?.....	183
5.2	RECOMMENDATIONS FOR FUTURE RESEARCH.....	184
5.2.1	Further explorations with the model as it stands.....	184
5.2.2	Augmenting the model.....	184
REFERENCES.....		185
APPENDIX A – PURCHASING INFORMATION FOR MATERIALS USED IN THIS STUDY.....		196
APPENDIX B – CREATING SHELL PHANTOMS.....		197
APPENDIX C – TISSUE-SIMULATING LIQUID RECIPES.....		201
APPENDIX D – DASY 4 UNCERTAINTY BUDGET		203
APPENDIX E – PREVIOUS RELEVANT PUBLICATIONS		204

Chapter 1: Introduction and literature review

This section provides an outline of the history of knowledge in the field of radiofrequency dosimetry up to the current date; outlines some of the unanswered questions and limitations of existing methodologies; and provides a rationale for undertaking the work described in this thesis.

1.1 Modelling humans for radiofrequency safety compliance

The history of modelling human bodies for RF safety reflects the development of scientists' knowledge about what factors influence absorption and the capability of their tools.

This work restricts itself to examining SAR in the human head; discussion is likewise limited to human head models rather than whole bodies.

The physical concepts behind interactions of RF exposure with human tissue are relatively well described. It is generally agreed that the only potentially harmful detectable effects of low RF exposure are thermal. Other biological effects exist, however they are not considered by most RF dosimetry experts to be associated with adverse health effects (ICNIRP 1998).

The question arises of how to model thermal rise in humans. Thermal changes cannot be measured inside sections of a living organism without causing damage (if not death). Hence, electrically equivalent physical or numerical models of human heads are constructed, exposed to RF, and E-field is measured within the model. The E-field value is converted to the SAR (Specific Energy Absorption Rate), which quantifies energy absorption, which in turn may be converted to temperature change.

In order to correctly approximate thermal change in tissue, SAR needs to be averaged over a volume of tissue (ICNIRP 1998; McIntosh and Anderson 2011). Higher averaging produces better matching with thermal change, however too much averaging reduces granularity. Sensitive tissues (in the head, this includes tissues such as brains and eyes) are in particular need of protection from potentially harmful effects, and it is important to be able to distinguish which tissue experiences higher absorption.

RF safety standards in the US, Japan, UK, Australia (ARPANSA 2002), New Zealand, and many European countries are based on recommendations made by one of two prominent expert bodies: IEEE (IEEE 2005), the Institute of Electrical and Electronic Engineers, and ICNIRP (ICNIRP 1998), the International Commission on Non-Ionizing Radiation Protection. These two bodies converged in their recommendations for the averaging volume for SAR being 10-gram in 2005 (Habash, Elwood et al. 2009).

To determine the location of 10-gram maximum SAR, guidelines recommend that E-field is measured (or numerically evaluated, in the case of numerical models) over the entire model. SAR between measured points is interpolated. SAR is averaged in 10-gram cubes (made of approximately 10 grams of tissue) and the cube with the highest average spatial SAR determines the maximum absorption in the model (IEEE 2003).

1.1.1 History of modelling humans for RF compliance

Human models used for RF dosimetry are designed to allow determination of E-field at all points inside the organism, which allows quantification of magnitude and location of absorption maxima.

Early physical and computational models consisted of shapes that were simple to create and analyse: rectangular slabs (Gandhi 1980; Institute 1998), spheres (Heyvaert and Martens 1998); and prolate spheroids (Durney, Iskander et al. 1979). Planar (Abdalla and Teoh 2005) and layered models (Okoniewski and Stuchly 1996; Cerri, De Leo et al. 1997; Nikita, Stamatakos et al. 2000) such as seen in Figure 1 were often used.

Box models (known as phantoms) with homogeneous dielectric properties were used for compliance and research before more sophisticated models became popular (Kuster and Balzano 1992; Institute 1998). Also used were human-shaped phantoms such as the homogeneous phantom developed at the Telstra Research Laboratories (McIntosh, McKenzie et al. 2001). Complex heterogeneous physical models of humans are difficult to construct and even more difficult to measure E-field within. Consequently, such work is rare – one example is the multi-tissue model built by Anderson (Anderson and Joyner 1995) for measuring SAR in the brain and the eye.

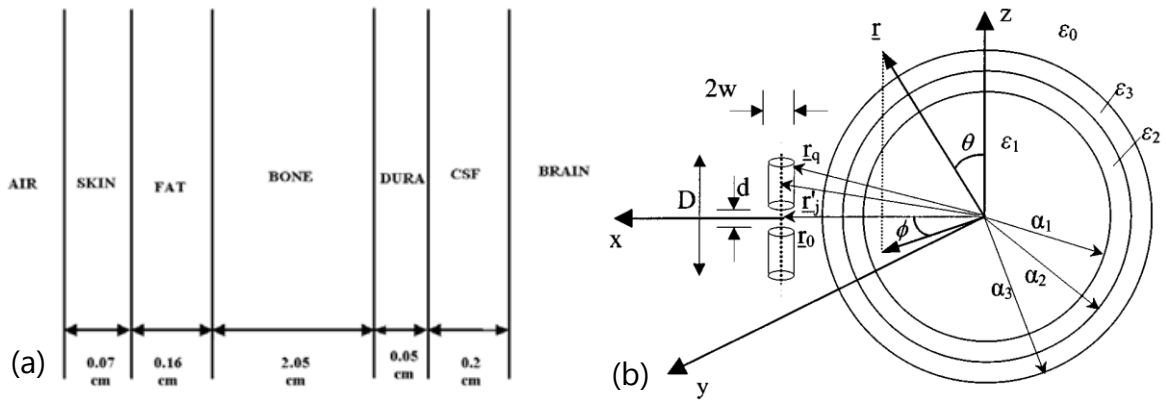


Figure 1: Examples of (a) planar model of human tissue (from (Abdalla and Teoh 2005)) and (b) layered sphere (from (Nikita, Stamatakos et al. 2000))

In 1996, the Visible Human (VH) model (Figure 2a) became available for RF dosimetry purposes (Spitzer, Ackerman et al. 1996). VH is a heterogeneous computational model based on cryosection images of a 38-year-old adult male. The anatomical data for the Visible Man originated at the U.S. National Library of Medicine and many individual researchers and research labs such as Brooks Air Force Base converted it into finite-difference time-domain (FDTD) models.

At the other extreme of complexity, the Standard Anthropomorphic Mannequin (SAM) in Figure 2b was chosen by the IEEE Standards Coordinating Committee 34, Subcommittee 2, Working Group 1 (SCC34/SC2/WG1) as a standards compliant measurement phantom and later also adopted by European standards (CENELEC 2006; IEC 2011). SAM is a sagittally-bisected lossless fibreglass shell phantom, whose dimensions and shape are based on the 90th percentile of an anthropometric study of 1774 U.S. army adult male recruits. SAM has been shown by several studies to provide a conservative SAR estimate when compared against other models (Schonborn, Burkhardt et al. 1998; Watanabe, Mochizuki et al. 2001; Lee, Choi et al. 2002; Lee, Choi et al. 2007). These studies tested SAM against one or several single-individual heterogeneous examples like Visible Human to determine its ability to provide conservative SAR estimates.



Figure 2: (a) Visible Human and (b) Specific Anthropometric Phantom, two extremes of tissue granularity

The factors incorporated into SAM and other parts of the measurement standards are ones identified by the IEEE to influence magnitude and distribution of SAR. These are: dielectric properties; relative location and power of exposure source; distance of exposure source from body - hence pinna (outer ear) size and morphology; overall head morphology; and head size (IEEE 2003).

Determining the contribution of the location, type and magnitude of power sources to SAR is relatively easy. Quantifying the contribution of anatomic parameters has been another matter. Christ's 2006 study (Christ, Klingenbock et al. 2006), for example, found that at 900 MHz, the worst-case SAR scenario of tissue layers using a planar model consisted of skin, followed by a layer of subcutaneous adipose tissue, and a layer of fat. The authors also noted that not including the skin did not result in accurate SAR predictions.

With the advent of high computing power and imaging techniques, the past ten years has seen a suite of new heterogeneous models become available. Studies like Beard et al.'s (Beard, Kainz et al. 2006) and Christ et al.'s (Christ, Kainz et al. 2010) describe SAR studies performed using a variety of highly heterogeneous imaging-based models, often attempting to determine how individual anatomic parameters help determine SAR. In the head alone, Visible Human numbers some 21 tissues.

Average rather than worst-case models have also been created: NORMAN (stands for NORmalised MAN) (Dimbylow 1997) features tissue sizes and locations based on average values of samples taken from a large population. NAOMI (Dimbylow 2005) is

a female model developed along similar lines. The Virtual Family (Figure 3) has recently become available, a collection of eight human models encompassing children and adults both male and female (Christ, Kainz et al. 2010), based to a certain extent on averaged morphological values.

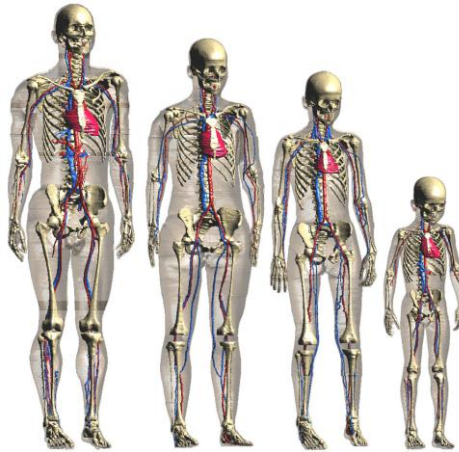


Figure 3: Virtual Family (from (Christ, Kainz et al. 2010))

The assumption has generally been that men's heads, being larger, provide a conservative SAR result which protects women and children as well (Petersen 2007), an assumption that has not been sufficiently tested in literature and may not be true for all populations. The standards define "conservative" to mean that the measured value will not be less than the expected value during normal use by a majority of users, not that that the measured value will not be less than the absolute maximum SAR value that could possibly occur under every conceivable combination head size, head shape, handset orientation, and spacing relative to the head (IEEE 2003). This may not be true for all populations; it is possible that many combinations of anatomic morphologies, dielectric properties and relative location of tissues cause unexpected 'hot spots'. Note also that average models like these are not representative of the extremes of populations, only the middle ground. Studies have found higher SAR in heads larger or smaller than average (Gandhi and Kang 2002).

All the models described so far are Caucasian; few models provide representation of other ethnic groups. Several notable exceptions are the Nagaoka Man and Woman (Nagaoka, Watanabe et al. 2004), Chinese Man and Woman (Wu, Liwen et al. 2011) and Korean Man (Kim, Choi et al. 2008). Until recently, no female models existed at all.

These models are also only representative of a single person, realistic or otherwise; each provides a single point of comparison. It is difficult to systematically test if and how the different parameters of human anatomy influence energy absorption from RF using the existing models. However, literature in the past few years has begun asking these questions. Effect of dielectric properties (Drossos, Santomaa et al. 2000; Kang and Gandhi 2004), head sizes (Hombach, Meier et al. 1996; Keshvari and Lang 2005; Bo 2007), and relative morphologies (Keshvari and Lang 2005; Christ, Kainz et al. 2010) on SAR have been examined to some extent. Heterogeneous and homogeneous models have been scaled, uniformly (Gandhi, Gianluca et al. 1996; Martínez-Búrdalo, Martín et al. 2004) or otherwise (Schonborn, Burkhardt et al. 1998; Wang and Fujiwara 2003; Hadjem, Lautru et al. 2005) (see Figure 4 for example), to closer resemble the heads of children (Wiert, Hadjem et al. 2007), women, and differently sized men (Kainz, Christ et al. 2005; Bo 2007). However, this is an arduous task, as properties of individual voxels (volume pixels) need to be adjusted to provide scaling, often manually. The only feature of homogeneous models that may be adjusted is the dielectric properties, and then only en masse. In some cases, canonical layered models have been used in an attempt to roughly determine how layered dielectrics of different thicknesses attenuate RF.

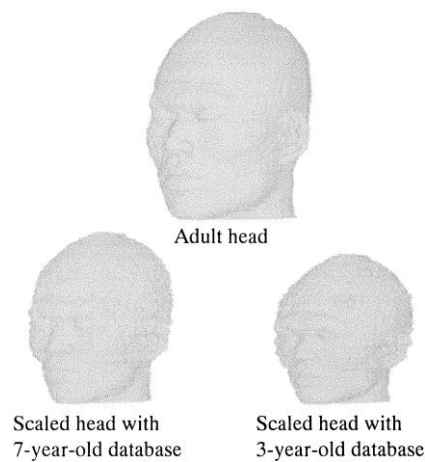


Figure 4: Non-uniform scaling of an adult heterogeneous head to derive children's heads (from (Wang and Fujiwara 2003))

The work described in this thesis attempts aims to overcome some of the shortcomings of the existing models used in RF dosimetry, and provide a more systematic approach to quantifying the effect of anatomic variations in the human head on energy absorption due to RF exposure (Christ, Klingebock et al. 2006).

1.1.2 Geometry Head

The question of how best to model humans for determining SAR for compliance with safety limits has not yet been answered, although much work has been done towards this goal over the past 60 years. Again, discussion is limited to modelling human heads, rather than whole bodies.

As covered in Chapter 2 below, existing dosimetric human models are of two types. At one extreme are highly heterogeneous models, closely representative of human anatomy, such as Visible Human, often used for research into energy deposition in different tissues. At the other extreme are the homogeneous models generally used for compliance, such as SAM, the Specific Anthropomorphic Mannequin. Traditionally, dosimetry studies assume that an adult Caucasian male model provides a worst-case conservative result, though the validity of this assumption has not been thoroughly tested. A number of models of Caucasian women and children as well as non-Caucasian adults (female and male) have become available in the past ten years. About 20 whole and partial body models of adults and about 14 models of children (from newborn to 14 years of age) are available, though the number is hard to estimate as different models were developed based on the same source data, or partial data sets of different patients or volunteers were combined to develop one complete body model. However, these are all individual comparison points, and do not provide enough information regarding how (and which) anatomic variations in humans, adult Caucasian male or otherwise, affect SAR distribution.

Models are only as good as their input parameters, and beyond a certain point, more complexity does not necessarily provide a better output. It is reasoned that there may be a reduced set of key tissues in the head that dominate the resultant SAR distribution, on which the compliance considerations depend most critically. For example, it is expected that surface tissues such as skin are the site of maximum SAR in the head, while the brain and eyes are the most critical organs in the head to be affected by RF exposure.

Investigating the relationships between energy absorption and specific anatomic variations in a systematic way is not easy using existing models. As a natural next step in this field, and taking advantage of the more mature modelling packages and

high solving power available, a new model has been created to better investigate this problem. The model, termed Geometry Head (GH) seen in Figure 5 includes a reduced set of only the most relevant tissues in a semi-homogeneous, simplified geometry. GH allows for easy parametric adjustment of tissue size, relative location, dielectric properties and morphology. Geometry Head aims to provide a point of diminishing returns in complexity somewhere between the homogeneous single-tissue model and the multi-tissue models.

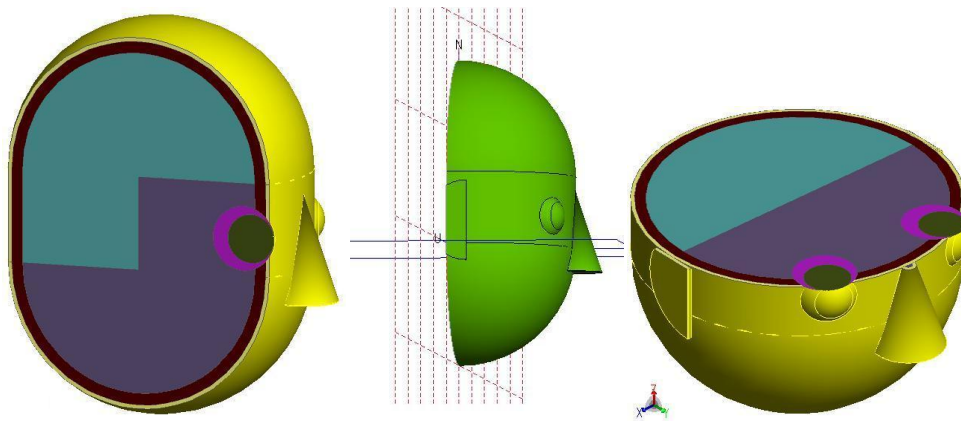


Figure 5: Geometry Head model, shown with various cutplanes

Initial anthropomorphic variable values such as tissue size and location were based on results of a large anthropometric study of adult males of multiple ethnicities (Farkas 1994), for higher comparability with existing models. Initial dielectric values of tissues are those used in SAR compliance studies (Gabriel 1996).

1.2 Original contributions

The original contributions of this thesis are:

- a) Creation of a unique parametric semi-homogeneous parametrically adjustable model of the human head suitable for modelling exposure of human heads to non-ionising radiation, named Geometry Head. Model was created using an appropriate commercially available software package (Section 3.1), with data originally taken from a large anthropometric study of adult Caucasian males
- b) Validation of the model at Ericsson Research Laboratories, Sweden, using simplified physical models of the human head, custom built for this purpose (Section 3.2)
- c) Gathering of data from literature regarding thickness of skin in adult humans, broken down into sub populations of sex (male and female), ethnicity (African-American, Caucasian, unknown/unspecified), and age groups (20-29, 30-39, 40-49, 50-59, 60+ years); and analysis of data for 5th, 50th and 95th percentiles of individual subpopulations as well as overall human variation (Section 3.3)
- d) Gathering of data from literature regarding thickness of the skull in adult humans, broken down into sub populations of sex (male and female), ethnicity (African, African-American, Australian Aboriginal, Bedouin, Caucasian, Chinese, Japanese, unknown/unspecified), and age groups (20-29, 30-39, 40-49, 50-59, 60+ years); and analysis of data for 5th, 50th and 95th percentiles of individual subpopulations as well as overall human variation (Section 3.4)
- e) Examination of the relationship between several anatomic parameters and SAR, to determine their effects on energy absorption in human heads from exposure to radiofrequency at 900 MHz:
 - i. cranial thickness (Section 3.3)
 - ii. skin thickness (Section 3.4)
 - iii. head size (Section 3.5)
 - iv. dielectric properties (Section 3.6)

1.3 Research questions

The current thesis is designed to address the following questions:

- What parameters of human head anatomy contribute to absorption of energy due to RF exposure?
- What variability exists in the relevant anatomic variations?
- What is the relationship between these anatomic parameters and SAR?
- What do these results imply for the safety standards for RF exposure?

While attempting to answer the above questions, another research question made itself evident:

- Given that existing models do not allow easy exploration of effect of anatomic parameters on SAR, can a new model be created without this limitation?

Chapter 2: Background concepts

The research described here combines concepts from electromagnetics, engineering and human anatomy. This chapter introduces some concepts required to understand the arguments, and experimental methods and results in this work.

2.1 Electromagnetics, mobile phones and safety standards

This section provides an introduction to the characteristics of electromagnetic fields, specifically the non-ionising radiofrequency radiation that is associated with mobile phones. A brief description of national and international radiofrequency safety guidelines in relation to GSM mobile phones is followed by a description of specific absorption rate (SAR), the metric used to measure radiofrequency absorption in biological tissue. Computational and experimental techniques used for measuring SAR are also explained.

2.1.1 Radiofrequency

The electromagnetic (EM) spectrum illustrated in Figure 6 extends from static fields, though frequencies associated with power lines and electrical appliances, up to x-rays and high-energy gamma rays. Frequencies are measured in Hertz (Hz), or wavelengths per second.

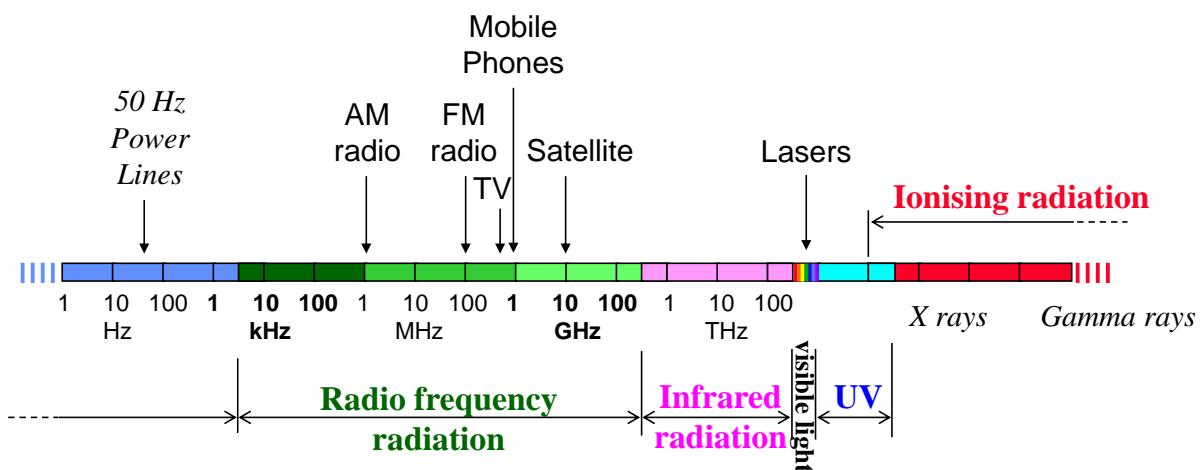


Figure 6: The electromagnetic spectrum (adapted from Telstra Research Laboratories training materials)

There are several ways to differentiate electromagnetic fields (EMFs). One of the key characteristics of EMFs is the energy level, which is easily derived from the frequency. At higher frequency region ($f \geq 10^{12}$ Hz), the energy is high enough (~ 5 eV) to ionise, i.e. break electron bonds in an atom. If this reaction occurs in living matter, it creates free radicals (atoms with unpaired electrons that are usually highly reactive), thereby increasing the risk of chromosomal damage or damage to biological tissue (ARPANSA 2002; Habash 2002). Therefore, this frequency band is identified as ionising radiation. X-rays and gamma rays are both classified as ionising radiation

and both have the ability to penetrate biological tissue and potentially cause damage.

The radiofrequency (RF) band of the electromagnetic spectrum is generally defined as the region between 3 kHz and 300 GHz. EMFs in this energy band do not carry enough energy to ionise material, hence the name non-ionising radiation. RF fields are used in numerous applications in modern society, most prolifically information transmission such as telecommunications, radio and television broadcasting. Other common usages for RF are heating, for example in microwave ovens, industrial applications such as RF welding and glue drying; and medical uses such as ablation and diathermy.

2.1.2 Radiofrequency and mobile telephony

A person in the vicinity of a base station is exposed to the radio frequency emissions from the base station; a person inside the same area using a mobile phone handset is additionally exposed to the RF emitted by the handset. This thesis is concerned with the emissions of handsets rather than base stations, specifically at the 900 MHz frequency used by technologies such as wide-band Code Division Multiple Access (w-CDMA), 3GPP Long Term Evolution (LTE), and GSM (Global System for Mobile Communications, originally *Groupe Spécial Mobile*).

As a general rule users are exposed to higher levels of emissions from handsets than from base stations due to the increased proximity of handsets to the body.

2.1.3 Propagation of EM fields

Under static conditions, the electric and magnetic fields form two individual vector quantities - E-field and H-field respectively. Electric fields exist whenever electric charges are present, and are produced by positive or negative charges that exert a force on other charged objects in the field. Magnetic fields are produced by the motion of electric charges, which exert force on other moving charges. Both electric and magnetic fields are strongest near the source and diminish as distance increases (Kraus 1992). Unlike E-fields, which exist even when no current is flowing, magnetic fields are produced only in the presence of moving charges (e.g. when a device is turned on).

EMFs can be mathematically defined in free space using four field quantities: electric field intensity (E , Volts/metre), the electric flux density (D , Coulombs/metre²), magnetic flux density (B , Webers), and magnetic field intensity (H , Ampere/metre). These four fundamental EMF quantities relate according to the Equation 1 and Equation 2 below:

Equation 1

$$B = \mu H$$

Equation 2

$$D = \epsilon E$$

where B = magnetic flux density (Wb), μ = permeability, H = magnetic field intensity (A/m), D = electric flux density (C/m²), ϵ = permittivity, and E = electric field intensity (V/m).

Propagation of electromagnetic waves in materials such as dielectrics and conductors is determined by their electrical parameters – permittivity, conductivity, and permeability. These constants further described in Section 2.1.6 are effectively the gradients of field propagation.

Under *time-varying* conditions, the time-varying magnetic and time-varying electric fields are coupled and propagate dynamically by one field component continuously producing the other over distance.

2.1.3.1 Plane waves

A transverse or a plane wave occurs when the electric and magnetic field components of EMF waves exist orthogonally (at right angles) to one another. The electromagnetic field plane is also at right angles to the direction of the wave propagation, as depicted in Figure 7 below.

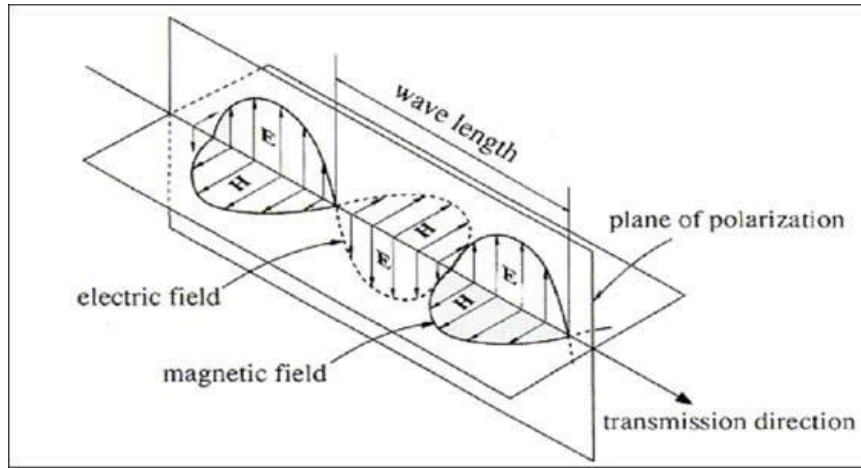


Figure 7: Propagation of an electromagnetic wave (adapted from <http://www.mike-willis.com/Tutorial/PF3.htm>)

A plane wave can also be described as a spherical wave of a suitably large wavelength. It is an ideal EMF used for the purpose of research simplicity, and cannot be replicated in real life. It must be treated as a source infinitely far away from every point, so it makes no sense to talk about it being nearer or further than any point. However, regions region deeper inside a body encounter the excitation once it has been attenuated by surface tissue layers, and therefore diminished.

2.1.4 Maxwell's equations

James Clerk Maxwell's work in describing the propagation of time-varying electromagnetic waves led to the development of four fundamental equations, valid in any point in free space. The differential forms of Maxwell's equations, and the corresponding integral forms are provided below in Table 1 (Kraus 1992).

Table 1: Maxwell's electromagnetic field equations, in differential and integral forms

Maxwell's Electromagnetic Field Equations	
Differential form	Integral form
$\nabla \times \mathbf{H} = \mathbf{J} + \frac{\partial \mathbf{D}}{\partial t}$	$\oint \mathbf{H} \cdot d\ell = I + \int \frac{\partial \mathbf{D}}{\partial t} \cdot d\mathbf{s}$
$\nabla \times \mathbf{E} = -\frac{\partial \mathbf{B}}{\partial t}$	$\oint \mathbf{E} \cdot d\ell = -\frac{d\Phi}{dt}$
$\nabla \cdot \mathbf{D} = \rho$	$\oint \mathbf{D} \cdot d\mathbf{s} = Q$
$\nabla \cdot \mathbf{B} = 0$	$\oint \mathbf{B} \cdot d\mathbf{s} = 0$

where ∇ = curl operator, J = total current density (A/m^2), ρ = total charge density (C/m^3), dl = differential displacement of charge, ds = vector surface element, Q = charge (C), Φ = magnetic flux (Wb), I = current (A), and t = time (s).

2.1.5 Near field and far field

Over a significant propagated distance, EMFs may be categorised into two regions: the near-field and far-field. The near-field can be further divided into two regions, *reactive* near-field and *radiating* near-field.

While specific field characteristics of an EMF may be quantified accurately by calculation in the far-field, in practice near-field calculations can carry large uncertainties given that in this region, plane wave characteristics have not been established and the relationship between the field quantities can be highly non-linear. The reactive near-field is typically described as the distance within $\lambda/2\pi$ from the radiating source, where λ is the wavelength. Therefore, the reactive near-field distance from a mobile phones radiating antenna at 900 MHz can be found to be approximately 5.3 cm - notably within the region of a mobile phone user's head. On the other hand, the far-field distance may be defined as the region extending beyond $2d^2/\pi$ (considering an antenna of dimension d) or $\lambda/2$, whichever is the greater (ARPANSA 2002). In the far-field region the electromagnetic field from the mobile phone forms a uniform plane wave such that the ratio of electric field intensity E to the magnetic field intensity H is constant.

2.1.6 Dielectrics

A dielectric is an electrical insulator that can be polarised by an applied electric field. When a dielectric is placed in an electric field, electric charges do not flow through the material, as in a conductor, but only slightly shift from their average equilibrium positions causing dielectric polarisation. Positive charges are displaced toward the field and negative charges shift in the opposite direction. This creates an internal electric field which reduces the overall field within the dielectric itself. If a dielectric is composed of weakly bonded molecules, those molecules not only become polarised, but also reorient so that their symmetry axis aligns to the field (Kraus 1992).

The study of dielectric properties is concerned with the storage and dissipation of electric and magnetic energy in materials.

Mammalian and other animal tissues classify as dielectrics. All tissues used in this study have permittivity, permeability and conductivity characteristics. The medium in which EMFs travel directly influence the relationship between E and D and between B and H, which in turn affect the speed of propagation. The relationship of permittivity and permeability of the material relate to the permittivity and permeability of free space.

2.1.6.1 Conductivity

Electrical resistivity (also known as resistivity, specific electrical resistance, or volume resistivity) is a measure of how strongly a material opposes the flow of electric current. A low resistivity indicates a material that readily allows the movement of electric charge. Electrical conductivity or specific conductance (σ) is the reciprocal quantity, and measures a material's ability to conduct an electric current (Kraus 1992).

2.1.6.2 Permittivity: an electric characteristic

Permittivity (ϵ) is a measure of how an electric field affects, and is affected by, a dielectric medium. It relates to a material's ability to transmit (or 'permit') an electric field. In most material, the permittivity is constant (where it is not, the material is said to be nonlinear) (Kraus 1992).

When solving electromagnetic propagation problems, it is often convenient to use the relative permittivity of a material, i.e. the ratio of its permittivity to that of a vacuum, which is a known measured quantity:

Equation 3

$$\epsilon_r = \epsilon / \epsilon_0$$

where ϵ_r is the relative permittivity, and ϵ_0 is the permittivity of free space. ϵ and ϵ_0 are expressed in Farads per meter, however the relative permittivity is a dimensionless ratio. Permittivity is a complex quantity which is affected by frequency:

Equation 4

$$\epsilon = \epsilon' - j(\epsilon'' + \sigma/\omega)$$

where ϵ' and ϵ'' are the real and imaginary parts of ϵ respectively, σ is the conductivity, and $\omega = 2\pi f$ is the angular frequency in radians (Kraus 1992).

Relative rather than absolute terms are generally used in electromagnetics for permittivity and permeability (Section 2.1.6.3 below) partly for historical reasons, and partly for ease of use. Using relative terms results in equations that are easier to manipulate and provide neat solutions, as well as easily comparable units. Further information regarding this topic is available in textbooks outlining basics of electromagnetics such as those by Sadiku (Sadiku 1989), Durney and Christensen (Durney and Christensen 1999) and Kraus (Kraus 1992).

2.1.6.3 Permeability: a magnetic characteristic

Permeability (μ) is the measure of the ability of a material to support the formation of a magnetic field within itself. In other words, it is the degree of magnetisation that a material obtains in response to an applied magnetic field (Kraus 1992).

As with permittivity, when solving electromagnetic problems it is often more convenient to refer to the ratio of the permeability of a given material (μ_r) to that of a vacuum (μ_0) than use the absolute value (Kraus 1992). This is given by:

Equation 5

$$\mu_r = \mu / \mu_0$$

Relative permeability μ_r is also dimensionless. Permeability may also be a complex quantity, whereby the real and imaginary parts (μ' and μ'' respectively) are related thus:

Equation 6

$$\mu = \mu' - j\mu''$$

2.1.6.4 Skin effect

Skin effect is the tendency of a time-varying current to distribute itself within a conductor with the current density being largest near the surface of the conductor, decreasing at greater depths. In other words, the electric current flows mainly at the "skin" of the conductor, at an average depth called the skin depth. In a good conductor, skin depth varies as the inverse square root of the conductivity. This means that materials with a higher σ value have a reduced skin depth. At higher frequencies, the skin effect reduces the depth of penetration of currents into a conductor (Kraus 1992).

2.1.6.5 *Intrinsic impedance of a medium*

The characteristic or intrinsic impedance of a medium denotes how resistive the material is to electrical fields. It derives from Ohm's Law (Kraus 1992):

Equation 7

$$Z_0 = \frac{E_0}{H_0} = \sqrt{\frac{\bar{\mu}}{\varepsilon}}$$

For dielectric materials that have permeability and conductivity characteristics, such as human tissues, the intrinsic impedance is (Kraus 1992):

Equation 8

$$Z_0 = \sqrt{\frac{\omega\mu'' + j\omega\mu'}{\sigma + j\omega\varepsilon}}$$

2.1.7 *Speed of EMF propagation*

The speed of propagation of EMFs in free space is known to be a constant 299,792,458 m/s, otherwise known as c , the speed of light. In other materials, the speed is different, as it relates to the gradients of E-field and H-fields:

Equation 9

$$c = 1/\sqrt{\varepsilon_r\mu_r}$$

2.1.8 *Refraction of EM waves in dielectrics*

The refractive index (also known as index of refraction) is a measure of the speed of light in that substance, and is calculated by:

Equation 10

$$n = \frac{c}{v_r}$$

where c is the speed of light, and v_r is the relative velocity of the EM wave in the material in question. The refractive index characterises not only the wave propagation speed, but also the amount of radiation transmitted and reflected by a material. It is dependent on the material's dielectric properties:

Equation 11

$$n = \sqrt{\epsilon_r \mu_r}$$

As the frequency changes, the values of ϵ_r and μ_r change, which changes the speed of the EM wave propagation, and the refractive index.

When an wave propagates through a layered dielectric, as inside a human head, its speed and absorption will change at each material boundary. The nature of the change may be calculated using Snell's law, which states that the ratio of the sines of the angles of incidence and refraction is equivalent to the ratio of the wavelengths in the two media, and equivalent to the opposite ratio of the indices of refraction (Kraus 1992):

Equation 12

$$\frac{\sin \theta_1}{\sin \theta_2} = \frac{\lambda_1}{\lambda_2} = \frac{n_2}{n_1}$$

The frequency, being the inverse of the wavelength, thus determines the angle of refraction as the EM wave passes from one material into another.

The amount of energy reflected from the material under normal incidence (R) is proportional to the square of the index change at the face (Kraus 1992):

Equation 13

$$R = \frac{n_1 - n_2}{n_1 + n_2}$$

2.1.9 RF safety standards

Established recommendations and guidelines limiting human and animal exposure to electromagnetic fields exist in order to provide protection against known adverse health effects. Safety recommendations for non-ionising radiation are mainly provided by large two international expert groups: ICNIRP, the International Commission on Non-Ionising Radiation Protection (ICNIRP 1998) and the IEEE Institute of Electrical and Electronic Engineers c95 subgroup (IEEE 2005). These guidelines are usually adopted and enforced by government bodies.

RF safety standards have grown more sophisticated and complex over the years of development, with advancements in methodology and application techniques. The

exact rationale behind the safety limits vary between standards, however most come with a background of thorough, critical literature evaluation. For example, during the development of the C95.1-2005 IEEE standards, Standards Committee 4 Literature Surveillance Working Group listed 1143 peer-reviewed papers and technical reports of original research that were evaluated and contributed to the standard development (Petersen 2007).

The biological bases for limits in the frequency range 100 kHz to 10 GHz are whole body heat stress, and excess localised tissue heating (CENELEC 2006; Petersen 2007), and are based on established biological mechanisms of interaction. Safety factors are built into these standards to ensure permitted exposures are well below levels at which biological effects are observed.

Australia follows the ICNIRP recommendations (ARPANSA 2002) which specifies three SAR limits which all have to be fulfilled irrespectively:

- whole-body average SAR limit, to avoid general thermal stress
- localised SAR for the head and trunk, to avoid local heating; this is based on danger of developing cataracts (this is the limit that is used for mobile phones)
- localised SAR limit for the limbs

In the case of mobile phone safety using 900 MHz, the most relevant situation is consider is that of head and trunk localised exposure. Handsets are usually held against the head during use, and it has been shown that mobile handset antennas produce highly localised exposures (Li, Leong et al. 2000). A whole body exposure would be more appropriate if radiation from the base station was being considered.

2.1.10 Dosimetry and SAR

Dosimetry (from 'dose' and 'metric') refers to the evaluation of the amount of absorption of EMF in biological tissue following exposure to sources such as mobile phones, based on the electric field strength, induced current density, and the rate of energy absorption (NRPB, 2003).

The E and H-fields are normally assessed when characterising RF exposure, since these field parameters are rather easier to measure than temperature change at all

points in the body. As previously mentioned, in the far-field region, E and H are coupled i.e. E is perpendicular to H and both are perpendicular to the direction of motion, and in free-space:

Equation 14

$$Z_0 = E/H = \sqrt{\mu_0/\epsilon_0} = 377 \Omega$$

where Z_0 is the intrinsic impedance of free air.

However, in most cases as in exposure from RF sealers and from mobile phones, the distance from the source to the exposed individual is too short, and near-field conditions exist. In such a case, E and H must be treated separately, since both contribute to the absorption (Kraus 1992).

The main exposure metric used in safety standards to describe the absorption of RF fields up to 6 GHz in tissues (or other matter) is the Specific Energy Absorption Rate (SAR). This term, first proposed in 1981 (Petersen 2007), is defined as the rate at which energy is imparted (dissipated) from electric and magnetic fields to charged particles (body dielectrics) in an infinitesimal volume of an absorber per unit mass. It is measured in W/kg:

Equation 15

$$SAR = \frac{\sigma |E|^2}{\rho}$$

where σ is the tissue conductivity (S/m), ρ is the tissue density (kg/m³), and $|E|$ is the magnitude of the total RMS (root mean square) E-field level (V/m) induced within the irradiated tissue:

Equation 16

$$|E| = \sqrt{|E_x|^2 + |E_y|^2 + |E_z|^2}$$

where E_x , E_y , and E_z are the RMS values of the x , y , and z components of the electric field.

Note that the B-field is not included in SAR calculations. This is because the B-field does not transmit energy to electric charges, which constitutes almost all of

biological tissue. E-field can transfer energy to electric charges through the forces it exerts on them, however forces exerted on charges due to B-field are perpendicular to the velocities of the charges. The B-field can change the direction of charges but not their energy. B-field can also transfer energy through forces on permanent magnetic dipoles, however biological tissues are mostly nonmagnetic (Durney and Christensen 1999).

SAR can be averaged over different volumes. Three specific averaging volumes are used in this thesis, as these are used in safety standards (IEEE 2005): whole body averaged (WBA) SAR, and localised peak-spatial SAR averaged over 1-gram (henceforth referred to as '1g SAR') or 10-gram (henceforth referred to as '10g SAR') cubes of material.

All three variables on the right hand side of Equation 15 are temperature dependent and the conductivity and induced electric field are also frequency dependent.

During far field conditions, absorption in the object is dependent on the frequency of the applied RF field. Roughly speaking, for E-polarization the SAR will increase with increasing frequency as a function of f^2 , up to the resonance frequency for the object, and then decrease as a function of $1/f$, see Figure 8 below.

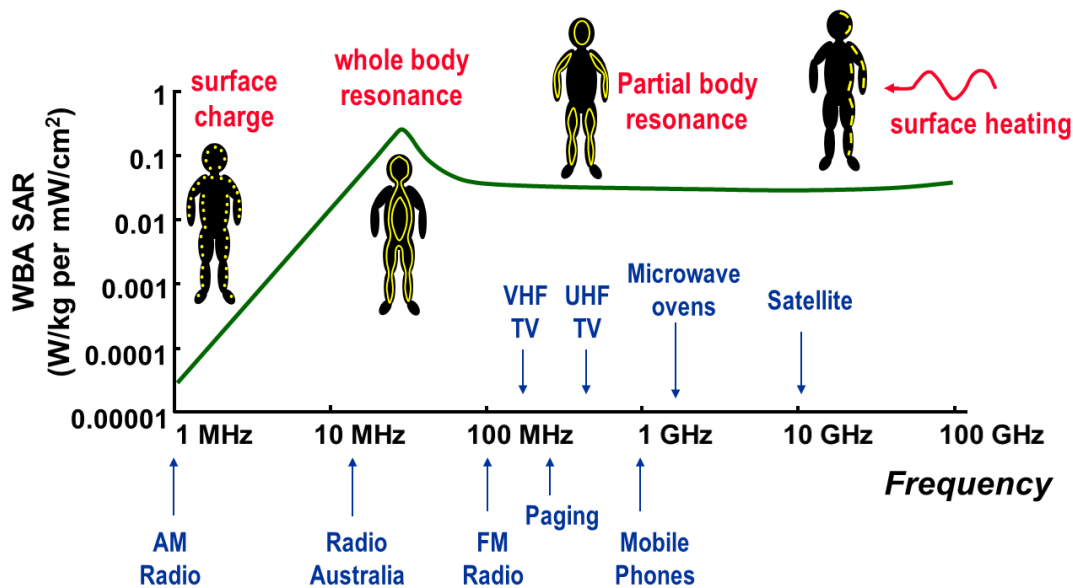


Figure 8: Effect of frequency on whole body average SAR (in far field). For E-polarization the SAR will increase with increasing frequency as a function of f^2 , up to the resonance frequency for the object, and then decrease as a function of $1/f$ (adapted from Telstra Research Laboratories RF training materials)

Other factors that affect the absorption are the polarisation, the density, and the electrical properties (also known as the dielectric properties) of the exposed object. The SAR value during exposure can be calculated using the measured field strengths or the induced current.

2.1.11 Field Strength

The *field strength* involved when biological organisms are exposed to electromagnetic fields must be specified, along with the type of tissue under discussion. Exposure to high intensity fields from parts of the spectrum might cause severe biological effects while very weak fields with the same frequency do not (Habash, Brodsky et al. 2003).

2.1.11.1 Power of phones

Usually, mobile phones transmit power in the range of 0.2 to 0.6 W (Habash, Brodsky et al. 2003).

2.1.12 Location of max SARs

Localised heating becomes more important than whole body heating for exposures very close to the RF source. Maximum SAR in the body occurs at locations closest to antenna currents where incident H is highest. Localised SAR generated by a nearby source decays exponentially as it passes into the body.

2.1.13 Basic restrictions and reference levels

More information about the history of RF safety standards and rationales used therein for units and measurement methods, please see Section 1.1.1. For more complete explanations regarding development and use of RF standards, please see (Habash 2002), (Habash, Elwood et al. 2009) and (Petersen 2007).

SAR and current density are termed as "Basic Restrictions" and refer to field or energy values inside the exposed tissue. In most cases it is inconvenient if not impossible to obtain such measures since invasive methods of measurement would be required, therefore direct assessment of compliance with basic restrictions is not usually feasible.

Instead, computational modelling can be performed: exposure guidelines define more usable exposure assessment metrics which do not require measurements within the exposed tissue. These are termed 'reference levels' and are based on measurements of ambient (free space) electromagnetic fields in close proximity to the exposed tissue. Reference levels are established via extrapolation from single frequency laboratory measurements using mathematical modelling. They are determined based on maximum energy coupling conditions, and therefore represent worst case scenarios (ICNIRP 1998). If the reference levels are fulfilled, it is not likely that the basic restrictions are exceeded. On the other hand, if the measured values do not comply with the reference values, numerical calculation must be used to ensure that the basic restriction is not exceeded. The reference values are electric and magnetic field strengths and currents flowing in the limbs.

ICNIRP has adopted more stringent exposure restrictions for the general population than for occupational exposure, and the division factor is 5 between those two. Table 2 provides a short summary of basic restrictions and reference values for the frequency range 1-2000 MHz.

Table 2: SAR Basic restrictions and fundamental limits (adapted from Telstra Research Laboratories RF training course)

Exposure category	Standard	Freq. range	WBA SAR (W/kg)	Localised SAR in head & trunk (W/kg)	Localised SAR in limbs (W/kg)
Occ.	ICNIRP 98	100 kHz - 10 GHz	0.4	10	20
Non-Occ.	ICNIRP 98	100 kHz - 10 GHz	0.08	2	4

2.1.14 Section summary

- radiofrequency is a non-ionising form of electromagnetic energy, nominally in the frequency range of 3 Hz – 300 GHz
- radiation safety standards protect humans and other animals from tissue damage
- limiting the absorbed power per unit mass in the whole body, localised to the head and the trunk and in the limbs, provides enough protection from RF heating effects, the only known effects to potentially cause damage
- mammalian tissues belong to a class of materials known as dielectrics, whose electrical properties (conductivity, permittivity and permeability) in the presence of radiofrequency are frequency dependent
- a material's conductivity, and to a lesser extent its permittivity, determine the amount of energy absorbed by the material due to the EM wave propagating through it
- at the interface of two dielectrics, the materials' dielectric properties, and therefore the frequency, determine the amount of energy reflected and absorbed by the materials
- this thesis is limited to exploring interaction of RF radiation at a frequency of 900 MHz with human head tissues rather than the whole body

2.2 Computational techniques

Computer power and software capabilities have increased substantially in recent years, and a variety of general purpose EM simulation tools are now commercially available for the analysis and design of antennas, microwave components, communication devices, and bioelectromagnetic problems.

Not all simulators have the same capabilities or performance, and each may be best suited for a particular type of problem. Factors including accuracy, speed of execution, and setup time, play important roles in selecting the proper simulator.

Computational methods generally involve the use of analytical and/or numerical techniques with a combination of techniques often useful in providing a more complete calculation of SAR (Habash 2002). Analytical techniques involve calculating the power absorption of incident fields in biological models of the human body or parts thereof relevant to the exposure source. Most of today's popular EM field simulation software packages for modelling SAR at RF frequencies are based on one or more of the following solving methods: Method of Moments (MoM), Finite Element Method (FEM), Finite Difference Time Domain (FDTD) and Finite Integration Technique (FIT). A brief description of each technique is provided below, along with advantages and drawbacks of each.

2.2.1 MoM

Electric dipole moment is a measure of the polarity of a system of electric charges. The Method of Moments (MoM) owes its name to the process of taking moments by multiplying with appropriate weighing functions and integrating. It is a boundary element method that involves breaking a model down into virtual wires and/or metal plates. Wires are subdivided into segments, and metal plates are subdivided into surface patches, both of which must be smaller than the wavelength of the device under investigation (Habash 2002). A virtual current source is then applied and the current on each wire segment and surface patch must be determined, allowing the electric field at any point in space to be calculated (Habash 2002).

The main disadvantage of using the method of moments is that it doesn't deal very well with complex geometry and heterogeneous dielectric models. It is applicable to problems for which Green's functions can be calculated, a mathematical method used

for solving inhomogeneous differential equations subject to specific initial conditions ('boundary conditions') (Kraus 1992). In a bioelectromagnetic problem, this usually involves fields in linear homogeneous media. This places considerable restrictions on the range and generality of problems to which boundary elements can usefully be applied. Since MoM requires calculation of boundary values only, rather than values throughout the space defined by a partial differential equation (PDE), it is significantly more efficient in terms of computational resources for problems where there is a small surface/volume ratio (Habash 2002).

2.2.2 FEM

The FEM solving method was originally designed for structural analysis problems. FEM is used for finding the approximate solution of partial differential equations (PDEs) and integral equations (Sadiku 1989) The solution approach is based either on eliminating the differential equation completely (steady state problems), or rendering the PDE into an equivalent ordinary differential equation, which is then solved using standard techniques such as finite differences, etc. The FEM is a good choice for solving PDEs over complex domains or when the desired precision varies over the entire domain. The finite element analysis of any problem involves basically four steps (Sadiku 1989): discretising the solution region into a finite number of subregions or elements; deriving governing equations for a typical element; assembling of all elements in the solution region; and solving the system of equations obtained. When meshing a volume by finite elements, the computational volume must be filled entirely, i.e. no space is left between elements; and all points inside the volume must lie in at least one finite element. If a point lies in more than one finite element, then the point is located in a common vertex or on a common edge or face (Sadiku 1989).

These rules mean that the complete volume of the configuration be meshed, rather than just the surface, with each mesh element able to have different properties where appropriate (such as biological tissue within a body). This can be a drawback as it is difficult to integrate the mesh elements for highly complex structures (Habash 2002)

2.2.3 FDTD

The Finite Difference Time Domain method provides a direct solution of Maxwell's curl equations in the time domain. FDTD techniques have emerged as the primary means to model many scientific and engineering problems dealing with electromagnetic wave interactions with material structures, and as such it is currently the most popular method used for estimating SAR (Roach 2009)

FDTD is a time-domain technique that alternately calculates the electric and magnetic fields in the defined region of a simulation, with the ability for different materials to be modelled within the computational domain. The advantages of using FDTD are its versatility - it is easy to understand and implement in software, and the analysis of a system covering a wide range of frequencies can be performed with a single simulation (Habash, 2002). However, this solving method is impractical for larger models. It requires that the entire computational domain be gridded, and the grid spatial discretisation must be sufficiently fine to resolve both the smallest electromagnetic wavelength and the smallest geometrical feature in the model. Very large computational domains can be developed, which results in very long solution times. Modelled shapes often suffer from a staircasing effect, where rounded shapes are approximated using cubic voxels (volume pixels), a drawback when dealing with rounded shapes such as exist in human bodies. Using FDTD there is also no way to determine unique values for permittivity and permeability at material interfaces.

2.2.4 FIT

The Finite Integration Technique gets its name from the fact that it discretises the integral rather than the differential form of Maxwell's equations. The resulting matrix equations of the discretised fields can be used for efficient numerical simulations on modern computers. All Maxwell's equations can be discretised with the FIT to yield their discrete counterparts with a compact and elegant matrix form (Sadiku 1989). The difference between modern FEM and FIT is only in the discretisation of the material property relations (Habash 2002).

2.2.5 Choosing a modelling package

Table 3 below lists seven of the most well-known commercial EM field simulators with their adopted numerical methods and applications.

Table 3: Seven of the most well-known commercial EM simulators and their adopted numerical methods

Simulator	Method	Type	Application	Provider	URL
HFSS	FEM	Frequency domain	3D Full-Wave-EM Field Simulation	ANSYS Inc., USA	http://www.ansoft.com
CST MWS	FEM/FIT	Time domain	3D Full-Wave-EM Field Simulation	CST Computer Simulation Technology AG.	http://www.cst.de
SuperNEC	MoM	Frequency domain	3D antenna design and analysis	Pointing Software (Pty) Ltd.	http://www.supernec.com
FIDELITY	FDTD	Time domain	3D Full-Wave-EM Field Simulation	Zeland Software Inc.	http://www.zeland.com
Feko	MoM and Hybrid MoM/FEM	Frequency domain	3D Full-Wave-EM Field Simulation	EM Software & Systems – S.A. (Pty) Ltd.	http://www.feko.info
xFDTD	FDTD	Time domain	3D Full-Wave-EM Field Simulation	Remcom (USA) State College, PA.	http://www.remcom.com
SEMCAD	FDTD and ADI-FDTD	Time domain	3D Full-Wave-EM Field Simulation	Schmid & Partner Eng. AG (SPEAG), Switzerland	http://www.semcad.com

2.3 Measurement techniques

Physical RF compliance measurement techniques as outlined in measurement standards (IEEE 2003; CENELEC 2006) are designed to provide a conservative SAR result while being not prohibitively complex to undertake. Heterogeneous head models with multiple tissues are difficult to construct. Moreover, measurements are often limited to specific regions of the phantom, due to restrictions imposed by bony structures.

A conservative approach for assessing SAR can be achieved by using a thin low-loss dielectric human-shaped shell ('phantom') filled with a homogeneous dielectrically equivalent tissue simulating liquid. A wireless device is positioned at various locations surrounding or abutting the phantom and operated at full power, while the computer-controlled electric field probe inserted into the tissue maps the electric fields inside. Computer algorithms determine the maximum electric field and then calculate the 1g or 10g SAR values throughout the phantom (IEEE 2003). For compliance measurements, a 1 mm * 1 mm * 1 mm grid is often used for probe measurements at the areas of interest. Since recipes for ingredients do not produce exactly correct values, partly due to inaccuracies in mixing and partly because of variations in the properties of each ingredient, the actual values (rather than the standard specification) must be measured and specified in tests.

2.4 Anatomy

This section describes structures of the human head and relevant measurement terms used elsewhere in this thesis.

2.4.1 Planes and directions of the human body

Figure 9 below shows some anatomic terms of location used in this thesis.

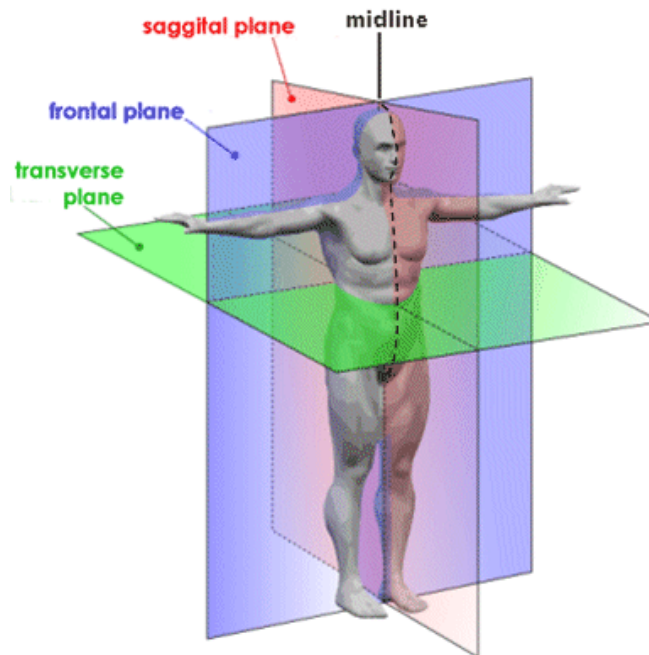


Figure 9: Planes and directions of the human body (adapted from http://staff.ucc.edu/alc-paez/biology/anat_planes/planes.htm)

The planes of the head body are:

- **Sagittal** – divides the body into right and left parts
- **Midsagittal or medial** – sagittal plane that lies on the midline
- **Frontal or coronal** – divides the body into anterior and posterior parts
- **Transverse or horizontal (cross section)** – divides the body into superior and inferior parts

The following relative directional terms are used to describe positioning of anatomic structures:

- **Superior and inferior** – toward and away from the top of the head, respectively
- **Anterior and posterior** – toward the front and back of the body

- **Medial, lateral, and intermediate** – toward the midline, away from the midline, and between a more medial and lateral structure
- **Superficial and deep** – toward and away from the body surface
- **Ipsilateral and contralateral** – on the same or opposite side as another structure

2.4.2 Anatomy of the human skull

The eight cranial and 14 facial bones comprise the human skull, some of which are named below in **Error! Reference source not found..** These bones in particular will be referred to again in later chapters.

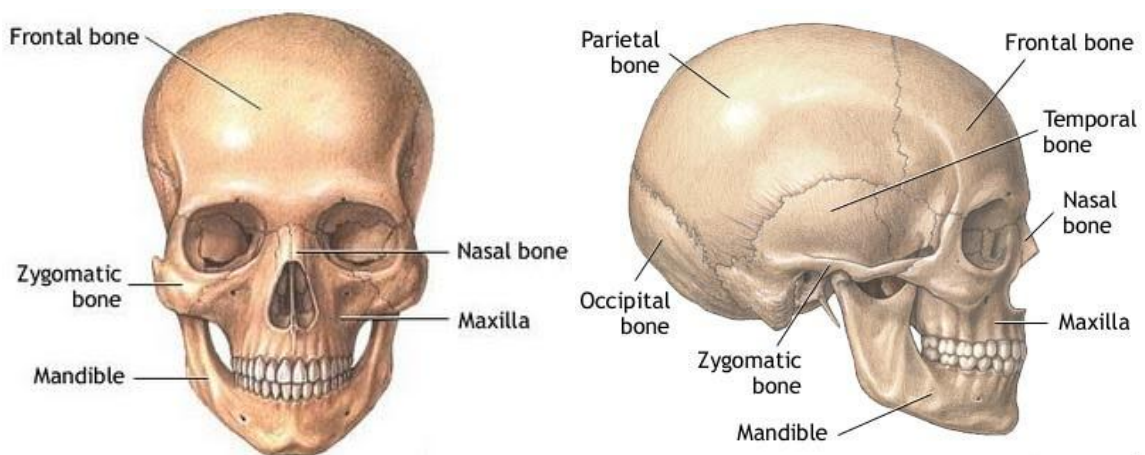


Figure 10: The human skull

2.4.3 Anthropometric measurements of the human head

Anthropometry is the measurement of the human bodies for the purposes of collecting and understanding human physical variation. Figure 11 below describes measurements of the human head and face used throughout this thesis.

For simplicity, measurement number 14 in Figure 11 (top of head to menton) is referred to in this thesis as 'head height'.

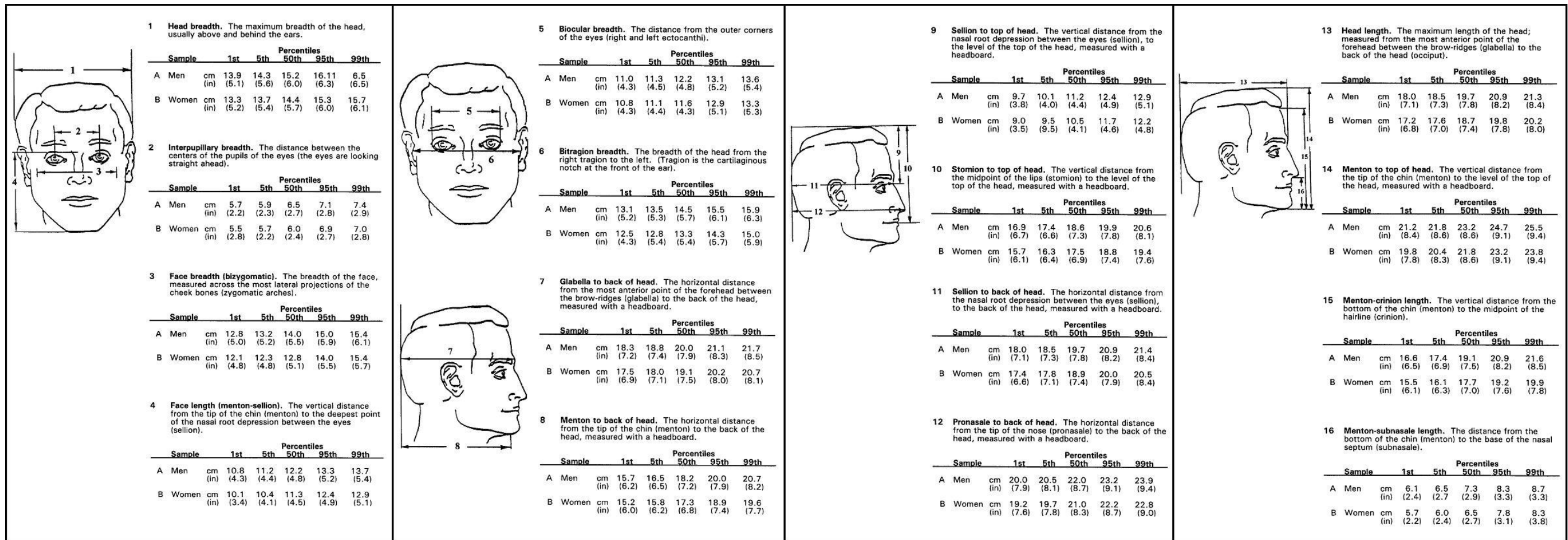


Figure 11: Anthropometric measures of the head and face (from Churchill 1976)

Chapter 3: Experimental methods, results and analysis

This chapter outlines the experimental procedures and materials used in this project. A rationale is provided for the specific structures of the model as it stands, and each step as it was performed. There are three sections of experimental procedure: construction of the model, detailed in Section 3.1; physical validation, Section 3.2; and testing individual parameters, Sections 3.2 to 3.6. Literature review pertaining to the tested variable and a discussion of results is provided in each section, along with a section summary.

3.1 Methodology: the Geometry Head model

An alternative computational model of the human head, named Geometry Head (GH) was created as part of this project using a commercially available electromagnetic solving package, with the intention of solving some of the existing limitations of human head models used for dosimetry compliance. Geometry Head consists of a semi-homogeneous reduced tissue set modelled as simplified geometries.

The GH model was initially created using the xFDTD modelling package (Remcom 2006), which uses the Finite Difference Time Domain solving method, and the first variable tests - effects of cranial thickness SAR in Section 3.3 - were performed using this version. However, one of the requirements of a model that allows systematic testing of variables is the ability to quickly and easily vary their values. This is not possible using the FDTD method, since it requires that the entire computational domain be gridded, and the grid spatial discretisation must be sufficiently fine to resolve both the smallest electromagnetic wavelength and the smallest geometrical feature in the model. Altering the relative location, morphology, or size of tissues in xFDTD requires manual manipulation of numerous individual voxels (volume pixels), rendering this software package unsuitable for the work undertaken here. For further discussion regarding advantages and disadvantages of electromagnetic numerical solving methods and modelling packages, please see Section 2.3.

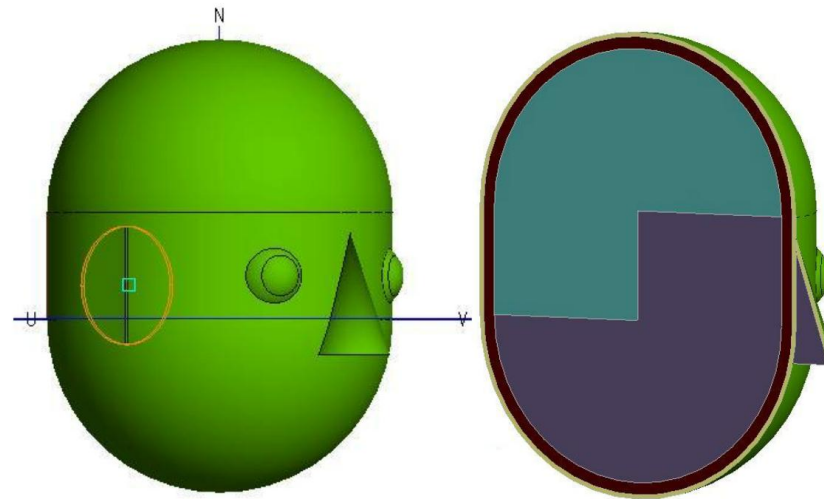
The final version of the GH model seen in Figure 12 was constructed (and is available for general use) using EMSS FEKO (EMSS 2009), a hybrid electromagnetic solver using Method of Moments/Finite Element Method. Several canonical models were tested using both packages; results were found to agree within a few percent variation.

Large volume sections

Top third: three concentric half spheres: filler tissue ($r = 80$), skull ($r = 86$), skin ($r = 88$)

Middle section: three concentric cylinders; the inner cylinder ($r = 80$) is split along the coronal plane to become two half-cylinders, 'brain' and 'filler' tissues; next layers are skull ($r = 86$) and skin ($r = 88$)

Bottom third: three concentric half spheres: filler tissue ($r = 80$), skull ($r = 86$), skin ($r = 88$)



Facial features

Eyes ($r = 8$) & fat ($r = 12$): two concentric spheres; centre point of fat is offset by 4 mm (anterior) to allow the eyes to protrude through fat. Eyes protrude 7 mm through the skin for a worst-case scenario of open eyelids

Nose: two concentric cones of 'filler' tissue ($r = 18$, $h = 55$) and skin ($r = 20$)

Ears: two half-cylinders ($r = 30$, thickness = 2) orthogonal to the rest of the 'head'

Figure 12: The Geometry Head model. Parentheses provide the dimensions used in the base-level model, based on anatomic measurements taken from a large sample of adult Caucasian males (Farkas 1994).

3.1.1 Features

Anatomic features included in this model are brain, skull, skin, eyes, ears and nose, as these are *a priori* considered to be most significant for the determination of the SAR distribution. A layer of fat surrounds both eyes, as in the human body, providing electrical isolation. The remainder of the model (termed 'filler') is comprised of an average head tissue, compliant with IEEE Measurement Standard (IEEE 2005), taking the number of tissues used in this model to six.

The brain, skull, filler and skin are modelled as a three concentric half-spheres separated by a cylindrical section. The head is modelled with uniform cranial and skin thicknesses. The top half-sphere is made up of brain, skull and skin; the bottom half-sphere comprises filler, skull and skin. Three concentric cylinders make up the middle section, where the inner cylinder is split along the coronal plane into a brain section at the back of the head, and a front 'filler' section. The nose is modelled as two concentric conic sections resulting in average head tissue covered with a skin layer of equivalent thickness to the rest of the head. The ear is composed of skin tissue. The fat and eyes are two concentric spheres with a centre point offset, allowing the eyes to protrude through the fat layer. Eyes protrude through the skin for a worst-case scenario of open eyelids.

The shapes in this model may be varied parametrically, greatly reducing the effort required to undertake this extensive modelling task. That is, as the size, morphology or relative location of any tissue or shape is altered, the rest of the head model automatically adjusts to accommodate the changes. This is achieved using complex variable dependencies. For example, the radii of the half-spheres and cylinders that make up the skull and skin are dependent on the brain radius, and if one is adjusted, the rest change accordingly.

Initial anthropomorphic dimensions such as tissue size and location were based on results of a large anthropometric study of adult males of multiple ethnicities (Farkas 1994); initial dielectric values of tissues are those used in SAR compliance studies (Gabriel 1996).

3.1.2 Parameters that may be varied

The following parameters of the Geometry Head model may be adjusted:

- radius of the inner half-spheres and half-cylinder (as a single variable), which determines head breadth and in part, the distance between the menton (bottom of chin) and top of the head
- skull thickness
- skin thickness
- height of the middle section, which contributes to the head height
- radius of the eye spheres
- radius of the fat spheres, i.e. thickness of fat layer
- offset of centre points of eye and fat spheres, which controls eye protrusion through fat layer
- vertical positioning of eyes relative to top of head
- interpupillary breadth (lateral separation of eyes)
- vertical positioning of the nose, which determines distance between sellion and top of the head.
- vertical height of nasal cone, which determines the vertical distance between sellion and subnasale
- radius of nasal cones, determining nose breadth and protrusion from face
- radius of the ear half-cylinders, which determines thickness of pinna (ear)
- tissue makeup each shape
- conductivity, permittivity and density of each of the six tissue types (brain, eye, fat, filler, skin, skull) as individual variables

3.1.3 Exposure

Exposure was treated as an experimental variable, and therefore was kept constant in all tests, permitting better comparison of anatomic variables. It is important to note that source intensity used in SAR computations can be scaled up or down after models are run. 900 MHz plane wave excitation propagating in the saggital plane was used as the exposure source, at an arbitrarily chosen power density of 10 W/m^2 . As this study is exploring the relationship between anatomic variables and SAR, the exposure source isn't overly relevant, as long as it is kept constant.

3.1.4 Validation

Ideally, to test the model's efficacy, SAR measurements inside a living human's head would be compared to predictions made by the Geometry Head model, with its parameters suitably adjusted to resemble the real head's anatomic features. As this option was not available, simplified models of the head were constructed specifically for this purpose, and GH parameters were adjusted to match anthropometry of the physical models as closely as possible. A model that can accurately predict SAR inside a real head should provide a reasonably accurate estimate of SAR when tested against a simplified solution space.

3.1.5 Parameter testing

In order to further test the efficacy of the Geometry Head model, the assumptions behind its construction, and attempt to determine relationships between tissue parameters and SAR, several parameters of the model were individually adjusted while all other variables were kept constant

Several anatomic parameters were chosen for initial investigation:

- cranial thickness
- skin thickness
- dielectric properties of each tissue
- head size

The Geometry Head model has been designed to resemble the anatomy of adults. It is not overly difficult to amend this model to closer reflect the morphology of children's heads, which is quite different to that of adults. Children's skulls are thinner, and the relative location of sensitive tissues such as brains is different. Moreover, the dielectric properties of children's heads are different to those of adults. Using directly scaled adult heads as a substitute for children's heads has been discouraged in the literature (Bit-Babik, Guy et al. 2005; Wiart, Hadjem et al. 2008), as this approach can lead to large uncertainties with respect to the local exposure of tissues and therefore to the interpretation of the findings. Some studies such as Schonborn et al's (Schonborn, Burkhardt et al. 1998) suggest using non-linear scaling algorithms to create child models. With current technology, it is simpler to derive

child models from imaging techniques such as MRI, and these are increasingly used for SAR investigations (Wiert, Hadjem et al. 2008; Christ, Kainz et al. 2010).

To establish what variations exist in the chosen anatomic features, a literature review was first undertaken to investigate the anatomic variability in humans. For some anatomic features, data is sparse and inconsistent, rendering comparisons between studies somewhat impractical. Where information was scarce, *a priori* reasoning was used to establish a parameter variation range that would encompass realistic variability.

3.1.6 Metrics examined

The **10g peak spatial SAR** (10g SAR) has been included in results of all tests, as it is the compliance metric used by ICNIRP (ICNIRP 1998) and IEEE (IEEE 2005) guidelines, and the ARPANSA radiofrequency standard which applies in Australia (ARPANSA 2002).

1g peak spatial SAR (1g SAR) has also been examined in most tests, as it was still a compliance requirement under IEEE recommendations until 2005 (IEEE 1999; IEEE 2005). The **whole head averaged (WHA) SAR** is included in most tests as it provides an indication of the overall absorption in the head.

For most tissue variations, the **average SAR in each tissue** of the model is also included. **SAR plots** showing the distribution of energy absorption through slices of the head have been included for one variable investigation. Along with **location of 1g and 10g SARs**, these metrics provide insight into regions of high SAR in the head, and how those change with variation in tissue parameters.

As well as raw SAR values, a calculation of the **SAR percentage variation** is included: how much the SAR value for any given tissue variation differs from the base-level GH SAR value, which acts as a point of comparison.

As the location of 1g and 10g SARs move, the tissue makeup of the cubes change. This creates some variability in results. As covered in Chapter 2, it is known that most absorption occurs at the surface; since the ear is modelled as skin, average skin SAR includes SAR in the pinna. Increasing the bulk averaging – from point SAR to 1g and 10g, all the way up to tissues and WHA SAR – provides an indication of

absorption trends. As the volume over which the SAR is averaged increases, the trends become clearer.

3.1.7 Section summary

- Geometry Head is a parametric, parametrically adjustable model of the human head, made of geometric shapes, suitable for testing relationships between anatomic variables in the human head and resultant energy deposition due to RF exposure
- Geometry Head is created using FEKO, a commercial Method of Moments/ Finite Elements Method (MoM/FEM) solver
- Initial anthropometric values used in the model are based on large multi-ethnic study of heads of adult males
- Model has been validated against physical simplified head models, see next section
- Several anatomic features were chosen for initial testing, see subsequent sections
- Metrics examined in this study provide a wealth of information regarding relationship between tissue parameters and SAR magnitude and distribution in the human head

3.2 Validation study

This section describes the creation of homogeneous and multi-tissue physical models approximating human heads, and SAR testing of those models under laboratory conditions. Details are provided regarding construction of analogous computational models using the Geometry Head model. Results of physical and computational models are compared to establish efficacy of the Geometry Head model at predicting SAR in realistic situations.

3.2.1 Rationale

The validation study was aimed at examining the Geometry Head model's ability to predict SAR in a realistic head.

Various studies indicate that in dosimetric studies where the computation model closely matches the physical model, the computational model provides highly accurate estimates of SAR (IEEE 2003).

The ideal way to test the model's accuracy at predicting SAR is to adjust the model parameters to known anatomic and dielectric attributes of those of a living human, and compare SAR results in GH with those measured *in situ* during similar exposures.

Instead of trying to undertake measurements likely to cause harm or death, simplified phantoms of the head were constructed, and GH parameters were adjusted to match the physical model as closely as possible. It was reasoned that a numerical model that can accurately predict SAR for a complex situation should be able to provide reasonable accuracy for a simplified solution space.

3.2.2 Methodology

3.2.2.1 Physical models

Custom-built phantoms resembling human heads were created specifically for this study. These were used in conjunction with two plastic human skull replicas and dielectrically-equivalent liquids to create homogeneous and heterogeneous head models of adult and child proportions. Since the E-field decays exponentially with depth into the phantom for closely coupled sources (Habash 2002; IEEE 2005), the maximum SAR was expected to occur at the inside surface of the phantom closest to the radiating source. With this in mind, models were designed to allow the probe to

reach inside the brain cavity, as close as possible to the source. Models were exposed to RF radiation in the form of a dipole antenna radiating 900 MHz. SAR in the 'brain' was measured using a compliance measurement and exposure system.

The physical models created are within realistic ranges of morphology, location, and size of tissues of real human heads, though they are not representative of any specific individuals' anatomy. These models were not intended to accurately represent reality, but rather to provide a comparison point for the computational model. Parameters of the computational model were matched to measured parameters of the physical models, and the SAR predictions in both models correspond reasonably well, suggesting the Geometry Head model is indeed viable for SAR predictions.

3.2.2.1.1 Measurement and exposure system

All tests were performed using the DASY4 (Dosimetric and near-field Assessment System, Figure 13) measurement system (Speag 2008) at the Ericsson Research Laboratories in Stockholm, Sweden. A similar DASY4 setup was used for initial testing at EMC Technologies, Melbourne, Australia. The DASY4 system comprises compliance testing equipment in accordance with regulatory standards. E-field probes were used to take volumetric scans of the 'brains' of custom made phantoms described below. From this, SAR values were derived using the SEMCAD software supplied with DASY systems.

Additional equipment used for testing and exposure:

- Signal generator, Rohde & Schwarz SMHU58
- Dielectric probe kit, HP 85070C
- Network analyser, HP 8752C
- Power meter, Rohde & Schwarz NRVS
- Power sensor, Rohde & Schwarz NRV-Z5
- Digital radio tester, Rohde & Schwarz CMU 200
- Thermometer, EBRO TFX-392SKWT
- Thermo/Hygrometer, Testo 608-H2

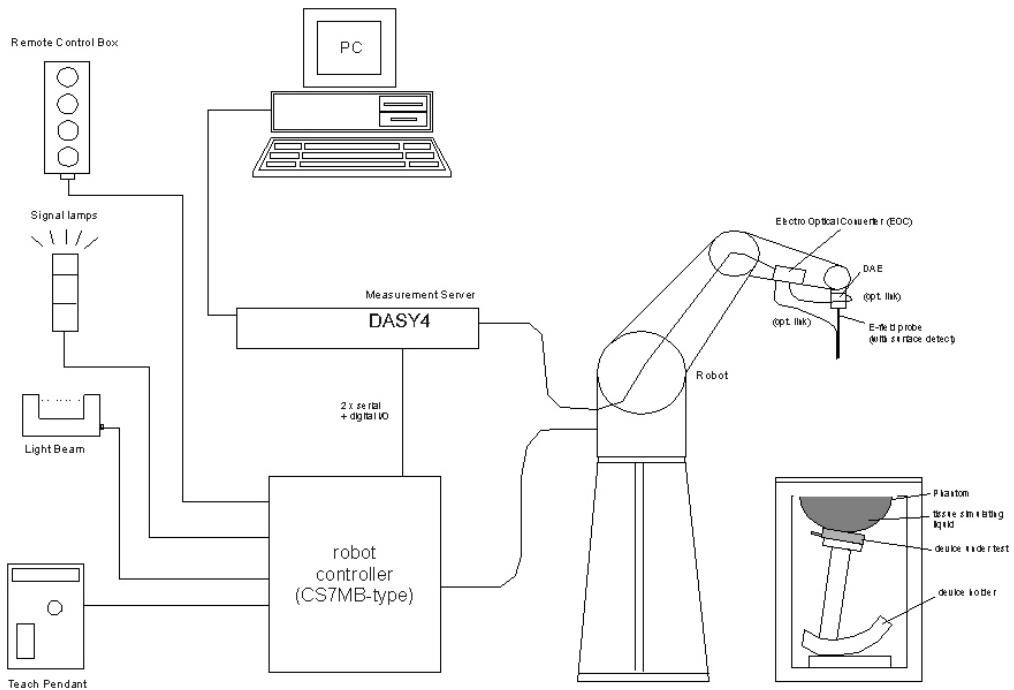
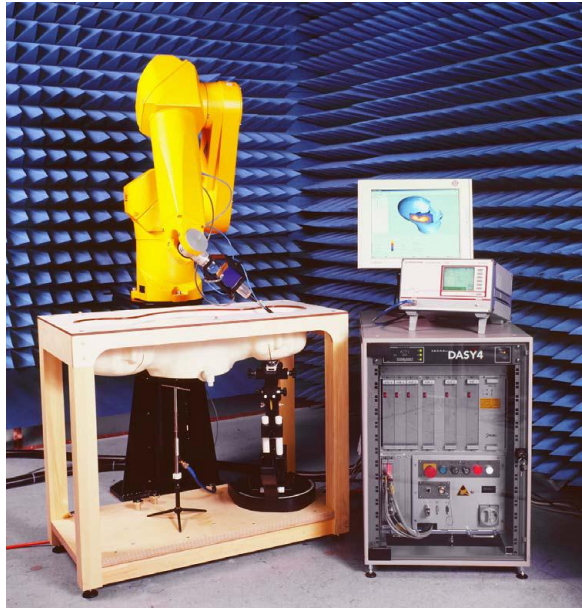


Figure 13: DASY4 exposure system and schematic of components

3.2.2.2 Skulls

Two commercially purchased plastic replica skulls were used for testing of morphological differences (full purchasing information is provided in Appendix A). Skull A is a replica of an adult African male skull; Skull B is of 5-year-old Caucasian child's skull, sex unknown. It was not possible to acquire real human skulls due to restrictions on trading in human parts, and skulls of other animals are

morphologically different. Although the dielectric properties of skull tissue are different to that of plastic (see Section 3.6 for more information regarding dielectric properties of human tissue), using the replicas in a model with other 'tissues' provided a pattern of high conductivity – low conductivity – high conductivity (from superior to deeper tissues) similar to reality.

Skulls came with a cut calvarium and/or metal clips. All metal parts were removed to minimise interference. Where necessary, 'hot glue' (hot melt adhesive) or sculptor's clay was used to secure mandible and/or calvarium to skull. An opening into the brain cavity was made in each skull by removing a piece of cranium along the saggital plane, to allow access into brain cavity by the measurement probe, see Figure 14.

3.2.2.3 Trial run at EMCT

A trial run was performed in Melbourne, Australia at a SAR compliance testing laboratory at EMC Technologies, using DASY4 setup. Adult skull was positioned inside the flat part of SAM phantom, in homogeneous average head liquid (see Figure 14). For detailed explanations and procedures of compliance SAR testing, please refer to the IEEE recommended practice guide for SAR measurement techniques (IEEE 2003).



Figure 14: Initial tests using adult skull in flat part of SAM phantom at EMC Technologies, Melbourne, Australia

SAR results are not included as they do not provide useful information pertaining to the aims of this thesis. The purpose of the exercise was to become familiar with the

peculiarities of the physical setup, and the software packages that control the robot and estimate SAR.

3.2.2.4 Phantoms

Two custom-made 'shell' phantoms resembling human heads were constructed (see Figure 15). A full protocol is provided in Appendix B: Creating shell phantoms. Before embarking on the phantom creation task, a literature review was undertaken to get a sense of how to reconstruct faces from skulls (Adeloye, Kattan et al. 1975; Ingerslev and Solow 1975; Siervogel, Roche et al. 1982; Stephan 2002; Stephan 2003; Swan and Stephan 2005), and several maxillofacial and forensic facial reconstruction experts were consulted for informal advice. In brief, artist's clay was used to create head casts by building up human 'faces' on the skulls. Placement of the facial features was dictated by skull anatomy; dimensions were appropriate to the age and ethnicity of the skull. The 'faces' were used to create moulds (negative impressions) using fast-set silicon. Fibreglass sheets were laid inside the mould and electrically inert epoxy resin was 'painted' on to create the shell phantoms and allowed to dry hard.

A support frame was made for each phantom, by cutting a hole just large enough to for the phantom to fit through in a wooden plywood sheet.

The thickness of the shell phantom varies from 2 mm to 5 mm. Thickness was minimised in order to reduce separation of the 'head' from the exposure source, however overly thin shells were found to leak.

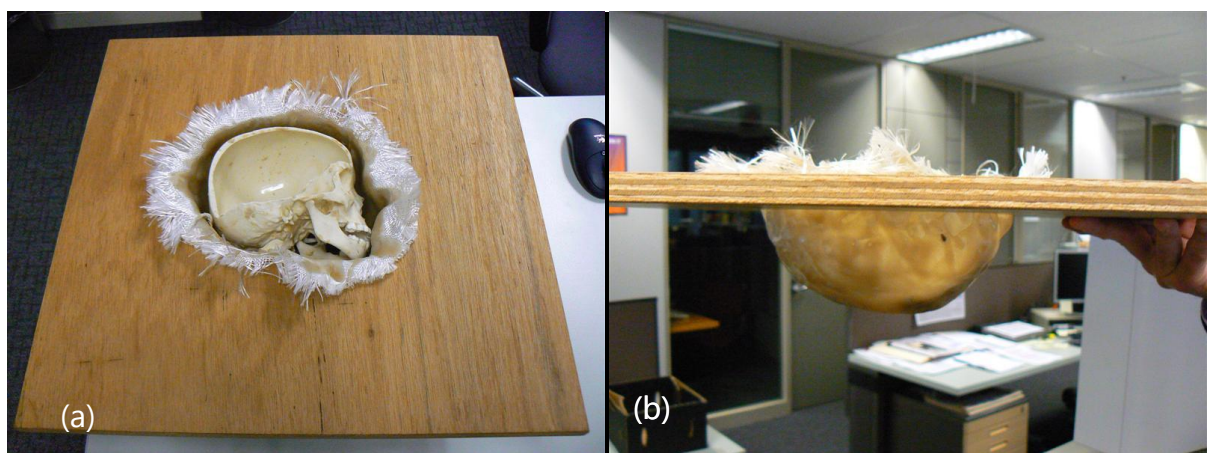


Figure 15: Shell phantoms with wooden support frame holding a skull, (a) top and (b) side (right) views.

3.2.2.5 Tissue simulating Liquids

Tissue simulating liquids were chosen here because they are malleable, relatively stable in their dielectric properties, and can be easily and cheaply mixed up.

Two kinds of liquids were used. The brain and 'average head' was simulated using a detergent based liquid. Hartsgrove liquids (Hartsgrove 1982) were used for all other tissues. Brain cavity was sealed from other liquids using a thin layer of artist's clay.

3.2.2.5.1 Detergent-based tissue simulating liquids

As these liquids are used for standards compliance testing, detergent based tissue-simulating liquids were available in the laboratory in large quantities. Protocols for mixing are available in measurement standards (IEEE 2005). 'Average head' detergent-based liquid was used in homogeneous tests. In multi-tissue models, 'average brain' liquid was used in brain cavity.

3.2.2.5.2 Hartsgrove liquids

Hartsgrove liquids (Hartsgrove 1982) are supersaturated deionised water solutions of sugar and salt. Salt increases conductivity, while sugar decreases permittivity and raises conductivity (though less so than salt) (Speag 2008). Hydroxyethylcellulose (HEC) sold under the brand name Natrosol©, a non-ionic water soluble polymer derived from cellulose, is added as a gelling agent. Bactericide is also added to keep the liquids foul-free.

The original formulae developed by Hartsgrove in 1982 (Hartsgrove 1982) only provide weights used for simulating muscle tissues. The formulae used for ingredient percentages in this study are line of best fit equations developed by Telstra Research Laboratories, based on extensive experimental data. Quantities used are provided in Appendix C. To create liquids, deionised water was warmed to 60° Celsius while required quantities of salt and sugar were stirred in until a clear solution formed. HEC and bactericide were added last, once dielectric properties were established to be correct, as these have a negligible effect on dielectric properties. Densities of tissues were not recorded as these have no influence on the field distribution in a phantom.

Points to note:

- Hartsgrove liquid recipes call for HEC at 0.5% concentration; for tissues that needed high viscosity, e.g. fat and eyes, this was increased to up to 10%, depending on resultant needs
- a high percentage of HEC causes the mixture to become grainy and almost solid to the touch; this renders it difficult to measure dielectric properties (see Figure 16)
- ϵ and σ of liquids drop with increased temperature and humidity
- water evaporation over time reduces ϵ and σ ; tissues were made no more than 2 days in advance, left in covered containers where possible, and dielectric properties measured immediately before construction of models
- of all ingredients, salt affects dielectric properties the most; if values were too high, water content was increased slightly, however this was not possible for thick mixtures
- food dye was occasionally added to differentiate tissues; some dyes were found to increase conductivity slightly; this was compensated for by the addition of a little extra water
- HEC can increase conductivity a little at high concentrations, this was compensated for with the addition of a little extra water

Resultant dielectric properties of high water content tissue equivalent liquids were found to be within 15% of expected value in most cases. Low water content 'tissues' were often well outside that range. This was not of great consequence here, as the aim of the exercise was to test how well GH predicts SAR in a physical model, and the dielectric parameters of the GH tissues were altered to match.

3.2.2.5.3 Other tissue equivalent options

Other tissue simulating options were considered but were deemed unsuitable, or were unavailable.

- Guy's recipe (Guy 1971) of TX-150 (a gelling agent), polyethylene powder, water and sodium chloride (NaCl) does not yield a useable low-water-content tissue simulant (Lagendijk and Nilsson 1985)

- oil-in-gelatine dispersions as proposed by Lazebnik et al (Lazebnik, Madsen et al. 2005) were deemed unnecessarily expensive when compared with other options
- carbon loaded silicon layers, where the carbon content determines the dielectric properties (Gabriel 2007), was considered viable for using as an outer layer between the skull and the phantom, or even moulded to resemble a skull and its outer layers; unfortunately these could not be sourced in time for testing



Figure 16: High concentration of gelling agent makes for a grainy texture; dielectric properties are difficult to measure. Food dye was added to differentiate tissues.

3.2.2.6 Measuring dielectric properties

Dielectric properties of liquids and were measured using a procedure outlined in the IEEE measurement standard (IEEE 2003). A listing of the equipment used in tests and exposure setup is provided at the start of this section. Three measurements were taken and the average used in each case.

Dielectric property measurement involves sending a RF signal (at the frequency of SAR testing) through the material, and measuring the reflection coefficient. Before each measurement, the probe was calibrated by measuring free space, deionised water, and a shorting block. This establishes the loss through the connecting coaxial cable and probe, by testing against the loss seen during measurement of known reflectors and absorbers.

A wide-diameter flask was used for measurements (100 mm or wider), with a liquid depth of at least 60 mm in flask. This allowed enough liquid in the flask for the signal to travel through the material being tested and return a reflection coefficient from the liquid, not air or the container material.

When measuring, the probe was slowly and carefully inserted into liquid at a 45 degree angle to the horizontal, to ensure a uniform amount of liquid covered the entire probe. Care was taken to remove any air bubbles or foreign matter as these would interfere with the measurement. Three readings were taken and averaged to obtain permittivity and conductivity values. The probe was wiped clean with a wet cloth between readings; a small amount of detergent was used to remove highly viscous liquids.

Hot glue, artist's clay and acrylic plastics such as the ones used in the manufacturing of the replica skulls are electrically inert, and have similar dielectric properties to air. In the analogous models, dielectric properties of skull tissue was set to that of air ($\epsilon = 1$, $\sigma = 0$).

3.2.2.7 Exposure source

A D900V2 dipole antenna and dipole position system supplied with DASY4 was used as the RF source (Speag 2008). The dipole physical dimensions are length of 148.5 mm, diameter 3.6 mm, with 15 mm spacer at the centre.

When adding the dipole into the computational FEKO model, the physical dimensions were closely approximated, while attempting to achieve ideal dipole impedance of $Z = 75 + j0 \Omega$. Closest approximation was found to be length of 154.5 mm, diameter 3.6 mm, and impedance of $Z = 74.1 - j0.03 \Omega$.

A schematic for the exposure setup used in all SAR tests in this study is shown below in 900 MHz signal at 250 mW power passed from the signal generator into an amplifier, then an RF coupler. Before each test, the reflection coefficients of the coupler ('B' in Figure 17) and the cable ('C' in Figure 17) were measured. Together with the coupling factor of the RF coupler ('A' in Figure 17, a constant), these gave the total reflected power, which was subtracted from the output power to give the total power delivered to the dipole.

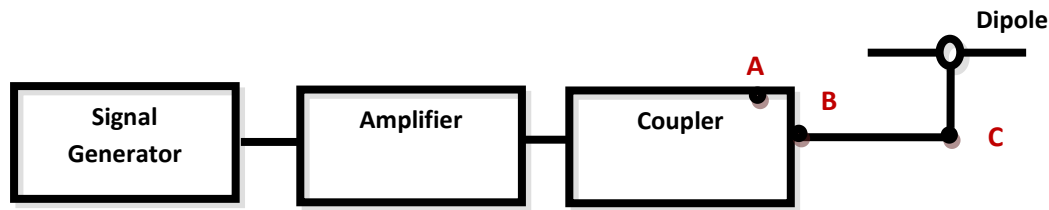


Figure 17: Exposure setup for SAR tests used in this study. $P_{\text{reflected}} = P_A$ (coupling factor) + P_B (measured reflection coefficient) + P_C (reflection coefficient through cable).

When testing phones (or other devices that run on batteries), it is standard to measure the power in an arbitrarily chosen point, e.g. above the antenna, before and after a SAR test, to check for power drift in the battery. This was not necessary here because a dipole with a well defined, non-drifting power source was used.

Power density in analogous computational models matches that of the physical models.

3.2.2.8 Dipole positioning

The centre of the dipole was positioned according to the IEEE SAR measurement standard (IEEE 2003), which specifies the antenna feed point be flush against the Ear Canal Reference Point (ERP). ERP is found by drawing a line passing through the ear canal and the mouth, and positioning the ERP 15 mm away from the ear canal towards the mouth – see Figure 19a.

ERP was clearly marked on both phantoms, and dipole positioned accordingly (Figure 19b). The dipole rotation angle was calculated using Pythagoras's Theorem to be 49.19° for Skull A and 48.19° for Skull B (where 0° is a line in the saggital plane). Dipoles were aligned in the 'tilt' rather than 'cheek' position – see Figure 18.

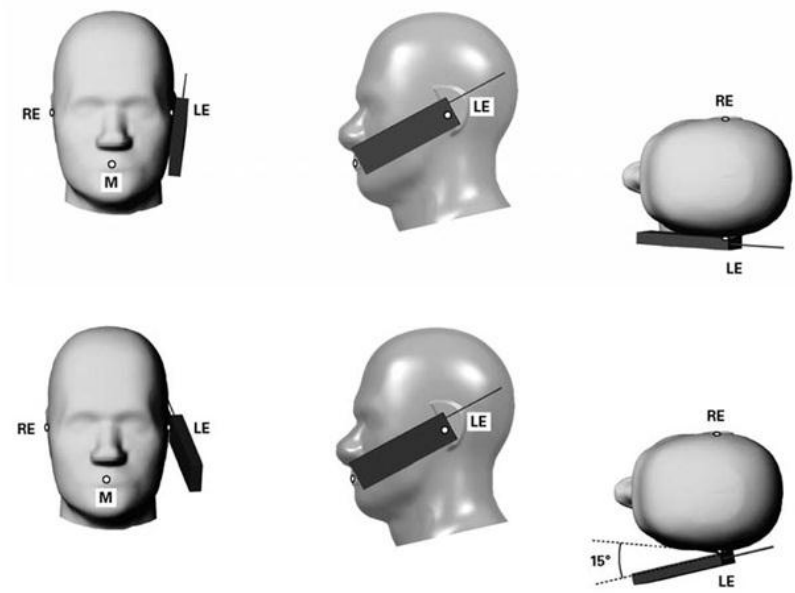


Figure 18: 'cheek' (above) and 'tilt' positions as shown on SAM phantom (image adapted from (IEEE 2003))

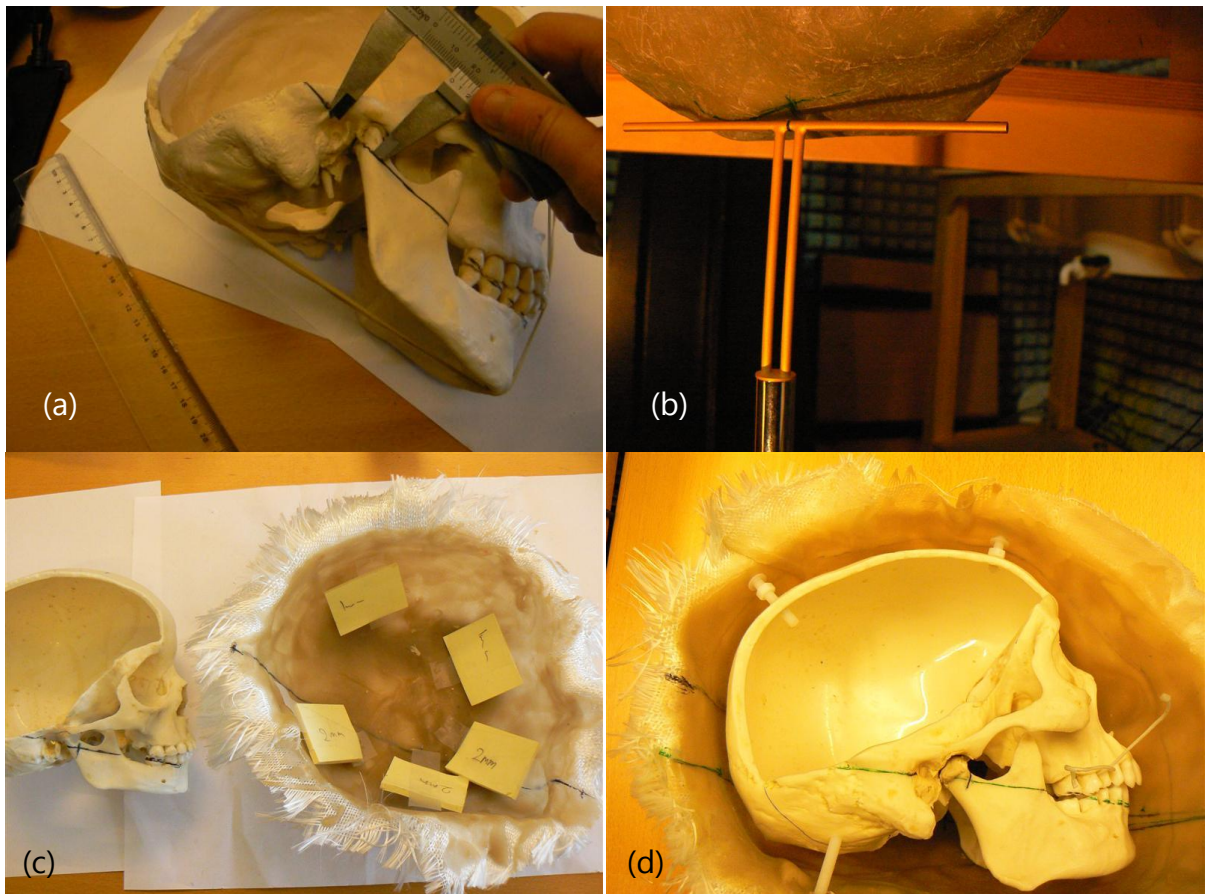


Figure 19: (a) establishing the Ear Canal Reference Point (ERP) on the skull; (b) Dipole was positioned with antenna feed point flush against the ERP, marked on the shell phantoms (c) 1 mm and 2 mm spacers between the skull and phantom; (d) skull is attached to shell using plastic screws to minimise electromagnetic interference

3.2.2.9 Constructing the physical models

To create a skin and muscle layer between the skull and phantom of consistent thickness, the skulls needed to be positioned at a fixed distance from the shell. This was achieved by placing appropriately placed 1 mm and 2 mm spacers inside the shell (Figure 19c), carefully locating the skull relative to facial features of the phantom, and attaching the skull to the shell using nylon (polyamide) screws (Figure 19d). Efforts were made to ensure all objects used in model construction were electromagnetically neutral. In cases where this was not possible, for example where clamps were used to attach frames, metal objects were kept at least 300 mm away from source and probe. Section 3.2.4 below lists the set of models constructed and tested.

3.2.2.10 Defining the measurement space

One of the implications of using non-standard models was the absence of a CAD schematic of the physical space, which could be uploaded to SEMCAD software for robot positioning: there was no pre-defined way to 'tell' the robot where to measure.

A workaround was used to overcome this limitation. Surface testing using probe positioning was used to 'teach' the robot various reference points, which were used to assign the phantom space and measurement regions.

Three reference points on the wooden support frames (visible in Figure 20a and c), plus an assigned depth value of 850 mm, 'told' the robot that measurement space was a rectangular box phantom. Overlapping two-dimensional regions were defined within the brain cavity (DASY software 'plane scans'), and the third dimension of depth was added for volume scanning ('volume scans').

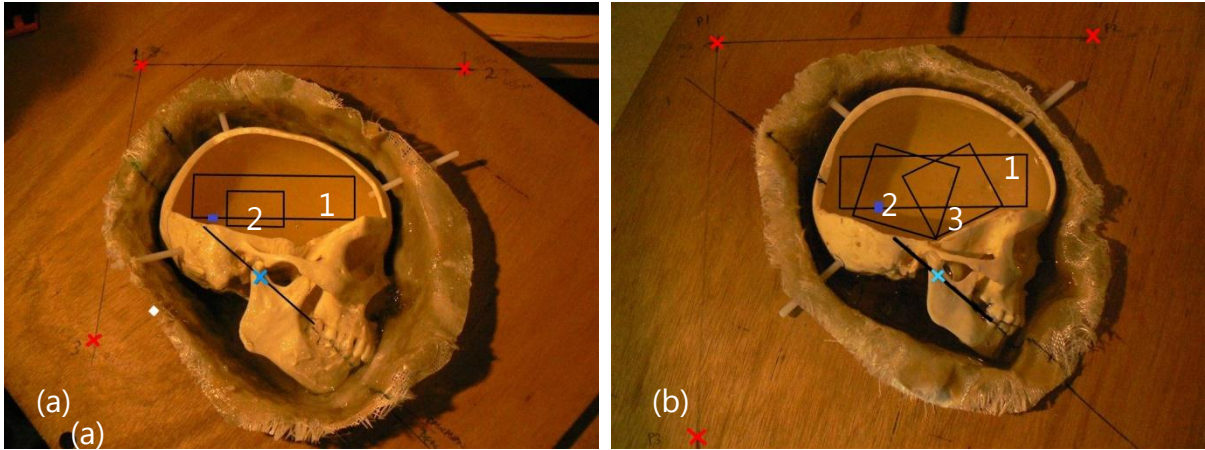


Figure 20: Defining measurement regions within (a) adult phantom and (b) child phantom. Measurement planes are marked and numbered. The three red crosses on each image identify the reference points used to 'teach' the robot the location of the measurement space. The blue cross in each image denotes position of the Ear Reference Point, the ERP was marked on the outside of the shell and the dipole was positioned against it. The blue rectangle in the brain area represents the point of comparison for physical and computational models, see Section 3.1.5.

Area scan regions measured are 50×82 (Region 1) and 30×50 mm (Region 2) in the adult phantom, and 30×70 , 40×40 and 40×40 mm (Regions 1, 2 and 3 respectively) in the child phantom. A third dimension of 30 mm depth, contralateral to the dipole, was added for the volume scans.

DASY probes have the ability to use optical surface testing, however the reflectivity of the surfaces of the skull was not known and the probe could not be effectively calibrated for such conditions. Once planes were defined, the robot 'learned' the inner surface of the skull for the area scan, see Figure 21.

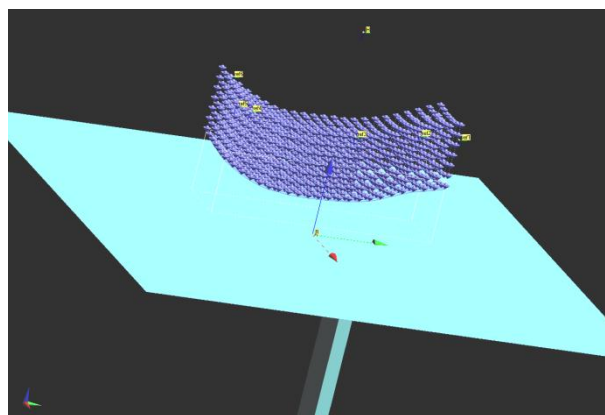


Figure 21: Measurement points used by the probe for a volume scan within adult skull. The skull surface was 'learned' by the robot for a plane, then extended contralateral to the dipole for 30 mm to obtain volume scan area.

It was possible to take field measurements inside the shell phantoms immediately next to the source while the phantoms did not contain a skull, i.e. during the entirely

homogeneous tests. However, to minimise uncertainty and maximise comparability, the measurement areas used in all model runs of the same phantom were identical, whether skulls were present or not. It may also have been possible to 'teach' the robot the entire inner surface of the phantoms (without the skulls) and use this information in conducting homogeneous tests to establish the location of 1g and 10g peak SARs in entire phantom, not just the brain. However, such resources were not available.

3.2.2.11 *1g and 10g volume cubes*

1g and 10g peak spatial SAR were calculated using SEMCAD software. This function uses a finer grid for measuring E-field over a cube of 30 mm³ volume, of dimensions 7×7×7 points. A minimum of 6 points are used for an area scan, and a minimum of 10 points for a volume scan. The volume required by the software for 1g and 10g peak SAR averages must be within 5% of the required mass, contain no more than 10% air, and must not contain any surface boundaries. If those three conditions are not met, and an appropriate cube cannot be found, the software uses an inverse polynomial approximation algorithm for spatial peak averaged SAR calculations (Speag 2008). For extrapolation calculations, the distance between the probe centre and the phantom surface was set to 5 mm.

At certain times, the required scan area contained points inaccessible to the probe due to the shape of the skull. In such cases, the scan area was shifted by the minimum distance necessary to allow the largest possible volume scan around the max SAR point. When doing a zoom scan, the measurement grid is automatically refined by a factor of 10. Values between points are interpolated by the software. To find maxima, the software uses a linear search; interpolated values and values above or below 2 dB of the global maxima are not included.

3.2.3 **Analogous models**

The physical models were replicated computationally using the Geometry Head model initially described in Section 3.1, with sizes and dielectric properties of tissues were adjusted to resemble the physical models as much as possible, including the addition of a dipole antenna. Further detail is provided in the following sections.

3.2.4 Details of physical and computational models

Further details of models and SAR tests are provided below. Radiated power of computational model dipoles was matched to the radiated power in the physical models. All 'tissues' named below are tissue simulating liquids as described in Section 3.2.2.5.

Adult phantom homogeneous			
<u>Physical model</u>		<u>Analogous GH model</u>	
Forward Power	= 24.05 dBm = 254.01 mW	Tissue	ε σ (S/m)
Return power	= 2.27 dBm = 1.69 mW	Brain	40.3 0.95
Radiated power	= 254.01 – 1.69 = 252.41mW	Eye	40.3 0.95
Temperature	22.5° C	Fat	40.3 0.95
Humidity	47.2%	Filler	40.3 0.95
		Skin	40.3 0.95
		Skull	40.3 0.95
Tissue	ε σ (S/m)		
Average head	40.3 0.95		
Protocol:			
<ul style="list-style-type: none"> 'average head' liquid was poured into phantom to a depth of 130 mm 			

Adult phantom homogeneous with skull			
<u>Physical model</u>		<u>Analogous GH model</u>	
Forward Power	= 24.05 dBm = 254.01 mW	Tissue	ε σ (S/m)
Return power	= 3.79 dBm = 2.39 mW	Brain	40.3 0.95
Radiated power	= 254.01 - 2.39 = 251.70 mW	Eye	40.3 0.95
Temperature (ambient)	21.5 ° C	Fat	40.3 0.95
Humidity	50.8 %	Filler	40.3 0.95
		Skin	40.3 40.3
		Skull	0 1
Tissue	ε σ (S/m)		
Average head	40.3 0.95		
Protocol:			
<ul style="list-style-type: none"> any clay blocking cavities within the head (e.g. orbital, nasal) was removed skull was secured in position using nylon screws 'average head' liquid was poured into the space between skull and phantom until all cavities were filled; care was taken not to create bubbles more 'average head' liquid was poured into skull cavity to a depth of 70 – 80 mm 			

Child phantom homogeneous			
<u>Physical model</u>		<u>Analogous GH model</u>	
Forward Power	= 24.01 dBm = 251.77 mW	Tissue	ε σ (S/m)
Return power	= 9.62 dBm = 9.16 mW	Brain	39.6 0.93
Radiated power	= 251.77 – 9.16 = 242.61 mW	Eye	39.6 0.93
Temperature	21.1° C	Fat	39.6 0.93

Child phantom homogeneous				
Humidity	35.5%		Filler	39.6 0.93
			Skin	39.6 0.93
			Skull	39.6 0.93
Tissue	ϵ	σ (S/m)		
Average head	39.6	0.93		
Protocol:				
<ul style="list-style-type: none"> 'average head' liquid was poured into phantom to a depth of 130 mm and left to settle for 30 minutes before testing 				

Child phantom homogeneous with skull				
<u>Physical model</u>			<u>Analogous GH model</u>	
Forward Power	= 24.01 dBm = 251.77 mW		Tissue	ϵ σ (S/m)
Return power	= 10.20 dBm = 10.47 mW		Brain	39.6 0.93
Radiated power	= 251.77 - 10.47 = 241.30 mW		Eye	39.6 0.93
Temperature	21.9 °C		Fat	39.6 0.93
Humidity	35.5%		Filler	39.6 0.93
			Skin	39.6 0.93
			Skull	0 1
Tissue	ϵ	σ (S/m)		
Average head	39.6	0.93		
Protocol:				
<ul style="list-style-type: none"> any clay blocking cavities within the head (e.g. orbital, nasal) was removed skull was secured in position using nylon screws 'average head' liquid was poured into the space between skull and phantom until all cavities were filled; care was taken not to create bubbles more 'average head' liquid was poured into skull cavity to a depth of 70 – 80 mm and left to settle for 30 minutes before testing 				

Adult phantom heterogeneous without eyes				
<u>Physical model</u>			<u>Analogous GH model</u>	
Forward Power	= 24.01 dBm = 251.77 mW		Tissue	ϵ σ (S/m)
Return power	= 3.49 dBm = 2.23 mW		Brain	42.3 0.82
Radiated power	= 251.77 - 2.23 = 249.54 mW		Eye [□]	38.8 0.92
Temperature	22.2 °C		Fat	6.8 1.0
Humidity	32.4%		Filler [¥]	33.7 0.96
			Skin	36.7 0.75
			Skull	1 0
Tissue	ϵ	σ (S/m)		
Average head	38.8	0.92		
Skin	36.7	0.75		
Fat	6.8	1.0		
Muscle	50.0	0.95		
Brain	42.3	0.82		
Protocol:				
<ul style="list-style-type: none"> inside of the shell phantom was covered with 'skin' tissue 				

Adult phantom heterogeneous without eyes

- 'fat' was applied to front part of the 'face': cheeks, maxilla, orbital cavities, mouth
- 'muscle' was smeared everywhere except the calvarium, also liberally applied under mandible, inside zygomatic arch and inside nose cavity
- the skull was attached inside the shell using the nylon screws
- 'brain' liquid was added inside brain cavity to a depth of 70 – 80 mm
- normal viscosity 'average head' liquid was poured into the gap between the skull and the shell, to fill in any air bubbles and fill the orbital cavities, and left for 30 minutes to settle

▫ highly gelled 'average head' liquid was used instead of eyes

¥ 'filler' tissue dielectric properties were calculated using a weighted average of the tissues used in the physical model: 40% 'muscle', 30% 'fat', 30% 'average head'

Adult phantom heterogeneous with eyes

Physical model

Forward Power	= 24.06 dBm = 254.68 mW
Return power	= 11.19 dBm = 13.15 mW
Radiated power	= 254.68 - 13.15 = 241.53 mW
Temperature	21.4 ° C
Humidity	42.4%

Analogous GH model

Tissue	ε	σ (S/m)
Brain	46.6	0.82
Eye	42.8	0.92
Fat	23.6	0.51
Filler ¥	42.5	0.83
Skin	36.7	0.75
Skull	1	0

Tissue	ε	σ (S/m)
Average head	38.7	0.92
Skin	36.7	0.75
Fat	23.6	0.51
Muscle	52.6	0.98
Brain	46.6	0.82
Eye	42.8	1.25

Protocol:

- inside of the shell phantom was covered with 'skin' tissue
- 'fat' was applied around the front part of the face: cheeks, eyes and mouth
- 'muscle' was smeared everywhere except the calvarium, also liberally applied under mandible, inside zygomatic arch and inside nose cavity
- 'fat' was smeared inside orbital cavities to a depth of up to 2 mm, and two approximately spherical balls of 30 mm diameter were rolled by hand and carefully inserted into eye cavities
- the skull was attached inside the shell using the nylon screws
- 'brain' liquid was added inside brain cavity to a depth of 70 – 80 mm
- normal viscosity 'average head' liquid was poured into the gap between the skull and the shell, to fill in any air bubbles, and left for 30 minutes to settle

¥ 'filler' tissue dielectric properties were calculated using a weighted average of the tissues used in the physical model: 60% muscle, 30% fat, 10% average head.

Child phantom heterogeneous

Physical model

Forward Power	= 24.04 dBm = 253.51 mW
Return power	= 11.69 dBm = 14.76 mW
Radiated power	= 253.51 - 14.76 = 238.75 mW
Temperature	21.5 ° C
Humidity	40.0%

Analogous GH model

Tissue	ε	σ (S/m)
Brain	45.3	0.83
Eye	42.4	1.24
Fat	17.5	0.38
Filler ¥	35.4	0.70

Child phantom heterogeneous					
Tissue	ϵ	σ (S/m)	Skin	36.7	0.75
Average head	38.7	0.92	Skull	1	0
Skin	36.7	0.75			
Fat	17.5	0.38			
Muscle	52.6	0.98			
Brain	45.3	0.83			
Eye	42.4	1.24			

Protocol:

- a thin skin layer was applied inside the shell
- 'fat' was applied at anterior part of face, under the chin
- thin layer of 'muscle' was applied everywhere except inside the cut calvarium, also liberally applied inside the zygomatic arch and under the mandible
- 'fat' was smeared inside eye cavities
- extra 'fat' was added around cheek pad, as appropriate for child anatomy
- extra 'muscle' was added at zygomatic arch
- 'eyes' of weight 18.05 ± 1 grams were made by hand, approximately spherical, and inserted into eye cavities
- skull was screwed into place
- the entire model was left for several hours to settle
- the top 'eye' leaked a little due to gravitational effects, the gelatinous liquid was moved back into place by hand
- average head liquid was poured into the gap between the skull and phantom and left to settle for an hour
- 'brain' liquid was added inside the skull cavity

¥ 'filler' tissue dielectric properties were calculated using a weighted average of the tissues used in the physical model: 45% 'fat', 45% 'muscle', 10% 'average head'

3.2.5 Results and discussion

3.2.5.1 Single point SAR comparison

A point was chosen for direct comparison between physical and computational models, shown as blue rectangle in Figure 20 for the physical models and in the Figure 22 in computational models. Location was chosen to provide a high SAR value; point is in the brain region against the skull, medially from the dipole antenna. Values of SAR in both models at the comparison point are shown in Table 4 and Figure 23. The comparison point was no more than 20 mm from the location of 1g and 10g SAR cubes in any direction the computational models.

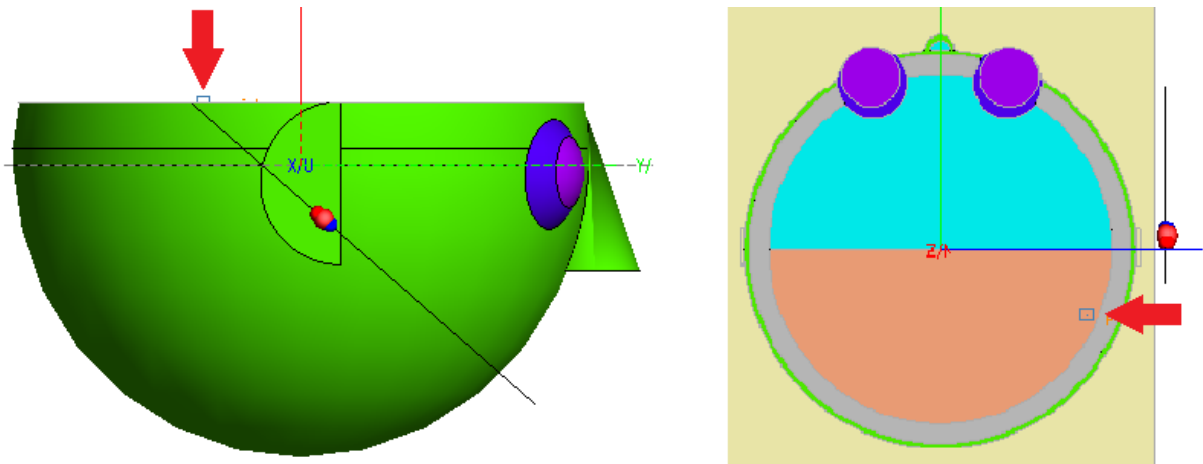


Figure 22: Comparison point used in computational models, shown in side and top view of the adult model

Table 4: Single point SAR comparisons between physical and computational models

	Adult homog	Adult homog with skull	Adult hetero with eyes	Adult hetero without eyes	Child homog	Child homog with skull	Child hetero
Computational	0.23	0.51	0.44	0.47	0.43	0.51	0.46
Physical	0.40	0.22	0.18	0.20	0.58	0.32	0.30

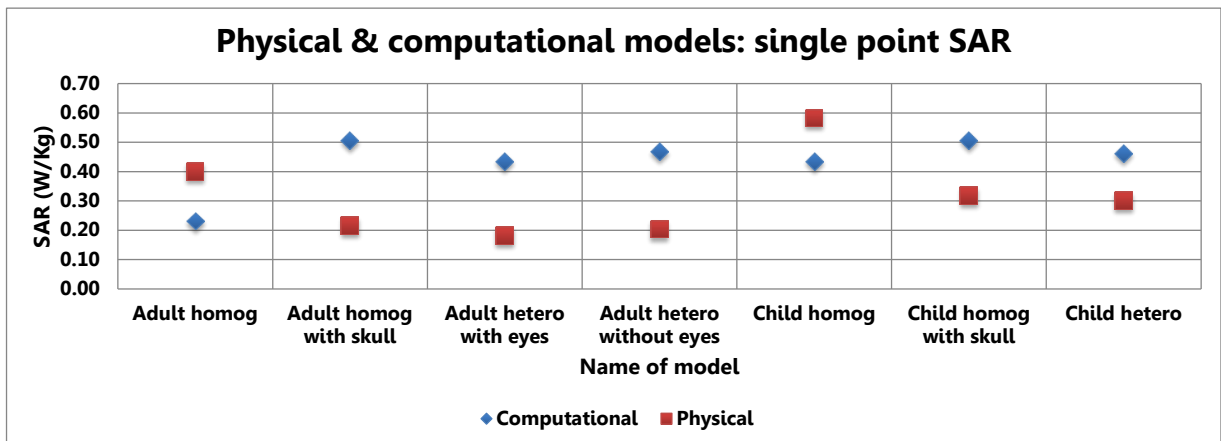


Figure 23: Single point SAR comparison in the physical and computational models

SAR in the child models varies by about 35% at the comparison point, and by about 57% for all the non-homogeneous adult models. Interestingly, computational GH models overestimate SAR in the non-homogeneous models, but underestimate it by about 30% for homogeneous ones, contradicting previous results (Gandhi, Gianluca et al. 1996; Hombach, Meier et al. 1996; Meier, Hombach et al. 1997) suggesting that a homogeneous model provides a more conservative estimate.

Please refer to Section 4.3.2 for an analysis of the uncertainties in this modelling work, both computational and physical. Safety guidelines consider variation up to $\pm 30\%$ between measured and numerically analysed results to be acceptable (ARPANSA 2002; IEEE 2003), which this work adheres to. The comparatively high level of uncertainty in the dielectric properties of the tissue-simulating liquids, and the human error introduced when creating the models, is likely the cause of the extra level of difference between what's seen here. As outlined in Section 4.3.2, every effort has been made to minimise human error, and its contribution to errors is considered minimal here, however it cannot be discounted. Human error cannot be quantified but is estimated to be no more than a 20% contributor to the uncertainty factor.

Note that agreement of computational and physical models is about $\pm 3\text{dB}$ (50% of the magnitude), which is a value treated as acceptable variation by most measurement work (Bassen and Babij 1990; Roach 2009). The consistent patterns across models also suggest that the results are reasonably accurate (correlation analysis was not performed). A similar difference between measured and numerical predictions is seen across models.

3.2.5.2 Averaged SAR

Table 5 and Figure 24, and Table 6 and Figure 25, show 1g and 10g SAR respectively in the brains of physical models, and 1g and 10g SARs in the analogous computational models, both in the entire head and in the brain tissue. 1g and 10g SARs in the original-sized GH model are also included. The discrepancies between SAR predictions in physical and computational models, and the similar pattern seen above in the point SAR comparison follow a pattern which suggests that the computational model predictions are reasonably accurate.

Recall that the measured volumes in the physical models are only a small part of the 'brain', whereas the computational models take into account the entire brain tissue.

Table 5: 1g peak SAR in physical and computational models

1g peak in brain (W/kg) comparison	Adult homog	Adult homog with skull	Adult hetero with eyes	Adult hetero without eyes	Child homog	Child homog with skull	Child hetero	Original (Caucasian adult)
GH brain tissue	0.84	0.98	0.82	0.83	0.92	0.87	0.79	0.30
Physical model	0.65	0.22	0.09	0.18	1.68	0.53	0.41	
GH entire model	2.48	1.20	1.09	1.32	2.26	1.07	0.99	0.36

Table 6: 10g peak SAR in physical and computational models

10g peak in brain (W/kg) comparison	Adult homog	Adult homog with skull	Adult hetero with eyes	Adult hetero without eyes	Child homog	Child homog with skull	Child hetero	Original (Caucasian adult)
GH brain tissue	0.39	0.48	0.42	0.44	0.47	0.48	0.46	0.22
Physical model	0.34	0.14	0.06	0.11	0.88	0.33	0.31	
GH entire model	1.60	0.83	0.77	0.87	1.54	0.76	0.71	0.29

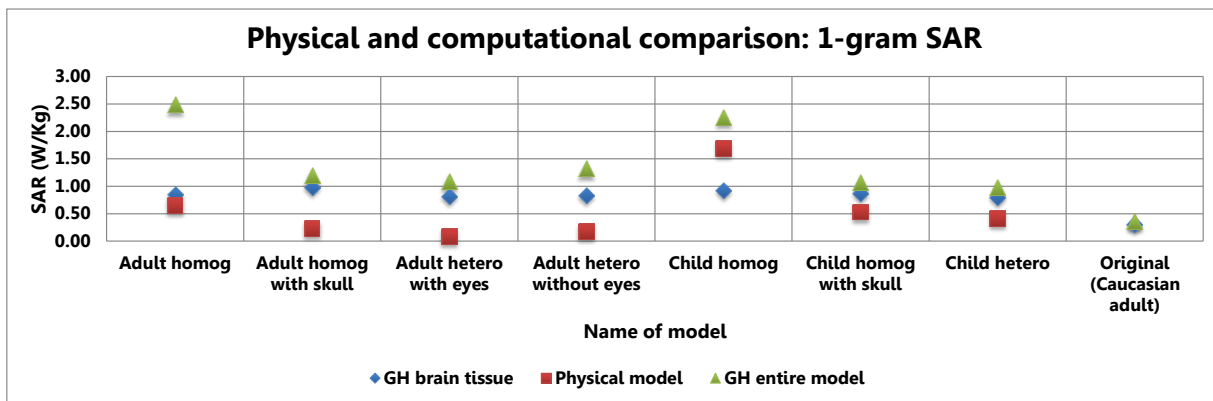


Figure 24: 1g peak spatial SARs in the physical and computational models

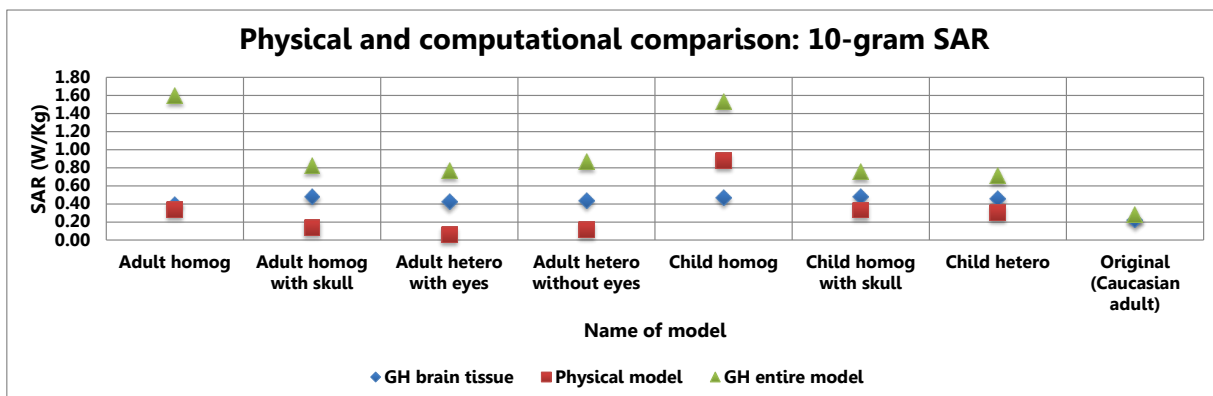


Figure 25: 10g peak spatial SARs in the physical and computational models

Figure 27 shows SAR plots of physical models as extrapolated by DASY4 software from E-field measurements taken in the 'brain' regions shown in Figure 20. The area scans on the left are measurements taken in the plane closest to the dipole. Energy absorption is seen to follow a spherical pattern, decreasing with distance from the source.

It is evident from Figure 20 and Figure 27 that measurements in the physical models were taken in the part of the 'brain' adjacent to the dipole, though location is at least 30 mm away from the feed point. This is consistent with the fact that measured 1g/10g SARs in the brain of physical models are lower than those predicted by GH for the brain tissue, and lower still than the 1g/10g SARs predicted for the entire head (with the exception of the homogenous child head). The regions of highest SAR found in the brain tissue of GH correlate closely to the measured regions within the physical models, see Figure 26 for example of 1g/10g SAR locations. In the physical (and computational) models, some of the 'brain' tissue was closer to the feed point than the measured regions, which explains the discrepancy between 1g/10g GH results in the brain and in the entire head. It is expected that the highest SAR in the physical models occurred in the skin tissue closest to the feed point, though it was not possible to take measurements in that area.

Measured SAR in the heterogeneous adult model with 'eyes' are surprisingly low, about half that of other non-homogeneous adult models. It is possible that an error was made during dipole positioning for that test, causing the source to be too far from the phantom, however the single-point measurements do not support that theory. A repeat of the test was not possible due to time constraints. It is more likely that a large heterogeneous head model using these parameters provides a low averaged SAR value.

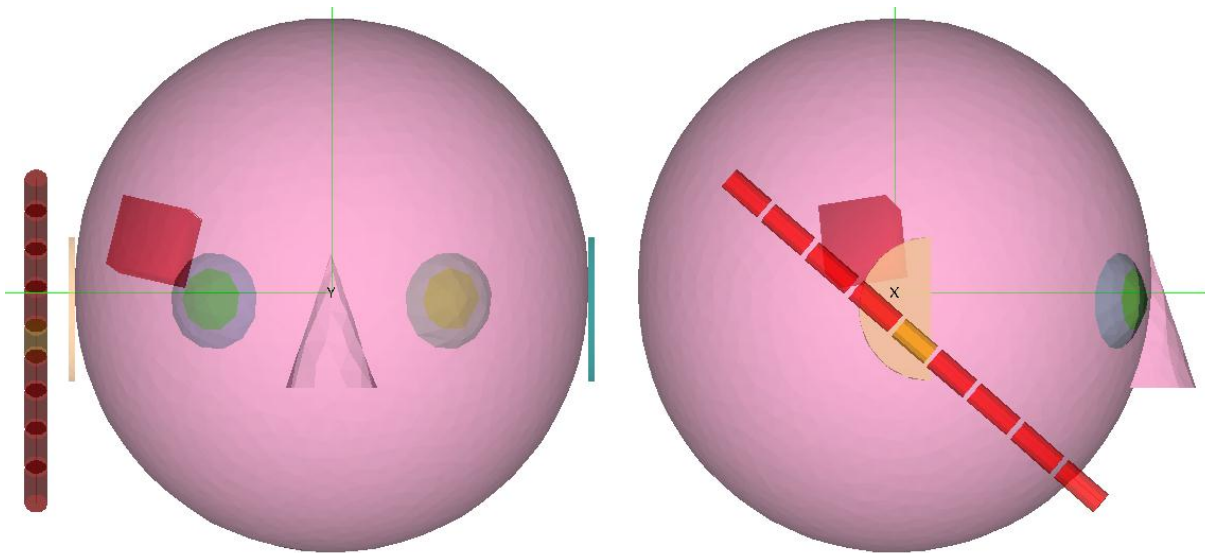


Figure 26: Location of 1g and 10g SAR cubes (10g SAR shown here) in the brain of computational models

Homogeneous models show significantly higher 1g and 10g SAR than heterogeneous models, up to 3 times as much in measured models; this agrees with others' previous work indicating SAM provides conservative results. However, the homogeneous child's head model shows higher SAR than the homogeneous adult one, suggesting that SAM may not provide the worst case result for all anatomic variations, particularly smaller heads.

Lowest 1g/10g SAR predicted by GH is in the adult Caucasian original model; that model has a smaller head than the rest of the ones tested here, again suggesting that SAM may not provide a conservative result for all heads.

In the non-homogeneous models (with the exception of the adult heterogeneous model with 'eyes'), the difference between predicted and measured SAR in the adult heads is in the order 0.35 W/kg; in the child heads, 0.15 W/kg; this consistency lends credence to the results of the validation tests, as well as the viability of the GH model at predicting SAR.

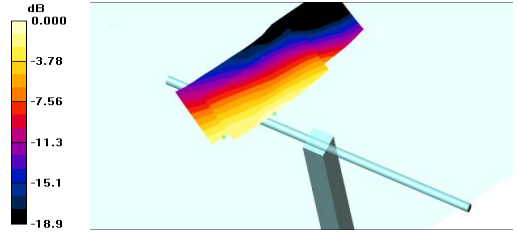
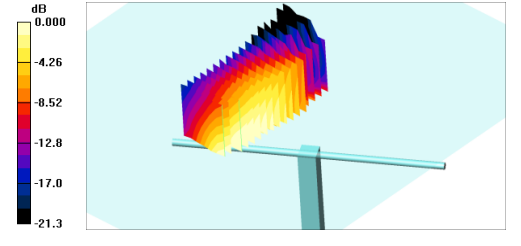
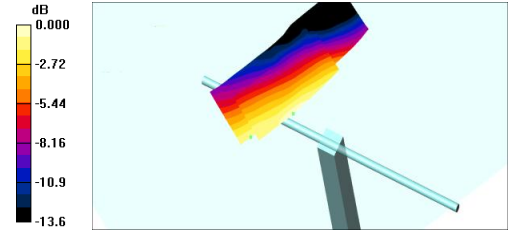
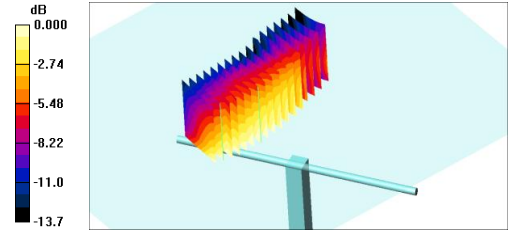
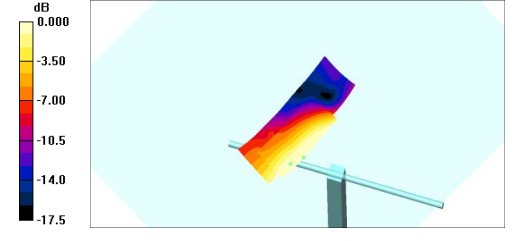
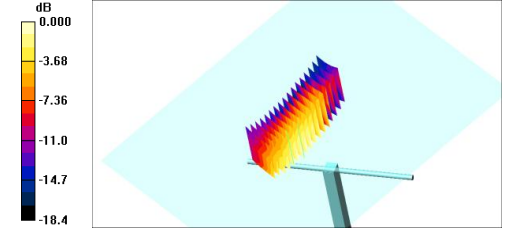
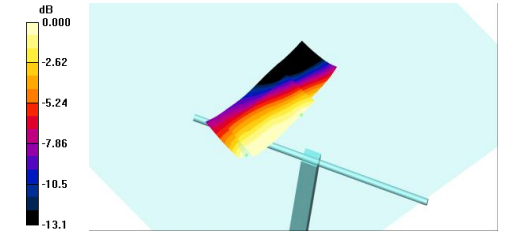
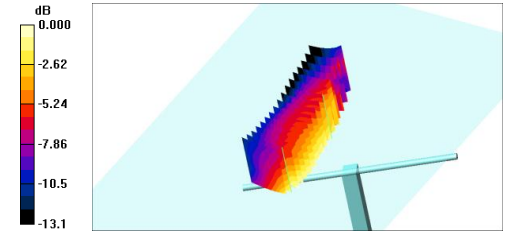
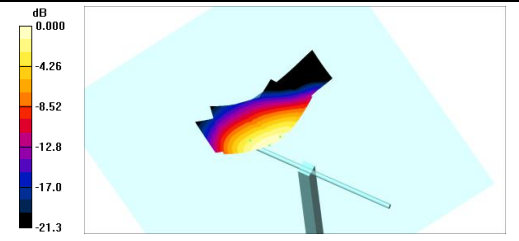
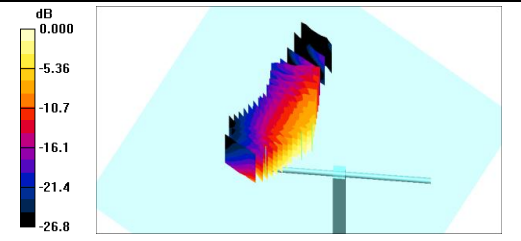
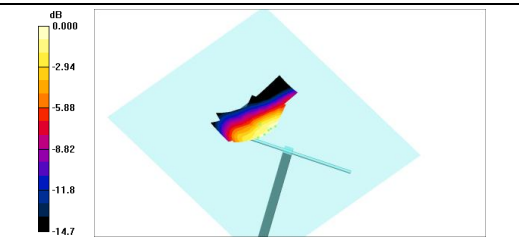
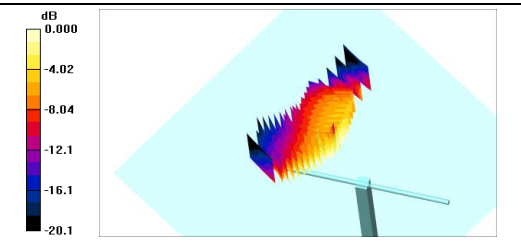
Model	Area	Volume
Adult homog		
Adult homog with skull		
Adult hetero with eyes		
Adult hetero without eyes		
Child homog		
Child homog with skull		
Child hetero	Image not available	Image not available

Figure 27: Area and volume SAR scans of physical models. Locations of measured areas are shown in Figure 20.

Recall again that the 1g and 10g SAR results from physical models are due to averaging of a section of the brain only; whereas the entire brain was averaged to derive 1g and 10g SAR results in computational GH models. It is expected that some variation will be seen. As with the point comparison, patterns across models suggest the results are within a reasonable margin of prediction, indicating the Geometry Head model provides accurate representation of SAR in a physical situation.

3.2.5.3 *Uncertainty of validation study*

For a discussion of the uncertainties of this study please see Section 4.3.2 below.

3.2.6 **Section summary**

- Tissue-equivalent liquids with dielectric properties resembling those of human tissues were used in combination with plastic replica skulls and custom-made phantoms to create several homogeneous and semi-homogeneous physical models of the human head
- Models anatomically resemble the heads of an adult African male and a Caucasian 5-year-old child
- Homogeneous and non-homogeneous models were used for performing SAR tests; exposure source was a dipole antenna radiating at 900 MHz; E-field measurements were taken inside the 'brain' tissue, as close as possible to the antenna feed point and SAR calculated
- Parameters of the Geometry Head model were adjusted to create analogous computational models, mirroring the physical models as closely as possible
- SAR predictions of computational and physical models are reasonably well matched, from which it is inferred that the Geometry Head model is able to accurately predict SAR in human heads

3.3 Cranial thickness

3.3.1 Why this variable is important

As discussed in Chapter 2, radiation decays exponentially as it is attenuated by the lossy dielectric absorbers that comprise the human head. Penetration of the electromagnetic wave at 900 MHz is only of a few centimetres, therefore most of the absorption happens near the surface. Thickness of the skull tissue, a tissue close to the surface of the head, is expected to play a large part in location and maximum values of SAR.

3.3.2 Literature review

Little difference is seen between male and female skulls of children, however in adulthood male skulls tend to be larger and more robust than female skulls, which are lighter and smaller, with a cranial capacity about 10 percent less than that of the male. However, the male body is larger than the female body, which accounts for the larger size of the male skull; proportionally, the male skull is about the same size as the female skull. Male skulls typically have more prominent supra-orbital ridges, a more prominent glabella (the space between the eyebrows and above the nose), and more prominent temporal lines. Female skulls generally have rounder orbits and narrower jaws. On average male skulls have larger, broader palates, squarer orbits and larger sinuses, than those of females. Male mandibles typically have squarer chins and thicker, rougher muscle attachments than female mandibles. Different thicknesses are seen on different points of the skull (Gray 1918).

3.3.2.1 Cranial thickness in human adults

Much disparity exists in literature as to cranial thickness in adults. Most available data was found in anatomy and archaeology texts and peer-reviewed journal papers.

Using sections excised from four cranial locations frontal and parietal regions, Ross et al. (Ross, Jantz et al. 1998) found mean cranial thickness to be between 7.03 mm and 8.97 mm in females and between 6.43 mm and 7.70 mm in males. They also noted that cranial thickness decreases with age in males and increases in females. Conversely, Lynnerup found no correlation between cranial thickness and sex, age or general body build (Lynnerup 2001). These findings are noted to be in agreement with several earlier studies that found little or no correlation. Simms and Neely

(Simms and Neely 1989) studied variability of temporal bone thickness in children aged 0-20 years of age; their findings also indicate no thickness variability between sexes but displayed large differences between age groups. Adult (20 years old) bone thickness was found to be between about 3 and 7 mm. Eshel et al. (Eshel, Witman et al. 1995) noted that cranial asymmetry needs to be taken into account.

Overall, categorising human skulls along delineations such as sex, age or race does not reduce the inter- or intra-category variation in skull thickness. As much variation may be found between, for example, two child skulls, as between a child skull and an adult skull (Anderson 2003). Definitions of 'child' and 'adult' range in the literature from 16, 18 to 21 years old (Anderson 2003).

3.3.2.2 Effect of cranial thickness on RF absorption

This variable has not been systematically explored much in literature, likely due to the difficulty of altering features in existing human models used for dosimetric studies. Heterogeneous models are closely representative of human anatomy, where skull thicknesses (and other features) vary greatly across the model. Homogeneous models obviously do not contain a separate skull tissue. Canonical layered sphere models have used cranial thicknesses ranging from 4.7 mm (Anderson, 2003) to 10 mm (Drossos, Santomaa et al. 2000), usually based on a value taken from literature. Where cranial thickness is varied across simplified models, other variables are too. Literature sources agree that in general, smaller heads absorb more energy than larger heads, but the specific contribution of skull thickness cannot be isolated. This effect is likely due to morphological differences and overall size of the head (Schonborn, Burkhardt et al. 1998). More information regarding effect of head sizes on SAR is found in Section 3.5.

3.3.3 What do we expect to see?

Little data is available regarding effect of cranial thickness on SAR. However, *a priori* reasoning suggests that SAR in the head would increase with decreased skull thickness.

3.3.4 Methodology, results and discussion

3.3.4.1 Variation of human cranial thickness

Information regarding human cranial thickness is readily available, unlike some other anthropometric measures. A literature review was undertaken to establish the 5th, 50th and 95th percentiles of thickness of the skull in human anatomy. In total, 27 literature sources were consulted yielding multiple measurements taken of 3103 skulls. Summary results are provided in Table 7 with full data available in Table 8.

Results were split for sex (female and male), age groups (20-29, 30-39, 40-49, 50-59, 60+ years old), and ethnicity (African, African-American, Australian Aboriginal, Caucasian, Bedouin, Chinese, Japanese, unknown/unspecified) sub-populations. Where more than one of the subpopulation criteria, (age, sex or ethnicity), measurements were placed into the 'Unknown' category (n = 609), so as not to skew the subpopulation percentile values. This category includes measurements of male and female skulls of various ages from Easter Island, Korea, Australia, New Zealand, and North and South America.

The overall 5th, 50th and 95th percentiles of skull thickness in adult humans were found to be 3.70 mm, 6.43 mm and 10.80 mm respectively. These values were rounded to **4 mm, 6 mm and 11 mm** respectively for modelling purposes.

In general, skulls of females (n = 778) were found to be thicker than those of males (n = 1716), with 5th, 50th and 95th percentiles of female skull thickness found to be 4.87, 7.16 and 9.34 mm versus male thicknesses of 3.91, 6.50 and 9.58 mm respectively. Japanese male skulls were the thinnest overall (5th, 50th and 95th percentiles at 4.00, 4.70 and 6.75 mm respectively, n= 105), closely followed by those of Japanese females (4.83, 5.60 and 6.90 mm respectively, n = 47).

The highest variation was seen in skulls of Australian aboriginal males (n=80), with a 5th percentile of 3.97 mm and the 95th at 15.28 mm. Female Australian aboriginal skulls (n = 32) show a similar range at 4.28 mm for the 5th percentile and 12.25 mm for the 95th. The 95th percentile values for male and female Australian aboriginals were also the highest values found.

Percentile values of three sub-populations – African males, African females, and Chinese females – were based on measurements taken of only one or two skulls.

Caucasian male skulls were the most often examined (n = 1308) in the found literature, with Caucasian females a poor second at 541 skulls.

Table 7: Overview of adult cranial thickness in literature (for full information see Table 8). n refers to the number of specimen – often multiple measurements are included of the same skull.

Overall				
	All	Unknown	Male	Female
5th percentile	3.70	3.50	3.91	4.87
50th percentile	6.43	5.60	6.50	7.16
95th percentile	10.80	11.28	9.58	9.34
n	3103	609	1716	778

Subpopulation –Age and/or Sex and/or Ethnicity Unknown	
5th percentile	3.50
50th percentile	5.60
95th percentile	11.28
n	609

Subpopulation - Male							
	Australian Aboriginal	African	African-American	Bedouin	Caucasian	Chinese	Japanese
5th percentile	3.97	6.54	6.10	5.42	3.65	6.07	4.00
50th percentile	7.80	7.94	7.00	5.60	6.39	6.71	4.70
95th percentile	15.28	9.33	9.40	7.67	8.38	7.51	6.75
n	80	2	133	11	1308	77	105

Subpopulation – Female							
	Australian Aboriginal	African	African-American	Bedouin	Caucasian	Chinese	Japanese
5th percentile	4.28	6.97	6.10	5.56	5.59	7.03	4.83
50th percentile	7.35	6.97	7.70	6.10	7.11	7.03	5.60
95th percentile	12.25	6.97	9.40	7.63	9.10	7.03	6.90
n	32	1	144	12	541	1	47

Table 8 Adult cranial thickness in literature (detail)

Ethnicity	Age	Reference	Notes	n	Thickness m	Thickness s.d.	Var
MALE							
Caucasian	20-29	(Adeloye, Kattan et al. 1975)	American	25	7.70	1.70	
					6.50	1.60	
					7.50	1.40	
					5.70	1.40	
		(Ross, Lee et al. 1976)	American, age unknown (17-95)	59	3.52	0.50	
		(Weber and Kim 1999)	European	1	5.37	1.87	
		(Getz 1961)	Norwegian (Sogn), age unknown	57	6.00	0.20	
					7.20	0.10	
					7.20	0.40	
					7.10	0.20	
			Norwegian (Oslo), age 20-59	30	5.80	0.30	
					5.90	0.30	
					6.50	0.20	
					7.00	0.40	
					7.40	0.30	
					7.00	0.60	
					7.10	0.30	
					7.70	0.40	
					7.60	1.10	
			Norwegian (Lapp), age unknown	33	5.60	0.20	
					6.10	0.20	
		(Zvyagin 1975)	Russian, aged 20-86. means of 3 skull tables added.	91	6.06		
					5.18		
					6.96		
					6.47		
					7.11		
					7.39		
					6.38		
					1.20		
	30-39	(Adeloye, Kattan et al. 1975)	American	16	7.10	1.40	
					6.20	1.50	
					8.20	1.30	
					5.90	1.30	

Ethnicity	Age	Reference	Notes	n	Thickness m	Thickness s.d.	Var
		(Todd 1924)	American, age unknown	448	11.26		
					5.75		
					3.56		
		(Todd 1924)	American, age unknown	169	11.80	0.32	
					6.10	0.23	
					6.20	0.15	
					3.70	0.12	
					11.50	0.23	
					6.00	0.16	
					5.80	0.13	
					3.70	0.13	
					11.00	0.26	
					5.70	0.19	
					5.90	0.15	
					3.50	0.97	
					9.80	0.25	
					4.90	0.14	
					5.20	0.10	
					3.10	0.08	
		(Todd 1924)	American, age unknown	167	3.93	0.15	
	40- 49	(Adeloye, Kattan et al. 1975)	American	17	7.50	2.40	
					6.6	1.9	
					7.3	1.5	
					5.6	0.9	
		(Lynnerup 2001)	Danish	43	7.044	1.273	
					7.825	1.657	
					5.04	1.25	
					5.034	1.328	
		(Ross, Jantz et al. 1998)	American, aged 18-86 (45+/-16)	122	6.43	1.43	
					6.57	1.31	
					7.67	1.72	
					7.7	1.82	
		(Weber and Kim 1999)	European	1	4.34	2.14	
	50- 59	(Adeloye, Kattan et al. 1975)	American	9	8.7	1.2	
					7.4	1.7	
					8.1	1.5	
					6.4	1.7	
	60+	(Adeloye, Kattan et al. 1975)	American	10	6.6	1.9	

Ethnicity	Age	Reference	Notes	n	Thickness m	Thickness s.d.	Var
					6.2	1.9	
					6.8	2	
					5.1	1.1	
		(Elahi, Lessard et al. 1997)	Canadian	10	5.43		
					4.72		
					4.87		
					5.19		
					6.89		
					4.77		
					6.57		
					0.74		
					4.58		
					4.87		
					5.73		
					4.23		
					5.84		
					4.81		
					6.43		
					4.65		
					7.15		
					6.5		
					5.13		
					7.61		
					5.69		
					5.9		
					7.72		
					5.34		
					7.16		
					4.73		
					5.78		
					7.07		
					7.66		
					6.44		
					7.68		
					5.43		
					7.29		
					6.74		
					7.35		
					5.53		
					8.1		
					7.41		
					6.22		
					6.55		
Japanese	20- 29	(Ishida and Dodo 1990)	Aged 17-90	105	4.00	1.03	1.06
					4.00	0.95	0.91
					6.30	1.26	1.59
					4.60	1.22	1.50
					4.80	1.17	1.38

Ethnicity	Age	Reference	Notes	n	Thickness m	Thickness s.d.	Var
					6.90	1.44	2.08
Australian Aboriginal	20- 29	(Brown 1992)	Ages unknown; late Holocene.	24	7.80	1.09	
		(Brown, Pinkerton et al. 1979)	Yuendumu tribe, aged 19- 34.	28	15.10	3.00	
					7.30	0.70	
					7.20	0.80	
					9.00	1.40	
					4.00	0.60	
					3.90	0.50	
		(Brown, Pinkerton et al. 1979)	Skulls from SA museum	27	14	2	
					8	1.2	
					7.7	1.3	
					8.9	1.4	
					4	0.9	
					4.30	1.00	
					15.70	2.30	
African	30- 39	(Weber and Kim 1999)	Bushman	1	6.38	3.43	
	50- 59	(Weber and Kim 1999)	Bantu	1	9.49	3.36	
African- American	20- 29	(Adeloye, Kattan et al. 1975)	American	28	6.80	1.40	
					6.60	1.50	
					8.80	2.40	
					6.60	1.80	
		(Ross, Lee et al. 1976)	American, exact age unknown (17-95)	50	4.03	0.70	
	30- 39	(Adeloye, Kattan et al. 1975)	American	16	7.00	1.90	
					6.40	1.60	
					9.60	2.50	
					7.00	1.70	
	40- 49	(Adeloye, Kattan et al. 1975)	American	14	7.40	1.70	
					6.30	1.30	
					8.70	2.30	
					7.40	1.50	
	50- 59	(Adeloye, Kattan et al. 1975)	American	11	7.00	1.80	
					6.10	1.60	
					8.50	1.70	
					6.90	2.40	

Ethnicity	Age	Reference	Notes	n	Thickness m	Thickness s.d.	Var
Bedouin	20-29	(Smith, Wax et al. 1985)	Early Bedouin 1800CE, exact ages unknown	11	7.90	1.70	
					5.60	1.80	
					5.40	1.20	
Chinese	20-29	(Brown 1992)	Exact ages unknown. South Chinese	38	7.60	1.40	
			Ages unknown. North Chinese	37	6.40	1.30	
	30-39	(Weber and Kim 1999)		2	7.01	3.00	
					6.01	3.08	
FEMALE							
Caucasian	20-29	(Adeloye, Kattan et al. 1975)	American	17	7.10	1.50	
					6.10	1.10	
					8.80	1.60	
					6.20	1.60	
		(Ross, Lee et al. 1976)	American, age 17-95	50	4.27	0.90	
		(Weber and Kim 1999)	European	1	6.35	3.39	
		(Weber and Kim 1999)	European	1	5.73	2.27	
		Tallgren 1974	Finnish, aged 20-73	32	7.11	1.47	
					7.09	1.72	
					8.20	2.05	
					7.30	1.68	
					15.74	3.30	
	30-39	(Adeloye, Kattan et al. 1975)	American	8	7.20	0.90	
					5.80	1.40	
					7.40	1.00	
					5.10	1.30	
		(Israel 1973)	American. Same population also measured at 50-59 (below).	20	7.80	1.70	
				20	7.70	1.80	
				20	6.80	1.80	
				18	7.60	1.90	
				21	8.60	2.00	
				20	9.10	2.10	
	40-49	(Adeloye, Kattan et al. 1975)	American	9	8.30	1.50	
					6.20	1.00	

Ethnicity	Age	Reference	Notes	n	Thickness m	Thickness s.d.	Var
					8.10	0.80	
					6.00	1.40	
		(Lynnerup 2001)	Danish	21	6.68	1.12	
					7.60	2.01	
					5.64	1.14	
					5.45	1.42	
	50-59	(Adeloye, Kattan et al. 1975)	American	4	7.80	0.50	
					7.00	0.80	
					8.00	0.80	
					8.00	1.20	
		(Ross, Jantz et al. 1998)	American, aged 18-87 (51±19)	58	7.03	1.57	
					7.23	1.68	
					8.87	2.74	
					8.97	2.51	
		(Israel 1973)	American. Same population also measured at 30-39 (above)	20	8.50	1.60	
				20	8.50	1.90	
				20	7.00	1.80	
				18	8.30	2.00	
				21	8.80	1.90	
				20	9.10	2.10	
	60+	(Adeloye, Kattan et al. 1975)	American	5	8.20	1.30	
					6.00	1.20	
					9.50	2.00	
					6.70	2.20	
		(Zvyagin 1975)	Russian, aged 20-86; added means of 3 skull tables.	97	6.58		
					5.83		
					7.10		
					6.64		
					6.99		
					6.55		
					6.25		
					5.75		
Japanese	20-29	(Ishida and Dodo 1990)	(age 17-90)	47	4.80	1.06	1.12
					4.90	1.25	1.57
					6.00	1.20	1.43
					5.50	1.22	1.48
					5.70	1.20	1.44
					7.20	1.33	1.78
Australian Aborigine	20-29	(Weber and Kim 1999)		1	4.53	1.73	

Ethnicity	Age	Reference	Notes	n	Thickness m	Thickness s.d.	Var
		(Brown, Pinkerton et al. 1979)	Yuendumu tribe, aged 19-27.	31	13.40	2.00	
					7.60	0.90	
					7.10	0.90	
					8.80	1.00	
					4.20	0.60	
African	20-29	(Weber and Kim 1999)	Bantu	1	6.97	3.25	
African-American	20-29	(Adeloye, Kattan et al. 1975)	American	31	7.80	1.80	
					6.40	1.40	
					9.40	2.30	
					7.70	1.80	
		(Ross, Lee et al. 1976)	American, age unknown (17-95)	59	4.22	0.60	
	30-39	(Adeloye, Kattan et al. 1975)	American	14	7.60	1.30	
					6.30	1.10	
					9.20	2.10	
					7.70	1.60	
	40-49	(Adeloye, Kattan et al. 1975)	American	16	7.10	1.50	
					6.30	1.20	
					9.30	1.60	
					7.70	1.60	
	50-59	(Adeloye, Kattan et al. 1975)	American	5	8.30	1.10	
					7.80	2.40	
					10.50	2.10	
					8.20	1.80	
	60+	(Adeloye, Kattan et al. 1975)	American	19	8.30	1.60	
					6.10	1.30	
					8.70	2.10	
					7.30	2.20	
Bedouin	20-29	(Smith, Wax et al. 1985)	Early Bedouin ~1800CE, ages unknown	12	7.80	1.80	
					5.50	1.60	
					6.10	1.10	
Chinese	30-39	(Weber and Kim 1999)		1	7.03	3.62	
>1 UNKNOWN							
Unknown		(Law 1993)	Male, American	1	5.20	0.89	0.80

Ethnicity	Age	Reference	Notes	n	Thickness m	Thickness s.d.	Var
		(Zipnick, Merola et al. 1996)	American (NY). Race, gender, age not mentioned	26	9.00	2.00	
					9.00	2.00	
					11.00	3.00	
					14.00	5.00	
					11.00	2.00	
					9.00	3.00	
					8.00	2.00	
					10.00	3.00	
					11.00	3.00	
					10.00	2.00	
					8.00	2.00	
					7.00	2.00	
					17.55	3.18	
Korean		(Hwang, Kim et al. 1997)	Korean	88	4.86	1.39	
			Age unknown		5.57	1.27	
			Males and females		6.43	1.16	
					6.67	1.41	
					5.35	1.31	
					5.86	1.33	
					6.29	1.31	
					6.10	1.35	
					5.52	1.24	
					5.45	1.31	
					5.91	1.25	
					5.54	1.29	
					4.73	1.19	
					5.21	1.21	
					5.31	1.32	
American		(Ebraheim, Lu et al. 1996)	Male American (Ohio)	25	6.20	1.30	
			Age unknown		6.50	1.30	
					7.60	1.70	
					9.10	1.80	
					11.60	2.60	
					15.10	2.60	
					11.50	2.60	
					9.00	2.10	
					7.40	1.50	
					6.90	16.00	
					6.60	1.60	
					5.60	1.70	
					5.50	1.90	
					5.50	1.90	
					5.70	1.90	
					7.20	2.70	
					11.10	2.50	

Ethnicity	Age	Reference	Notes	n	Thickness m	Thickness s.d.	Var
					6.70	2.20	
					5.90	1.80	
					5.70	1.70	
					6.40	1.50	
					6.10	1.90	
					4.30	1.40	
					4.60	1.80	
					4.20	1.60	
					4.70	1.60	
					5.90	2.10	
					9.00	2.00	
					5.30	2.60	
					4.50	1.40	
					4.30	1.70	
					5.20	1.80	
					5.70	1.50	
					4.00	1.70	
					4.20	1.50	
					3.70	1.20	
					4.70	1.60	
					5.90	2.10	
					6.80	1.40	
					4.90	2.20	
					4.30	1.70	
					3.80	1.30	
					4.60	1.60	
					4.50	1.10	
					4.30	2.00	
					3.90	1.50	
					3.90	1.60	
					5.10	2.00	
					5.60	1.70	
					6.10	1.80	
					5.40	1.80	
					4.50	1.80	
					3.70	1.10	
					4.80	1.90	
					4.70	1.50	
American		(Ebraheim, Lu et al. 1996)	Femle American (Ohio)	27	5.40	1.20	
			Age unknown		5.70	1.30	
					6.50	1.50	
					7.70	1.50	
					9.80	2.10	
					12.00	1.90	
					9.70	2.10	
					7.50	1.70	
					6.10	1.60	
					5.60	1.40	
					5.10	1.10	

Ethnicity	Age	Reference	Notes	n	Thickness m	Thickness s.d.	Var
					4.90	1.70	
					4.70	1.40	
					4.30	1.50	
					4.30	1.30	
					5.10	1.60	
					9.50	2.20	
					5.00	1.60	
					4.40	1.20	
					4.80	1.60	
					5.10	1.50	
					5.40	1.30	
					5.00	1.40	
					3.98	1.20	
					3.40	1.20	
					3.80	1.00	
					3.90	1.10	
					7.80	1.70	
					4.20	1.60	
					3.60	1.00	
					3.40	1.10	
					4.20	1.40	
					5.00	1.70	
					3.90	1.30	
					3.40	1.30	
					3.10	1.30	
					3.70	1.30	
					4.30	1.50	
					6.60	1.30	
					3.90	1.40	
					3.40	1.40	
					3.10	1.20	
					3.90	1.50	
					5.00	1.70	
					4.10	1.80	
					3.30	1.80	
					3.50	1.60	
					4.10	1.10	
					5.00	1.70	
					5.60	1.30	
					4.60	1.30	
					3.50	1.60	
					2.90	1.50	
					3.60	1.40	
					4.30	0.90	
		(Olivier 1975)	male	125	15.60		
			female		13.90		
		(Grob, Jeanneret et al. 1991)	males & females	10	14.00		
					6.60		

Ethnicity	Age	Reference	Notes	n	Thickness m	Thickness s.d.	Var
					5.70		
		(Pensler and McCarthy 1985)	males & females,	200	6.80	1.04	
			caucasian &		7.03	1.06	
			African- American		7.45	1.03	
			aged 18-91		7.72	1.07	
					6.86	0.99	
					7.03	1.05	
					7.46	1.09	
					7.72	1.11	
		(Garfin, Botte et al. 1985)	age/sex/race unknown	47	8.70		
					9.60		
					6.70		
					6.60		
					6.10		
					10.60		
					6.10		
					5.30		
		(Getz 1961)	Greenland (age/sex unknown)	10	5.70	0.40	
					6.40	0.40	
			Easter Island (age/sex unknown)	10	7.20	0.30	
					7.60	0.30	
			Australia (age/sex unknown)	10	5.60	0.30	
					6.50	0.20	
			New Zealand (age/sex unknown)	10	7.10	0.20	
					7.30	0.20	
			South America (age/sex unknown)	10	5.40	0.40	
					7.50	0.20	
			North America (age/sex unknown)	10	5.70	0.30	
					6.10	0.30	
		No. of literature sources: 27					

3.3.4.2 Modelling the variable

The Geometry Head model was initially created using xFDTD, a finite-difference time domain software package (Remcom 2006), and cranial thickness tests were performed using that version.

Recall from Section 3.1 that the base-level cranial thickness was chosen as a uniform 5 mm. Thickness was varied to the 5th, 50th and 95th percentiles of human variation – 4 mm, 6 mm and 11 mm – with all other variables kept constant, and SAR results compared.

3.3.4.3 Effect of cranial thickness on SAR

The whole head average (WHA) SAR, 10g peak spatial SAR (10g SAR) and peak point SAR results are tabulated and plotted in Table 9 and Figure 29 respectively. SAR plots of the Geometry Head model with 4, 6 and 11 mm cranial thicknesses are seen in Figure 28 below (the 4 mm model is shown with the FDTD mesh).

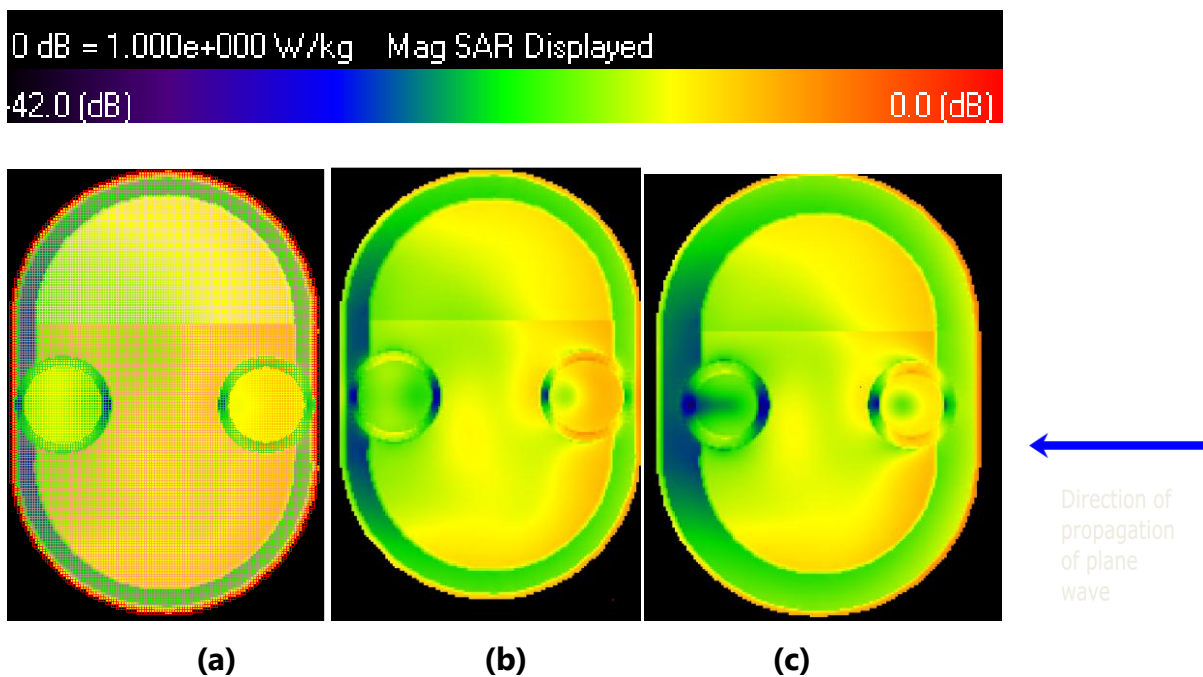


Figure 28: SAR plots of Geometry Head with (a) 4 mm (b) 6 mm and (c) 11 mm cranial thicknesses.

The SAR plots show that most of the absorption happens in the outer skin layer. Not much is absorbed in the skull tissue, likely due to its low conductivity and hence absorbance. A region of high SAR is seen further inside the head model, just inside the skull, medial to the ear.

The fat layer around the eyes shows higher absorption than the eye itself. This lends credence to the assumption that electrically isolating this tissue provides protection, and that the fat parameter needs to be included in human head models.

Table 9: Cranial thickness and SAR

Cranial thickness (mm)	4	6	11
WHA SAR (W/kg)	0.04	0.04	0.04
10g SAR (W/kg)	0.12	0.13	0.13

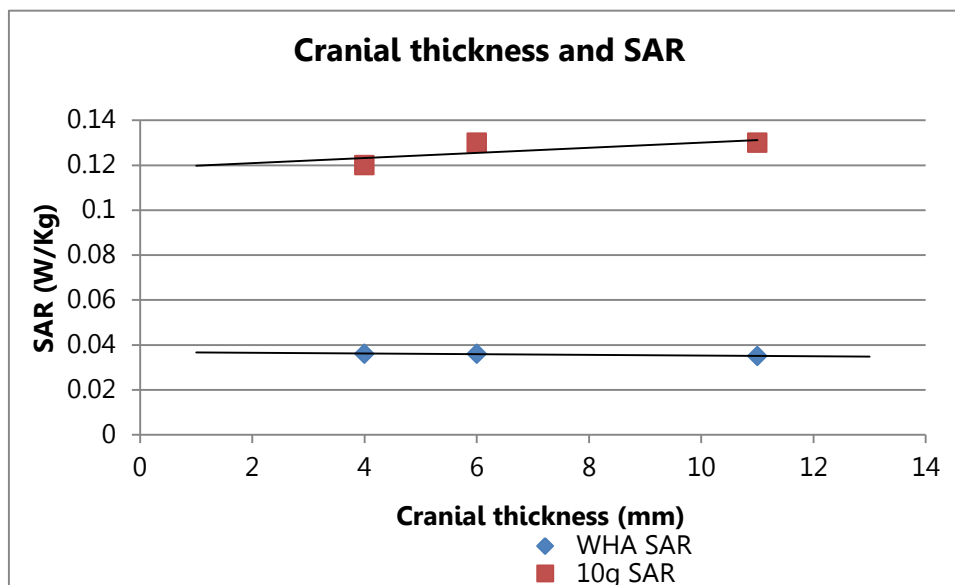


Figure 29: Relationship between cranial thickness and SAR

Figure 29 above charts the relationship between WHA and 10g peak spatial SAR and cranial thickness in adult human in the range of 5th to 95th percentiles. Lines of best fit are shown. However, only 3 points are used for analysis so results must be considered with caution.

At the range of human anatomic variation, adult cranial thickness is predicted by this model to have little effect on SAR. The SAR values themselves are not critical, rather the relationship between SAR variable is worth noting

3.3.5 Section summary

- Literature provides much data regarding cranial thickness in humans, but little regarding the effect of this variation on SAR
- 27 literature sources were consulted, yielding numerous measurements of 3103 adult human skulls

- The 5th, 50th and 95th percentiles of adult human cranial thickness were found to be 4, 6 and 11 mm respectively; percentiles of human sub-populations broken down into different sexes, ages and ethnicities are also available
- Cranial thickness at the range of human anatomic variance, despite expectations, was found to make little difference to SAR using the Geometry Head model, but only 3 points were used for analysis so results must be treated with caution

3.4 Adult skin thickness

3.4.1 Why this variable is important

This variable was chosen for testing (and for inclusion in the Geometry Head model) because its location at the surface of the head provides a shield for the sensitive tissues further inside the organ. As discussed previously in Chapter 2, at a frequency of 900 MHz, the electromagnetic excitation source is expected to penetrate no more than a few centimetres into the head, before decaying to a negligible level.

3.4.2 Literature review

Human skin consists of two layers: the stratified, cellular epidermis and an underlying dermis of connective tissue. Below the dermis is the subcutaneous fat, which is further separated from the rest of the body by a striated muscle layer known as the panniculus carnosus (Maximow and Bloom 1943). Ridges of the epidermis protrude into the dermis, creating a poorly defined dermal–epidermal junction. Some glabrous or hair-bearing skin such as found on fingers and toes contains a further keratinous outer layer known as the stratum corneum (Kligman 1969).

Skin on the face and head is thinner than many other parts of the body. The epidermal layer on feet, for example, can be up to 10 mm thick, and only 1-2 mm on the face (Gray 1918; Montagna 1962).

3.4.2.1 Skin thickness in adult humans

Skin thickness data was found primarily from medical and anatomic texts and academic papers, often exploring skin thickness for medical, dermatological or beauty treatments. Results of data gathering are provided in Section 3.4.4 below.

3.4.2.2 Effect of skin thickness on SAR

Little data is available in literature regarding effects on skin thickness on SAR. Studies exploring effect of body composition on SAR studies generally select a single skin thickness value (often taken from one or more literature sources) rather than create models of varying skin thicknesses for comparison (Cerri, De Leo et al. 1997; Bashayreh, Omar et al. 2010). When using layered sphere models, skin thickness is varied at the same time as other variables (Anderson 2003; Christ, Klingenbock et al. 2006; Wang, Fujiwara et al. 2006), making it difficult to isolate contribution of this parameter.

For comparison, skin thickness of existing heterogeneous models of adults and children, for example Visible Human (Spitzer, Ackerman et al. 1996), Norman (Dimbylow 1997), Naomi (Dimbylow 2005), and the Visible Family (Christ, Kainz et al. 2010), is in the range of 1 – 2 mm.

3.4.3 What do we expect to see?

Most of the absorption at 900 MHz happens at near or at the surface, and much of the energy absorption is expected to occur in the skin tissue, including the ear, modelled here as skin tissue. As skin thickness increases, we expect to see a drop in SAR.

3.4.4 Methodology, results and discussion

3.4.4.1 Range of skin thickness in humans

A literature review was undertaken in order to establish the 5th, 50th and 95th percentiles of variation in skin thickness of human adults. Since work involved examining skin thickness of the head, collation was restricted to skin measurements taken from areas of thinner skin where no stratum corneum is found: face (Diridollou, Vienne et al. 1999), forearm flexor (Takema, Yorimoto et al. 1994), groin, thigh (Southwood 1955), lower back, and scalp (Hori, Moretti et al. 1972). Information regarding scalp thickness is scarce; scalp thickness measurements were discarded if they included lower tissue layers such as subcutaneous connective tissue, muscle and fascia.

In total, 16 literature sources were consulted yielding 1520 measurements taken from numerous cadavers or live volunteers; often multiple measurements were taken from the same specimen at different points. Summary results in Table 10 show the 5th, 50th and 95th percentiles of skin thickness in adult humans are 0.03 mm, 0.84 mm and 1.86 mm respectively, rounded to **0.05 mm, 1 mm and 2 mm** for modelling purposes. Table 10 also shows results split for sex (female and male), age groups (20-29, 30-39, 40-49, 50-59, 60+ years old), and ethnicity (Caucasian, African-American, unknown/unspecified) sub-populations. Where two or more subpopulation criteria were unknown or unspecified (age, sex or ethnicity), measurements were included in the 'unknown' category, so as not to skew the population percentile values.

Female skin thickness (n = 845) was found to be lower than male (n = 554), with the 5th, 50th and 95th percentiles of female skin at 0.04, 0.77 and 1.68 mm versus male thicknesses of 0.89, 1.18 and 1.62 mm respectively. Caucasian and African-American male and female results in the literature review show no variability over the 5-95 percentile range (female African-American: 1.06 mm, n=60; male African-American: 1.17, n=40; female Caucasian: 1.05, n=141; male Caucasian: 1.17, n=177).

Table 10: Adult skin thickness in literature (summary). For full detail see Table 11. All measurements in millimetres, and include dermis and epidermis. Note that n denotes the number of measurements taken, not the number of cadavers or live volunteers.

Overall	Subpopulations			
	All	Unknown	Male	Female
5th percentile	0.03	0.03	0.89	0.04
50th percentile	0.84	0.91	1.18	0.77
95th percentile	1.86	3.57	1.62	1.68
n	1520	121	554	845

Subpopulation – sex and ethnicity unknown	
5th percentile	0.03
50th percentile	0.91
95th percentile	3.57
n	121

Subpopulation – Male			
Ethnicity	Unknown	Caucasian	African-American
5th percentile	0.88	1.17	1.17
50th percentile	1.19	1.17	1.17
95th percentile	1.63	1.17	1.17
n	337	177	40

Subpopulation - Female			
Ethnicity	Unknown	Caucasian	African-American
5th percentile	0.04	1.05	1.06
50th percentile	0.75	1.05	1.06
95th percentile	1.69	1.05	1.06
n	644	141	60

Table 11 Adult skin thickness in literature (detail)

Ethnicity	Age	Reference	Notes	n	Thickness mean	Thickness s.d.
MALE						
African-American	20-30	(Bliznak and Staple 1975)	aged 37.4+-16.3	40	1.17	1.08
Caucasian	20-30	(Bliznak and Staple 1975)	aged 36.9+-16.7	177	1.17	1.07
Unknown	20-30	(Meema, Sheppard et al. 1964)	aged 15-65	26	1.46	0.20
			aged 65+	45	1.19	0.23
		(Tan, Statham et al. 1982)		44	1.02	0.10
				16	1.01	0.13
				12	0.91	0.08
				11	0.93	0.10
				7	0.90	0.12
				9	0.81	0.16
		(Black 1969)	mean age 32	51	1.30	0.02
			mean age 78.6	14	0.90	0.04
		(Upham and Landauer 1935)		40	1.53	0.06
				42	1.61	0.06
		(Hori, Moretti et al. 1972)	cadavers, age 16-83	6	1.67	
			measured at scalp	2	1.52	
				5	1.46	
				7	1.18	
FEMALE						
African-American	20-30	(Bliznak and Staple 1975)	aged 44.1+-17.6	60	1.06	1.07
Caucasian	20-30	(Bliznak and Staple 1975)	aged 46.3+-16.4	141	1.05	1.08
Unknown	20-30	(Meema, Sheppard et al. 1964)	aged 15-65	62	1.33	0.17
			aged 65+	40	1.06	0.21
		(Dahan, Lagarde et al. 2004)	aged m=45, face & neck	20	1.42	0.14
					1.79	0.19
		(Tan, Statham et al. 1982)	forearm flexor	36	0.81	0.08
				17	0.82	0.08
				12	0.77	0.11
				27	0.76	0.09
				11	0.74	0.13
				16	0.70	0.12
		(Black 1969)	mean age 32	53	1.10	0.01
			mean age 77.2	22	0.90	0.03
		(Upham and Landauer 1935)	cutis	38	1.21	0.05
				41	1.29	0.05

Ethnicity	Age	Reference	Notes	n	Thickness mean	Thickness s.d.
		(Takema, Yorimoto et al. 1994)	ages 17-76, measured on different locations on face & forearm	170	0.45	0.12
					0.44	0.13
					0.53	0.11
					0.62	0.23
					0.70	0.11
		(Diridollou, Vienne et al. 1999)	measured on face	21	0.01	0.01
					0.01	0.01
					1.58	0.01
					1.41	0.01
		(El-Domyati, Attia et al. 2002)		2	0.07	0.00
					0.05	0.00
				5	0.06	0.00
					0.05	
				5	0.07	
					0.06	
				5	0.07	
					0.06	
				21	0.06	
		(Hori, Moretti et al. 1972)	cadavers, aged 16-83; measured at scalp	5	1.83	
				4	1.66	
				3	1.35	
				8	1.52	
> 1 UNKNOWN						
Unknown	Unknown	(Maximow and Bloom 1943)	histology text, general info given	1	1.01	
			added dermis + epidermis values for inclusion	1	2.12	
		(Miyauchi and Miki 1983)	quoted figures; added min/max	1	1.08	
			dermis + epidermis	1	4.15	
		(Southwood 1955)	dermis + epidermis; n = at least 20	20	0.42	
					3.50	
		(Tan, Statham et al. 1982)		12	0.84	0.13
					1.58	0.52
					1.48	0.50
				7	0.91	1.33
				4	0.89	0.06
					1.14	0.02
					1.15	0.11

Ethnicity	Age	Reference	Notes	n	Thickness mean	Thickness s.d.
		(Whitton and Overall 1973)	only included measurements from face	17	0.05	0.02
				10	0.05	0.03
				3	0.04	0.01
				30	0.05	0.02
		(Evans, Cowdry et al. 1943)		7	0.03	
				7	0.03	
No. of literature sources: 16						

3.4.5 Modelling the variable

Recall from Section 3.1 that the base-level skin thickness for the Geometry Head model was chosen as a uniform 2 mm. Due to computer hardware limitations, 1 mm was the smallest skin thickness able to be modelled, so the 5th percentile was not tested. Skin thickness in the entire model was altered to 1 mm, 5 mm and 10 mm, with all other variables kept constant. The two latter values were used to test how variations outside the range of normal anatomic values affect results obtained using this model, and further insight into the relationship between skin thickness and SAR.

The relative position of the eyes was not altered with skin thickness; even at skin thickness of 10 mm, the eyes were modelled with open eyelids.

3.4.6 Relationship between SAR and human skin thickness

Percentage variations in WHA, 1g and 10g SARs as skin thickness was altered relative to the base level models are shown below in Figure 30. Figure 31 plots the SAR in each of the six tissues (brain, eye, fat, filler, skin, skull) for the same models. Table 12 provides the raw SAR values and percentage SAR variations used in both figures.

Table 12: Skin thickness and SAR

		Skin thickness (mm)			
	Metric	1	2	5	10
WHA	SAR	0.079	0.082	0.077	0.060
	% SAR variation	-4%	0%	-5%	-27%
Brain	SAR	0.089	0.089	0.075	0.050
	% SAR variation	1%	0%	-16%	-44%
Eye	SAR	0.098	0.048	0.080	0.052
	% SAR variation	104%	0%	66%	7%
Fat	SAR	0.050	0.212	0.040	0.027
	% SAR variation	-77%	0%	-81%	-87%
Filler	SAR	0.210	0.097	0.185	0.123
	% SAR variation	117%	0%	91%	27%
Skin	SAR	0.126	0.118	0.093	0.064
	% SAR variation	6%	0%	-21%	-46%
Skull	SAR	0.027	0.027	0.022	0.015
	% SAR variation	1%	0%	-17%	-45%
1g SAR	SAR	0.372	0.364	0.354	0.337
	% SAR variation	2%	0%	-3%	-7%
10g SAR	SAR	0.27	0.29	0.25	0.19
	% SAR variation	-4%	0%	-11%	-34%

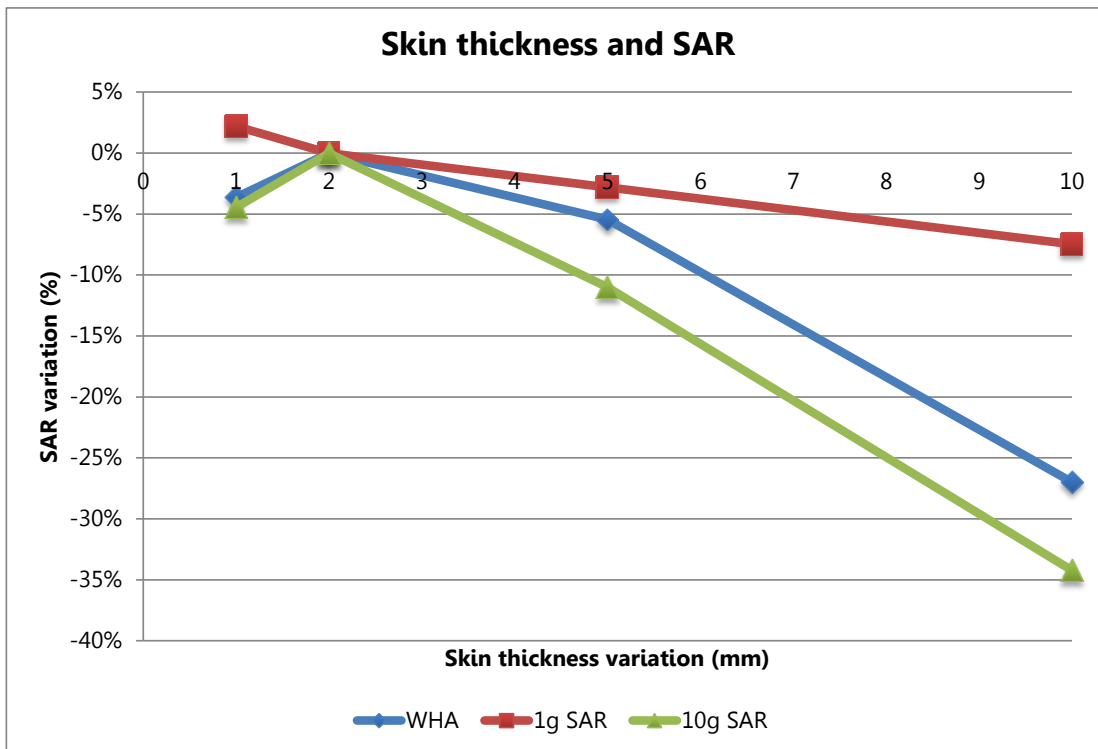


Figure 30: Skin thickness and SAR

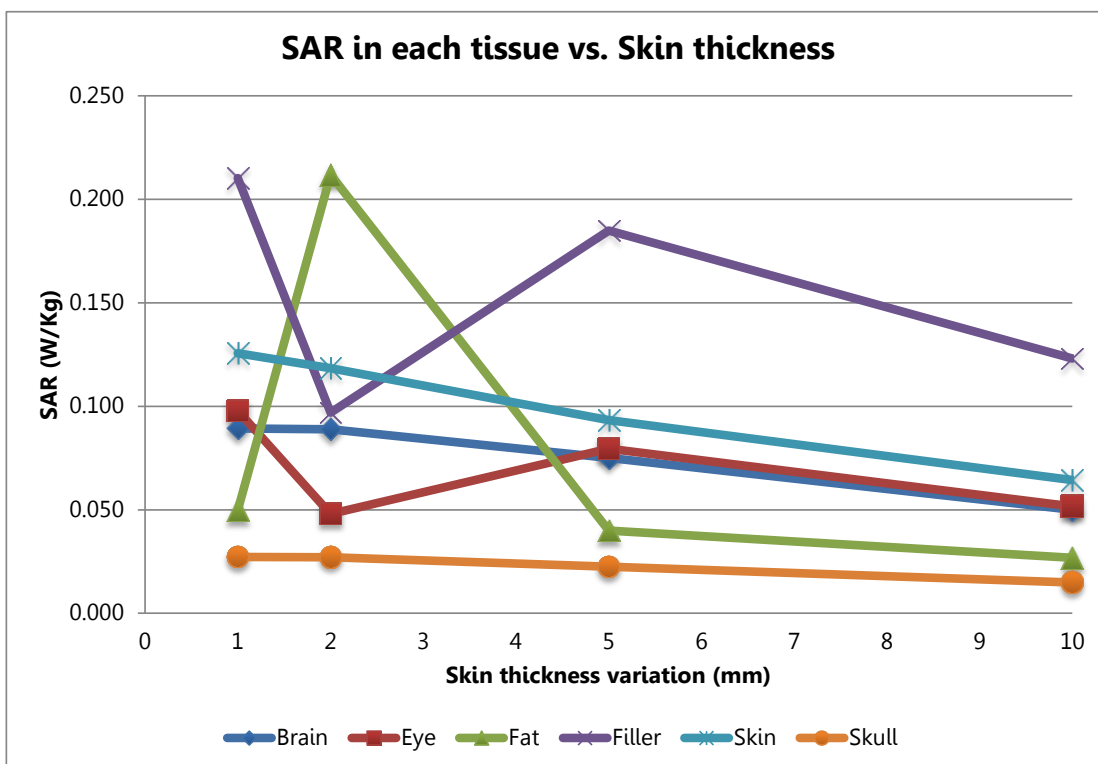


Figure 31: SAR in each tissue as skin thickness is varied

Interestingly, WHA and 10g SARs in Figure 30 are lower in the 1 mm skin model than in the 2 mm one. As skin thickness increases beyond that, both metrics are seen to sharply drop (WHA SAR by 27%, 10g SAR by 34% at the 10 mm skin model). 1g SAR drops by 12% as skin thickness increases from 1 to 10 mm.

Examining Figure 31, some of this effect is likely explained by a changed location of the max SAR, and along with it the makeup of the 10g SAR cubes. SAR in skull, brain and skin tissues steadily decreases with increasing skin thickness. In three of the four skin variations tested, highest SAR occurs in the filler tissue (0.210 – 0.123 W/kg), followed by skin (0.126 – 0.064 W/kg); brain and eye, of closely matching values (brain 0.089 – 0.050, eye 0.098 – 0.052 W/kg); then the low conductivity tissues, fat (0.050 – 0.027) and lastly skull (0.025 – 0.015). When the skin thickness is 2 mm, this model predicts highest SAR in the fat tissue (0.212 W/kg), a dramatic drop in filler SAR (0.097 W/kg), and a smaller drop in eye SAR (0.048 W/kg). It is not known whether this pattern is due to an artefact in the model which would not be repeated in a real head.

At the range of normal human skin thickness on the head as tested here (50th and 95th percentiles), the SAR differences are minor, with variation of less than 5% seen in WHA, 1g and 10g SAR metrics. Some aspects of the difference in SAR values are due to change in volume of the head (with the cube of the diameter) and also the change in placement and therefore tissue makeup of the 10g blocks used for averaging. The shielding provided to the internal parts of the head increases with increased skin thickness, suggesting that other parts of the body where skin is thicker are well better protected than the head – SAR in individual tissues drops by up to about 50% as skin thickness increases from 1 mm to 10 mm. Over than range, WHA and 10g SARs drop by over 30%, and 1g SAR drops by about 10%.

However, these results should be treated with some caution, as they are based on only 4 data points, and trends are largely interpolated.

3.4.7 Section summary

- Literature provides much data regarding skin thickness in humans, but little regarding the effect of this variation on SAR
- 16 literature sources were consulted, yielding 1520 skin thickness measurements from numerous adult humans, either live volunteers or cadavers, but only of regions of thinner skin as found on the head and face
- The 5th, 50th and 95th percentiles of skin thickness in adults were found to be 0.03 mm, 0.84 mm and 1.86 mm respectively, rounded to 0.05 mm, 1 mm, and 2 mm for modelling purposes
- Skin thickness in the base-level Geometry Head of 2 mm is comparable to that existing heterogeneous models VH, Norman, Naomi and the Visible Family (1 – 2 mm)
- Results using the Geometry Head model demonstrates a direct correlation between increase in skin thickness and decrease of SAR in the head, except for a skin thickness of 2 mm; this variation is likely due to altered location of region of maximum SAR
- At the range of human anatomic variation that was able to be modelled (1 - 2 mm), skin thickness is predicated by this model to make little difference to SAR in the head – less than 5% variation is seen
- Skin thickness of 5 and 10 mm such as found on other parts of the body provides a good level of shielding for the whole head, with a significant drop in SAR seen in all SAR metrics examined here

3.5 Head size

3.5.1 Why is this variable important?

Whole body exposure is affected by frequency, intensity and polarisation of the incident field, as well the size of the person and the person's electrical grounding, as explained in Chapter 2.

In this study, the frequency is kept constant. Whole body SAR is not being considered as only absorption in the head is considered. However, some of the same factors are true for body parts as for whole body exposure. As the head size changes, the whole head or different parts of it become resonant objects for the exposure frequency. The regions of maximum SAR may occur in different tissues, or be higher or lower depending on the head size.

3.5.2 Literature review

3.5.2.1 Head size in human anatomy

Much anthropometric data is available regarding head sizes of humans at different ages, sexes and ethnic groups (Baer 1956; Farkas, Katic et al. 2005). In this case it was decided to simply scale the base-level Geometry Head model up and down as far as possible within the software and hardware limitations, so a large collection of data was not undertaken.

Figure 11 in Section 2.4 provides some anthropometric measurements for human the head. The 5th and 95th percentiles of the adult head breadth (combined men and women) are 137 mm and 161.1 mm respectively; for head length, 176 mm and 209 mm respectively; and head height, 204 mm to 247 mm respectively.

3.5.2.2 Effect of head size on RF compliance

Effects of head size on SAR have been studied in the literature, though not systematically. Most studies that have explored this issue have compared adult heads to realistic child models, either derived from imaging techniques (Beard and Kainz 2004; Christ, Chavannes et al. 2005; De Salles, Bulla et al. 2006) or by using non-uniform scaling on adult heads (Lee, Choi et al. 2007). Studies that have used directly scaled heads to compare results (Gandhi, Gianluca et al. 1996; Anderson 2003; Kainz, Christ et al. 2005) used different exposures and modelling techniques, making it difficult to compare results.

Hombach et al. (Hombach, Meier et al. 1996), Kuster and Balzano (Kuster and Balzano 1992) and Schönborn and Kuster (Schonborn, Burkhardt et al. 1998) have all reported that the peak spatial-average SAR is not significantly dependent on the head size, provided that the geometrical relationships between the handset and the head are the same. The IEEE measurement standard asserts that a head geometry that results in overall smaller distances between the handset and the tissue boundary, for example where the ear is smaller, will provide more conservative results, because of the smaller separation between the equivalent current densities on the device under test and the tissue equivalent liquid. Thus, a larger anthropomorphic head model, with larger local radii of curvature, will satisfy the criterion for minimal distances (IEEE 2003). This was used to assign a larger male head for SAM, with a constant pinna thickness, as this is reasoned to represent a conservative case for men, women, and children.

3.5.3 What do we expect to see?

Results of previous tests comparing head sizes and SAR show mixed results. We expect that SAR in the head will vary to some extent with overall head size.

3.5.4 Methodology

The size of the entire Geometry Head model was scaled up and down by $\pm 30\%$ (70% to 130% of original size). The model could not be altered beyond those values due to hardware limitations. Table 13 below shows dimensions of GH at different sizes.

The parametrically adjustable nature of this model made such an adjustment quite easy. In the software, each of the variables affecting the size of the tissues is multiplied by a head size scaling factor (HSSF) variable. Altering the single value of the HSSF variable augments the sizes of all the geometric shapes by the same scaling value, altering the dimension of each tissue (for example, radius of eyes and thickness of skin) by the required factor.

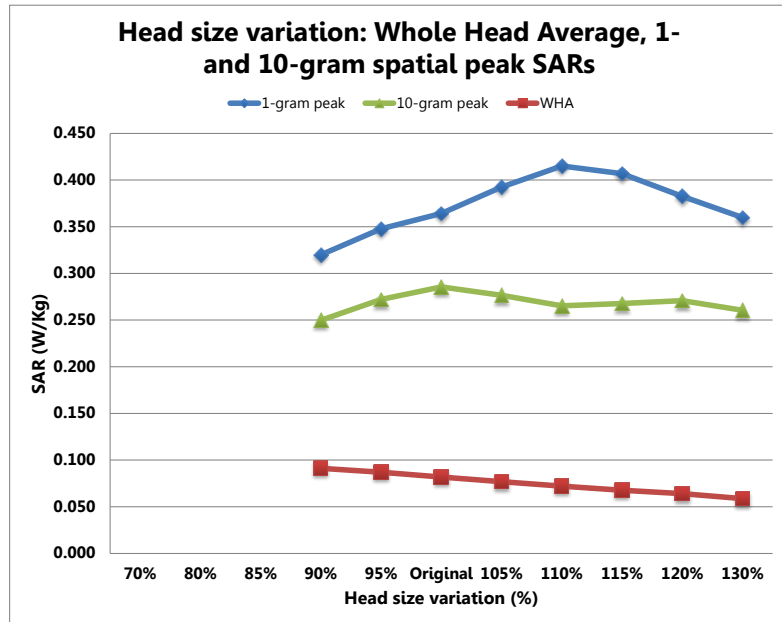
In Table 13 head, skull and brain 'height' measurements refer to dimensions from the top of the tissue to the bottom in the vertical. As the shapes of this model are symmetrical in the saggital plane, the breadth and length of the head are identical.

Table 13: Geometry Head size variation relative to wavelength

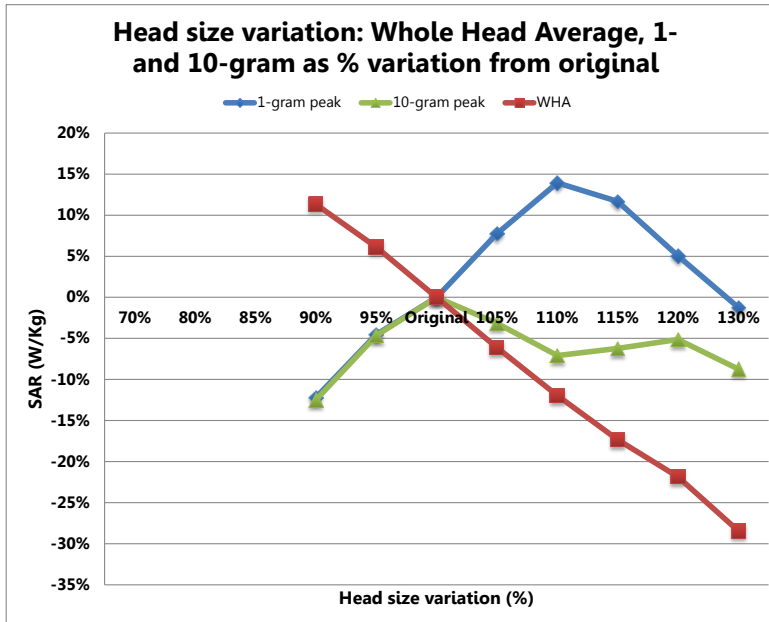
Head variables (mm)	Geometry Head size variation										
	70%	80%	85%	90%	95%	100%	105%	110%	115%	120%	130%
Head breadth	123.20	140.80	149.60	158.40	167.20	176.00	184.80	193.60	202.40	211.20	228.80
<i>Head breadth/λ</i>	<i>0.37</i>	<i>0.43</i>	<i>0.45</i>	<i>0.48</i>	<i>0.51</i>	<i>0.53</i>	<i>0.56</i>	<i>0.59</i>	<i>0.61</i>	<i>0.64</i>	<i>0.69</i>
Skull breadth	120.40	137.60	146.20	154.80	163.40	172.00	180.60	189.20	197.80	206.40	223.60
<i>Skull breadth/λ</i>	<i>0.36</i>	<i>0.42</i>	<i>0.44</i>	<i>0.47</i>	<i>0.50</i>	<i>0.52</i>	<i>0.55</i>	<i>0.57</i>	<i>0.60</i>	<i>0.63</i>	<i>0.68</i>
Brain breadth	112.00	128.00	136.00	144.00	152.00	160.00	168.00	176.00	184.00	192.00	208.00
<i>Brain breadth/λ</i>	<i>0.34</i>	<i>0.39</i>	<i>0.41</i>	<i>0.44</i>	<i>0.46</i>	<i>0.48</i>	<i>0.51</i>	<i>0.53</i>	<i>0.56</i>	<i>0.58</i>	<i>0.63</i>
Head height	161.00	184.00	195.50	207.00	218.50	230.00	241.50	253.00	264.50	276.00	299.00
<i>Head height/λ</i>	<i>0.49</i>	<i>0.56</i>	<i>0.59</i>	<i>0.63</i>	<i>0.66</i>	<i>0.70</i>	<i>0.73</i>	<i>0.77</i>	<i>0.80</i>	<i>0.84</i>	<i>0.91</i>
Skull height	158.20	180.80	192.10	203.40	214.70	226.00	237.30	248.60	259.90	271.20	293.80
<i>Skull height/λ</i>	<i>0.48</i>	<i>0.55</i>	<i>0.58</i>	<i>0.62</i>	<i>0.65</i>	<i>0.68</i>	<i>0.72</i>	<i>0.75</i>	<i>0.79</i>	<i>0.82</i>	<i>0.89</i>
Brain height	149.80	171.20	181.90	192.60	203.30	214.00	224.70	235.40	246.10	256.80	278.20
<i>Brain height/λ</i>	<i>0.45</i>	<i>0.52</i>	<i>0.55</i>	<i>0.58</i>	<i>0.62</i>	<i>0.65</i>	<i>0.68</i>	<i>0.71</i>	<i>0.75</i>	<i>0.78</i>	<i>0.84</i>

Table 14: SAR and percentage SAR variation in each tissue as the head size is altered

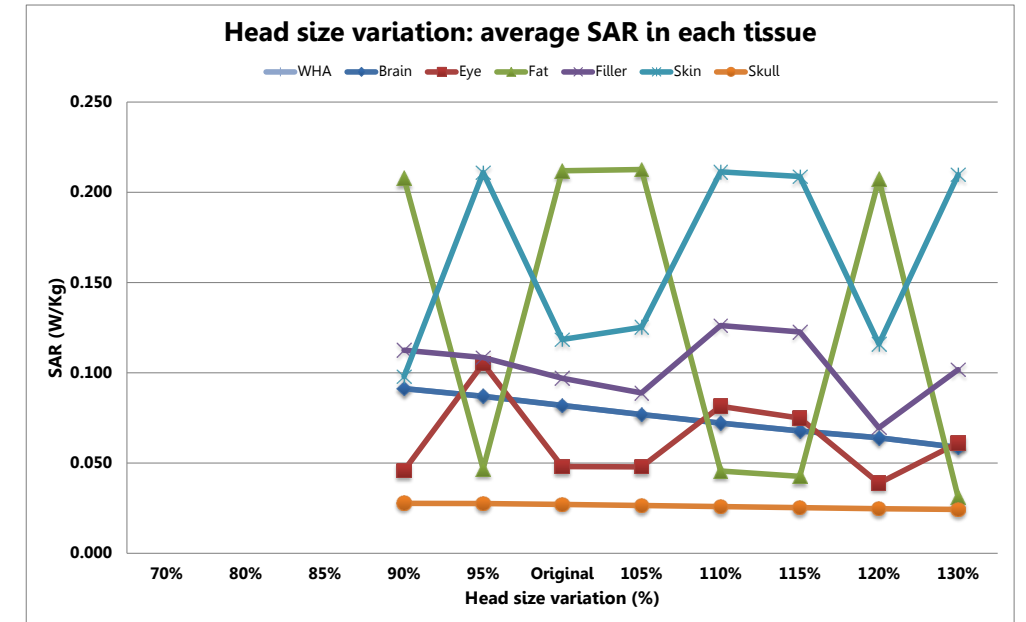
		Head Size Scaling Factor																							
				70%		80%		85%		90%		95%		Original		105%		110%		115%		120%		130%	
Tissue type	WHA	SAR	%var	0.120*	47%	0.099*	20%	0.095*	15%	0.091	11%	0.087	6%	0.082	0%	0.077	-6%	0.072	-12%	0.068	-17%	0.064	-22%	0.059	-28%
	Brain	SAR	%var	0.140*	57%	0.113*	27%	0.107*	20%	0.101	14%	0.095	7%	0.089	0%	0.082	-7%	0.076	-14%	0.071	-21%	0.066	-26%	0.059	-34%
	Eye	SAR	%var	0.051*	5%	0.127*	164%	0.119*	148%	0.046	-4%	0.105	119%	0.048	0%	0.048	0%	0.081	70%	0.075	56%	0.039	-19%	0.061	27%
	Fat	SAR	%var	0.209*	-2%	0.044*	-79%	0.045*	-79%	0.208	-2%	0.047	-78%	0.212	0%	0.213	0%	0.046	-78%	0.043	-80%	0.207	-2%	0.031	-85%
	Filler	SAR	%var	0.159*	64%	0.083*	-14%	0.090*	-7%	0.113	16%	0.108	12%	0.097	0%	0.089	-8%	0.126	30%	0.123	26%	0.069	-28%	0.102	5%
	Skin	SAR	%var	0.085*	-28%	0.191*	61%	0.200*	69%	0.098	-17%	0.211	78%	0.118	0%	0.125	6%	0.211	78%	0.209	76%	0.116	-2%	0.210	77%
	Skull	SAR	%var	0.030*	13%	0.027*	-1%	0.027*	1%	0.028	2%	0.028	2%	0.027	0%	0.026	-2%	0.026	-4%	0.025	-7%	0.025	-9%	0.024	-10%



(a)



(b)



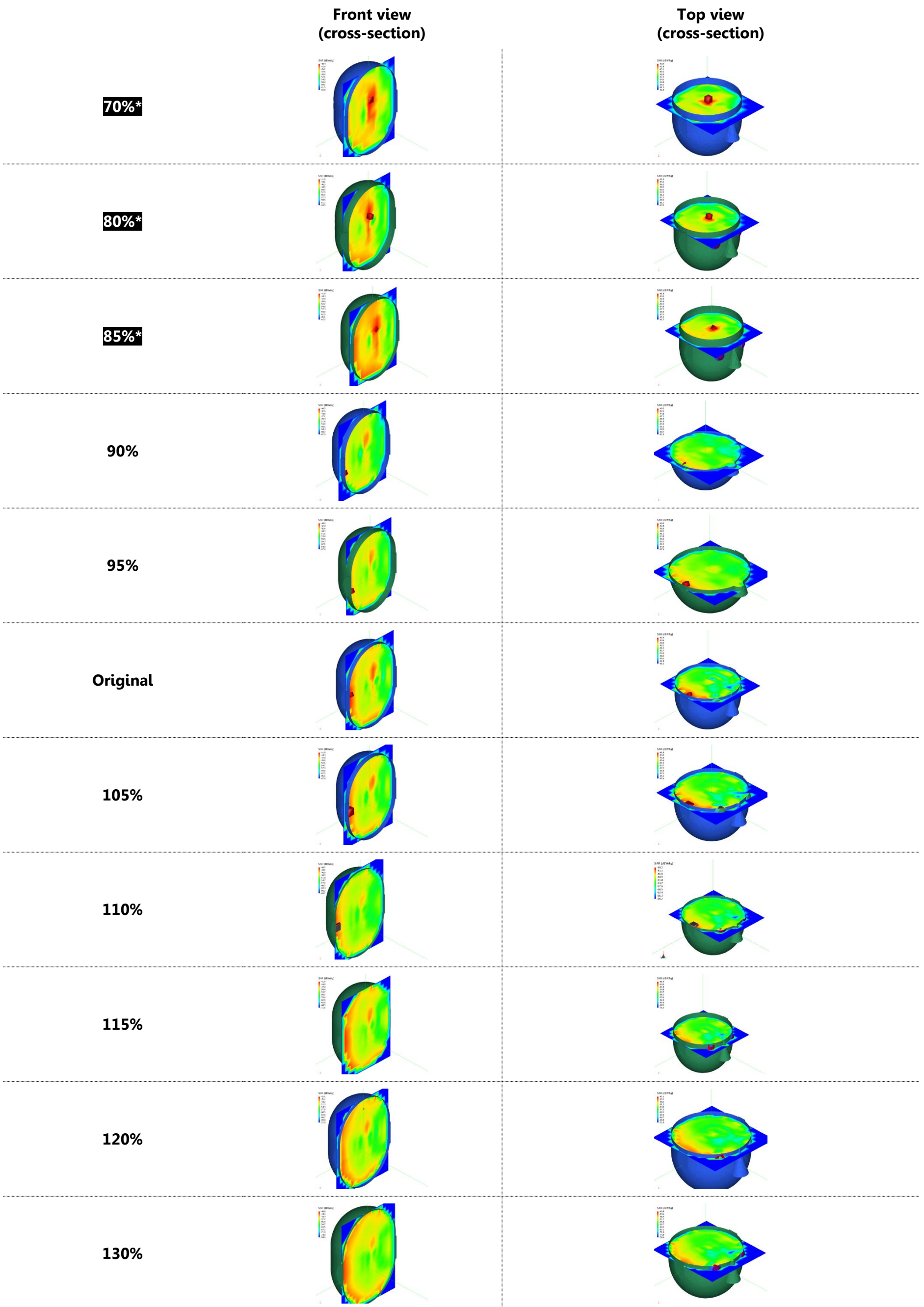
(c)

Figure 32: Relationship between head size and (a) WHA, 1g and 10g SAR as raw SAR values (b) WHA, 1g and 10g SAR as percentage variation (c) SAR in each tissue

Table 15: Relationship between head size and 1g and 10g SARs

				70%		80%		85%		90%		95%		Original		105%		110%		115%		120%		130%	
1g peak (W/kg)	SAR	%var	0.750*	106%	0.547*	50%	0.485*	33%	0.320	-12%	0.348	-5%	0.364	0%	0.392	8%	0.415	14%	0.407	12%	0.383	5%	0.360	-1%	
	Location		Artefact point		Artefact point		Artefact point		Near ear, ipsilaterally		Near ear, ipsilaterally		Eye		Eye, ipsilaterally		Eye, ipsilaterally		Eye, ipsilaterally		Eye, ipsilaterally		Eye, ipsilaterally		Eye, ipsilaterally
10g peak (W/kg)	SAR	%var	0.498*	74%	0.375*	31%	0.332*	16%	0.250	-13%	0.272	-5%	0.285	0%	0.276	-3%	0.265	-7%	0.268	-6%	0.271	-5%	0.260	-9%	
	Location		Artefact point		Artefact point		Artefact point		Near ear, ipsilaterally		Near ear, ipsilaterally		Ear		Near ear, ipsilaterally		Near ear, ipsilaterally		Near ear, ipsilaterally		Near ear, ipsilaterally		Near ear, ipsilaterally		Eye, ipsilaterally
1g peak location																									
10g peak location																									

* These results are explained in the text, and should be ignored. Artefact results are omitted in charts.



* These results are explained in the text, and should be ignored

Figure 33: SAR plots inside Geometry Head as head size is varied

3.5.5 Results and analysis

WHA, 1g and 10g SAR results may be seen in Figure 32 (a) as raw SAR values and (b) as percentage variation from the original GH model. Figure 32 (c) shows SAR in each tissue as head size is varied. Values are shown in Table 14 and Table 15. Table 15 also shows location of 1g and 10g cubes.

3.5.5.1 Artefact point

The images in Table 15 and Figure 33 (SAR plots inside the model of different head sizes) show that for head sizes of 70 – 85% of the original, the regions of maximum SAR are at the artefact point. SAR values in those models are far higher than the rest. These results have not been plotted in Figure 32, and should be ignored.

In a realistic head, the position of the spatial-average cubes seen in those smaller head sizes might be the position of the midbrain or the pituitary gland. In this case, it is likely that these peaks are seen in that area due to an artefact of the model. Recall from Section 3.1 that the middle section of the head shapes is modelled using a set of concentric cylinders. The relationship between the wavelength at 900 MHz, and height and breadth of the larger head objects used in GH – whole head, skull, and brain/average head tissue spheroids – is provided in Table 13. It can be seen that at 900 MHz, where $\lambda = 33$ mm, certain head sizes of GH create resonances in either the whole head or the skull cavity. When the diameter of the cylinder that makes the middle part of the head shape is near $\lambda/2$ or $\lambda/4$, the highest SAR is found at the artefact point. At 900 MHz, $\lambda = 33$ mm.

3.5.5.2 SAR results

The highest WHA observed using all three SAR metrics is at the smallest viable head size, 90% of the original-sized GH (head height of 207 mm, head diameter 158.4 mm), with SAR of 0.091 W/kg or 11% increase on the base-level model. For a head size variation of -5 to 30%, WHA SAR varies by 39%. A clear inverse relationship is seen between head size and WHA SAR, with SAR decreasing with increase in head size.

Over the same range of GH head size, 1g and 10g SARs vary by $\pm 15\%$ (only twice by more than 10%) in an irregular pattern. This is due to the changing location of the cubes between eye and ear (ipsilateral to the direction of plane wave propagation).

SAR plots in Figure 33 show areas of high SAR regions near both regions for all head size models, but the location of actual maxima are different at different sizes of the head. In Figure 32(c) it is seen that the brain and skull tissue SARs drop with increased head size over the modelled range. The SAR in other tissues changes dramatically. The eye SAR increases by 119% at a head size of 95%, though SAR in the eye is comparatively low.

The **worst case SAR** is observed by this model to occur at the smallest head size of 90%, with increases in both the WHA and the highest increase seen in the sensitive eye tissue.

3.5.6 Section summary

- Whole head average SAR decreases linearly as the head size increases; for a -5 to +30% variation in head size, a 39% variation is seen in WHA SAR, with highest SAR found in the largest head size
- Location and therefore magnitude of 1g and 10g SARs vary $\pm 15\%$ over the same range of head size using this model
- 119% increase in eye SAR is seen at head size of 95%, though the actual SAR value in the eye tissue is comparatively low

3.6 Dielectric properties of tissues

3.6.1 Why this variable is important

Section 2.1 describes the basic concepts governing interaction of electromagnetic waves and dielectric materials. There it is described how the conductivity and permittivity of individual tissues play a part in dielectric attenuation, which affects energy absorption due to electromagnetic exposure.

3.6.2 Literature review

3.6.2.1 Dielectric properties of human tissues in literature

Various authors outline measurements of dielectric properties of human tissues (Chakkalakal, Johnson et al. 1980; Behari and Singh 1981; Pethig 1987; Bao, Lu et al. 1997; Alanen, Lahtinen et al. 1998), or mathematical models used to extrapolate and interpolate such properties at various frequencies (Cole and Cole 1941; Khalafalla, Turner et al. 1971; Gabriel, Lau et al. 1996). Grant et al.'s 1988 study (Grant, Clarke et al. 1988) measured dielectric properties of skin at 50 MHz to 2.0 GHz of a single male individual at four points on the body. High variability in results was attributed to differences in adipose tissue deposits, presence of sweat ducts and composition of underlying tissue. This study applied a different mathematical analysis technique to the measuring equipment (open-ended coaxial line sensor), which cast doubts on results previously obtained by Grant and others. The uncertainty in estimates of human tissue dielectric properties is a source of uncertainty in the resultant SAR calculations. Raicu (Raicu, Kitagawa et al. 2000) used a different dispersion function and open-ended coaxial cable to explore the dielectric properties in skin in 2000. Their study concluded that the coaxial probe reports on the properties of the superficial layer, the stratum corneum, when the skin surface is dry, whilst the signal from deeper skin layers becomes dominant if the skin is wetted with saline. *In vivo* measurements quoted in the above studies were often obtained from a single individual, with no indication as to the possible range. Results of different studies vary by a factor of 50%.

Often, studies investigating the variation in dielectric properties examine the age related variation, i.e. how the dielectric properties change as the body ages. Wang et al. (Wang, Fujiwara et al. 2006) suggested using the total body water as a proxy to model the impact of age-dependent changes on the dielectric properties of tissues

relevant for SAR calculation in the head. Wang et al.'s work used the parameters of rat tissues of differently aged samples to extrapolate permittivity and conductivity. Their model predicts age-dependent changes of high water content tissues with satisfactory accuracy (tissues such as brain and skin), larger deviations from the experimental results are reported for the skull, a low water-content tissue.

Christ et al. (Christ, Gosselin et al. 2010) compares results of Peyman et al's 2009 study (Peyman, Gabriel et al. 2009) with those obtained using Gabriel's interpolating model based (Gabriel, Lau et al. 1996) on the Cole-Cole prediction method (Cole and Cole 1941). Peyman et al. (Peyman, Gabriel et al. 2009) report the measured dielectric properties of different porcine tissues, taken from pigs aged approximately 35, 100 and 600 days old. Christ et al. (Christ, Gosselin et al. 2010) note that as in Wang's study (Wang, Fujiwara et al. 2006), tissues with high water content only show small changes with age and are in generally good agreement with the Cole–Cole model (Cole and Cole 1941). However, significant differences at young age can be observed for tissues that have a low water content i.e. the skull, fat and bone marrow. These tissues show a significantly higher permittivity and conductivity for the younger age groups. With increasing age, they tend toward the values of the Cole–Cole model.

Wang et al. (Wang, Fujiwara et al. 2006) found that applying different dielectric property parameters to tissues to peak spatial SAR calculations does not reveal any systematic changes within different groups. Christ et al.'s study (Christ, Gosselin et al. 2010) supports Wang et al.'s conclusions that no age-related systemic changes could be found between peak-spatial SAR and dielectric properties of tissues, and furthermore noted that the SAR differences due to dielectric property variations are about 0.5 dB. SAR changes, Christ et al. conclude, are attributable to individual anatomic features.

3.6.2.1.1 [Can we use dielectric properties of animal tissues?](#)

Various studies have investigated the dielectric properties of mammalian animal tissue, before and after death. However, it is not certain how representative these results are of variance within human populations. Insufficient literature is available regarding the comparability of human and animal tissues with regards to dielectric properties.

Kraszewski et al. investigated the dielectric properties of various tissues in cats, including changes in dielectric properties for up to 4 hours after death (Kraszewski, Stuchly et al. 1982). Foster et al. (Foster, Schepps et al. 1980) details dielectric properties of white and grey brain tissue in dogs for frequencies between 100 MHz and 10 GHz (Foster, Schepps et al. 1979). Thurai et al. explored dielectric properties of mouse and rabbit brains (Thurai, Goodridge et al. 1984; Thurai, Steel et al. 1985).

Peyman et al. (Peyman, Rezazadeh et al. 2001) showed that dielectric properties of rat tissues change after death. Eight years later, Peyman et al. published another (Peyman, Gabriel et al. 2009) study showing that in vitro dielectric properties of porcine tissues in the frequency range of 50 MHz – 20 GHz show statistically significant reduction with age in both permittivity and conductivity of 10 out of 15 measured tissues. They ascribe this change to a reduction in the water content of tissues as animals age. Peyman et al. then used these results to calculate the SAR values in human children of age 3 and 7 years when exposed to 446 MHz RF

Schwartz's 1985 study into dielectric properties of frog blood and skin of dead animals are unusual in providing a comparison to human tissue properties (Schwartz and Mealing 1985). He noted no drifts in dielectric properties for several days after death.

A literature review of dielectric tissue properties by Foster and Schwan also notes several studies which show that variation in dielectric properties relating to time after excision was comparable to normal variability in the studied tissues (Foster and Schwan 1989). Schwan et al. performed several investigations of their own into this matter (Schwan and Foster 1980; Schwan 1981).

Pethig's 1987 paper (Pethig 1987) provides a similar review of the dielectric properties of various mammalian tissues, both human and other animals, and various biological fluids, for the frequency range from 1 Hz to 10 GHz.

Several studies do show that the differences of mammalian animal studies and adult human tissues are within the variation of the dielectric properties among different species of fully grown animals (Pethig 1987; Gabriel, Lau et al. 1996; Stauffer, Rossetto et al. 2003).

Methodology and results of animal dielectric properties vary from study to study. Little work has been done to correlate animal tissue dielectric properties to those of human tissues. It is therefore assumed here that animal studies cannot be taken into account.

3.6.2.2 *Effect of dielectric properties on SAR*

The literature is scarce regarding tissue dielectric properties' effect on SAR.

Drossos et al. (Drossos, Santomaa et al. 2000) provide a detailed discussion of the validity of the simple one-dimensional layered model, and comparison to realistic anatomic phantoms in the near field of sources.

Christ et al. (Christ and Kuster 2005; Christ, Klingenbock et al. 2006) have tested the effects of these properties on SAR.

As mentioned above in section 3.6.2.1, a paper by Peyman et al. (Peyman, Gabriel et al. 2009) showed the effect of dielectric properties of SAR in children, as derived from an a porcine tissue model. This work used 446 MHz as exposure frequency, so cannot be directly extrapolated to 900 MHz, however it is interesting to note that no significant differences between the SAR values for children or for adults were observed.

Keshvari et al. (Keshvari, Keshvari et al. 2006) varied dielectric properties of tissues in existing models by up to 20% and observed variation of up to 5% in computed SAR.

3.6.2.2.1 *Effects of fat dielectric properties*

Christ et al.'s 1996 paper (Christ, Klingenbock et al. 2006) considers the effect of body composition on SAR using a layered planar model and transmission-line models of dielectric property testing. They argue that the current dielectric definitions for head and body dielectric parameters in compliance standards were designed on the assumption that the source was placed near the ear and temporal bone. Their study expanded the planar model to worst-case scenarios of multiple tissue combinations (not head) with a far-field source. Their investigations found that at 900 MHz, the worst-case scenarios for 1g and 10g peak SARs were in a combination of high water content – low water content – low water content - high water content (specifically, skin - subcutaneous adipose tissue – fat – muscle) and high – low –high (skin -

subcutaneous adipose tissue - intestines) layers, respectively. The layers of fat with a relatively low water content only slightly attenuate the propagating waves. Christ et al. argue that sequences like these will lead to standing-wave effects in the low-permittivity layer, and if the thickness of this layer, including the outermost layer of skin, corresponds to an electric length of approximately $\pi/2$ or wavelength of approximately $\lambda/4$, the reflection of the inner high-permittivity layers will lead to (a) impedance-matching effects, which will allow a significant amount of the electromagnetic power to enter the tissue and (b) constructive interference, giving rise to a significant SAR increase in the skin layer.

Guy et al's 1968 (Guy 1968) study investigated the validity of different dielectric measurement systems on physical and numerical planar tissue models, using fat and muscle layers and neglecting the skin. The skin layer, however, significantly affects absorption characteristics (Schwan 1981) and should not be discounted.

3.6.2.2.2 Effects of skin dielectric properties

Meier et al.'s 1997 studies (Meier, Hombach et al. 1997) into absorption at 1800 MHz and 900 MHz noted that neglecting skin when modelling humans distorts SAR results.

Standing wave of impedance-matching effects in the tissue layers can lead to an increase of the local SAR in the skin if the thickness of the fat layer is of the order of magnitude of $\lambda/4$. However, if the SAR is averaged over a cubical volume of a mass of 1 or 10g, a conservative exposure assessment is possible using homogeneous material distribution, such as 'average head' tissue simulating liquid.

Keshvari et al.'s 2006 paper reports that varying dielectric properties of tissues in existing models by up to 20% creates variation of up to 5% in computed SAR (Keshvari, Keshvari et al. 2006). In 2007, Fujiwara et al approximated the electrical properties of skin using a different method (Debye dispersion characteristics) at 1.5 GHz (Fujiwara and Takai 1997), and noted that permittivity of skin is about 10% lower, and conductivity about 30% lower, than previous estimates.

3.6.2.2.3 What dielectric properties are used for compliance?

Gabriel et al. published dielectric properties of various tissues in the frequency range of 10 Hz to 20 GHz (Gabriel, Lau et al. 1996). Gabriel's samples were taken from freshly killed animals, human skin and tongues *in vivo*, and human autopsy material, the latter measured 24-48 hours after death. Her study reports variability in dielectric properties of $\pm 5\text{-}10\%$ above 100 MHz and $\pm 15\text{-}25\%$ at lower frequencies, but also note that variation within species may well exceed variations between species. These values became the accepted values of dielectric properties used for modelling humans for compliance (ICNIRP 1998; IEEE 2005) and research. These values are also available online for free download (FCC).

3.6.2.3 Literature review summary

- Studies into dielectric properties of human tissues have been performed using different methods and materials, comparing results is therefore difficult
- Several studies provide information about dielectric properties of animal tissues, however not enough information exists about how these compare to human tissue properties
- Some attempts have been made to establish what relationship exists between dielectric properties of human tissues and SAR; results are variable
- The accepted standard values of human dielectric property use for compliance are those provided by Gabriel et al in 1996

3.6.3 What do we expect to see?

Permittivity is greatly affected by the reflection coefficients of consecutive tissue layers, and the direction of incidence of the excitation. Reflections of propagating waves at different tissue layer interfaces can give rise to standing-wave effects and impedance matching, which can lead to local SAR increases.

Re-examining Equation 15 of SAR:

$$SAR = \frac{\sigma |E|^2}{\rho}$$

where σ is the tissue conductivity (S/m), ρ is the tissue density (kg/m³), and $|E|$ is the magnitude of the total RMS E-field level (V/m) induced within the irradiated tissue. It

becomes clear that tissue conductivity has a direct effect on SAR, whereas permittivity, which contributes to E , has a secondary effect.

Furthermore, in 1992 Kuster and Balzano (Kuster and Balzano 1992) demonstrated that during reactive near-field exposure (see Section 2.1 for a definition), i.e. where the exposure source is within 53 mm of the head at 900 MHz frequency, SAR is mainly proportional to the square of the incident H-field, and therefore the conductivity. The incident E-field, and therefore the material's permittivity, play a lesser role in SAR.

It is reasoned based on the literature survey and *a priori* that:

- some direct relationships exist between tissue dielectric properties and SAR
- tissues near the surface of the model closest to the source (in this model these are skin and skull) will play a greater role in SAR distribution than deeper layers
- tissue permittivity plays a smaller part in SAR than tissue conductivity
- small tissue volumes situated relatively far from the source (eyes, fat) will have little effect on SAR
- fat and skull, the two tissues with low water content, and therefore low σ values, will provide insulation to sensitive tissues within them – eyes and brain respectively
- the brain and filler tissues' dielectric properties are quite similar; as their values become closer, SAR absorption in those tissue is expected to be more uniform
- some results will be obscured by this model's artefact (see Section 3.5 for a fuller explanation of the artefact in this model)

3.6.4 Methodology

3.6.5 Modelling the variable

Section 3.1 details the anatomic features and tissues chosen for incorporation into the Geometry Head model. Dielectric variable analysis was performed using the FEKO software (EMSS 2009) version, see Figure 34 below. As discussed, anatomic features incorporated into both versions of this model are identical.

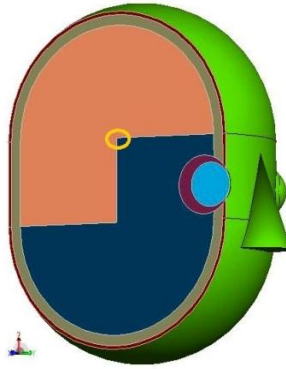


Figure 34: Geometry Head model created in FEKO software package, shown here with a cutplane. Different colours denote different tissues, and therefore regions of different dielectric properties. The yellow circle denotes the artefact point, explained above in Section 3.5.

The dielectric constant, and therefore SAR, is heavily affected by water content of the tissue. Tissues chosen for inclusion in the GH model include skin, skull, brain, average head, eye, and fat. The fat layer around the eyes (modelled as intersecting spheres, see Figure 34) has a relatively low water content and acts as electrical insulation. It is also expected that dielectric variations of the skull tissue, which has a much lower dielectric constant than either the skin or the inner parts of the head, will change the absorption characteristics of the whole head. In this model, the skull encases the brain/average head regions; the intersecting eye and fat spheres provide the only gaps.

Dielectric properties in the model were initially set to those used for compliance measurement (IEEE 2003) as described by Gabriel (Gabriel, Gabriel et al. 1996) see Table 16 below (density of tissues was not altered from the values shown).

Table 16: initial values of tissue dielectric properties and densities used in the Geometry Head model.

Tissue	Conductivity (σ, S/m)	Permittivity (ϵ)	Density (ρ)
Brain	0.77	45.8	1030
Eye	1.64	68.9	1000
Fat	0.05	5.40	1000
Filler	0.97	41.5	1000
Skin	0.87	41.4	1000
Skull	0.24	16.6	1850

Due to the scarcity and unreliability of available data regarding dielectric properties as explored in Section 3.6.2 above, it was not possible to determine a range of percentiles of human variability of dielectric properties. Instead, the initial ϵ and σ

values of any given tissue were individually varied, one at a time, to ± 10 , ± 20 and ± 30 per cent (see Table 17 below for full data) while all other variables were kept constant. $\pm 30\%$ variation was chosen based on the assumption of an approximately linear association with SAR and the observation that a variation for SAR of 30% is an acceptable uncertainty in SAR measurement standards (ICNIRP 1998). The full list of dielectric property variations modelled is provided in Table 17.

Table 17: Dielectric properties used in this study. Conductivity and permittivity as described by Gabriel were used varied to ± 10 , ± 20 and ± 30 per cent with all other variables kept constant for each test.

Conductivity variations							
Tissue	70%	80%	90%	100%	110%	120%	130%
Brain	0.54	0.62	0.69	0.77	0.85	0.92	1.00
Eye	1.15	1.31	1.48	1.64	1.80	1.97	2.13
Fat	0.04	0.04	0.05	0.05	0.06	0.06	0.07
Filler	0.68	0.78	0.87	0.97	1.07	1.16	1.26
Skin	0.61	0.70	0.78	0.87	0.96	1.04	1.13
Skull	0.17	0.19	0.22	0.24	0.26	0.29	0.31

Permittivity variations							
Tissue	70%	80%	90%	100%	110%	120%	130%
Brain	32.06	36.64	41.22	45.8	50.38	54.96	59.54
Eye	48.23	55.12	62.01	68.9	75.79	82.68	89.57
Fat	3.78	4.32	4.86	5.40	5.94	6.48	7.02
Filler	29.05	33.2	37.35	41.5	45.65	49.8	53.95
Skin	28.98	33.12	37.26	41.4	45.54	49.68	53.82
Skull	11.62	13.28	14.94	16.6	18.26	19.92	21.58

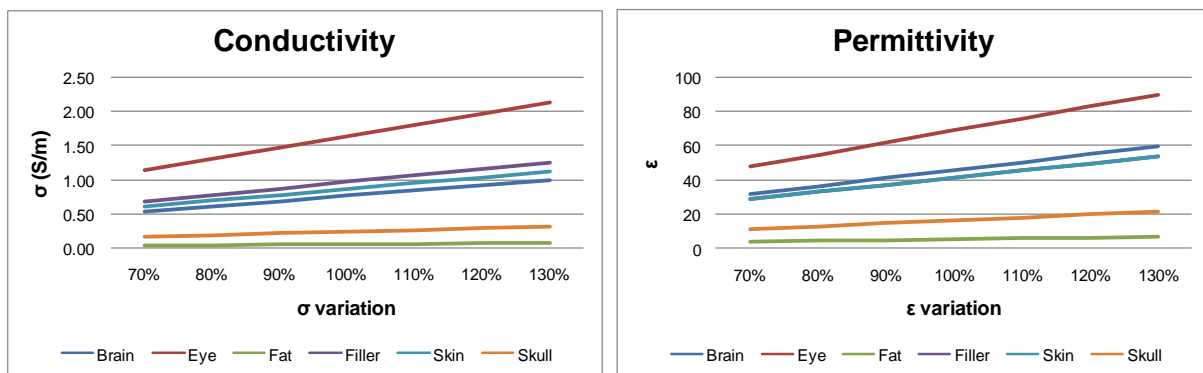


Figure 35: Dielectric properties used in this study. Conductivity and permittivity as described by Gabriel were used varied to ± 10 , ± 20 and ± 30 per cent with all other variables kept constant for each test.

3.6.6 Results and analysis

Figure 36 to Figure 44 and Table 18 to Table 26 show the WHA (whole head average) SAR, 1g and 10g peak spatial SAR, and average SAR in each tissue, for each variation of tissue dielectric properties. Raw SAR values at exposure of field intensity of 10 W/m² are provided, as well as a percentage variation of the given SAR value from the value predicted by the original, base-level GH model. The range of variability is provided in each case. Location of 1g and 10g SAR is also provided.

SAR results have been examined in four ways:

- Figure 36-Figure 38 and Table 18 to Table 20 show how WHA, 1g and 10g SARs vary with σ or ϵ variations, with a view to see which dielectric property values have significant effect on these metrics
- Figure 39-Figure 44 and Table 21 to Table 26 show the SAR variations in individual tissues, as the σ and ϵ of all tissues are altered in the range of $\pm 30\%$. These are used to examine how the SAR in any particular tissue is affected by dielectric property variations; for example, which tissue's σ or ϵ value have a greater effect on SAR in the skin tissue
- Table 27 describes the locations of the 1g and 10g SARs as the dielectric properties are altered, indicating where the peak absorption happens
- Figure 45 show the WHA SAR and SAR in each tissue (as raw SAR values) as the σ and ϵ values of one tissue at a time are altered, demonstrating how the SAR within the head model is re-distributed with the changes

Graphs showing the same type of results are plotted against identical axes for easy comparison. The graphs showing SAR variation in a given tissue vs. σ or ϵ are all plotted on a y-axis of value $\pm 35\%$; some points overshoot these limits (1g vs. brain ϵ , 1g vs. brain σ , and 10g vs. brain σ), explanations are provided below.

As the spatial averaging is increased – that is, as SAR is averaged over a larger volume, from 1g and 10g through to tissue type and WHA – the spikes in SAR variation smooth out, and the trends of SAR absorption become clearer. This is obvious from the increased linearity of the 10g graphs over the 1g graphs, and the increased regularity of location of 10g cubes, as the dielectric properties are varied.

Not all tissue properties play a big part in peak or spatially averaged SAR. Only significant variations, i.e. 5% or above, are individually listed here. Regularity of relationships is noted. More specific information about SAR distribution in individual tissues is provided in the sections below.

3.6.6.1 *Artefact*

As explained in Section 3.5 above, the Geometry Head model contains an artefact: sharp angles exist at the intersection of the filler and brain tissues (modelled as adjoining half-cylinders) along the frontal plane. This is clearly not an accurate representation of reality, as human heads do not contain 90° angles between tissues, and it causes misleading regions of high SAR along the joining 'seam'. The highest point SAR and 1g/10g SAR predicted by GH is sometimes at the sharp angle towards the top of the GH, termed the 'artefact point', and denoted by a yellow circle in Figure 34. These results are misleading. Using the FEKO modelling package, it was not possible to easily determine the regions of next highest SAR. Where the model predicts highest 1g or 10g SAR at the artefact point, the values are discounted. SAR range calculations do not include artefact point results.

3.6.6.2 *1g and 10g SAR*

Location of 1g and 10g SARs occurs in one of four regions in this model (Table 27): at the ear closest to the exposure source (comprising mostly skin and skull tissues); inside the head between the eye and the ear, ipsilaterally to the source – this is likely to be the brain tissue; at the eye (encompassing eye, fat and skin tissues); and at the artefact point (head and filler tissues). Artefact points have been ignored. As explained above, artefact point results have been ignored as they are due to a limitation of the 'blockiness' of this model. Where the cubes stay in roughly the same region, incremental changes are seen in SAR values and percentage SAR variation. Where the cubes change region dramatically, the metrics vary accordingly.

3.6.7 *What tissue dielectric properties affect WHA, 1g and 10 SAR?*

1g and 10g SARs show complex relationships to tissue dielectric properties. Most 1g and 10g SAR variations are in the order of 5 – 20%, with the exception of some brain tissue dielectric variations. At the two lowest brain σ values (70 and 80% of original σ value), the SAR of 1g and 10g cubes are very high: 89% and 65% change respectively at the lowest σ , 43% and 27% respectively at next lowest. The other exception is the

39% increase in 1g SAR seen at the highest value of brain ϵ . Exceptions are due to the makeup of the cubes changing dramatically with these dielectric property variations (see Figure 36 to Figure 38 and Table 18 to Table 20 **Error! Reference source not found.**) from the ear or eye region, to the artefact point. These results should be ignored.

1g SAR bears a complex relationship to most dielectric variations.

Over a $\pm 30\%$ range of σ and ϵ , 1g SAR significantly increases with (figures in brackets denote the range of SAR variation):

- increasing average filler σ (21%)
- increasing eye σ , but only for two highest values of σ
- increasing skin σ (8%)
- increasing eye ϵ (20%)

1g SAR significantly decreases with:

- decreasing fat ϵ (12%)
- increasing skin σ (8%)

The WHA plots show at most 5% variation, regardless of what dielectric variation occurs in individual tissues.

Using the GH model, WHA SAR is predicted to be unaffected by:

- eye ϵ or σ variations (0%)
- fat ϵ or σ variations (0%)

WHA SAR increases linearly (or mostly linearly) with:

- increasing brain σ (2%)
- increasing filler σ (2%)
- increasing skin ϵ (5%)

WHA SAR decreases linearly with:

- increasing skin σ (5%)

- increasing skull σ (2%)
- increasing skull ε (2%)
- increasing brain ε (5%)

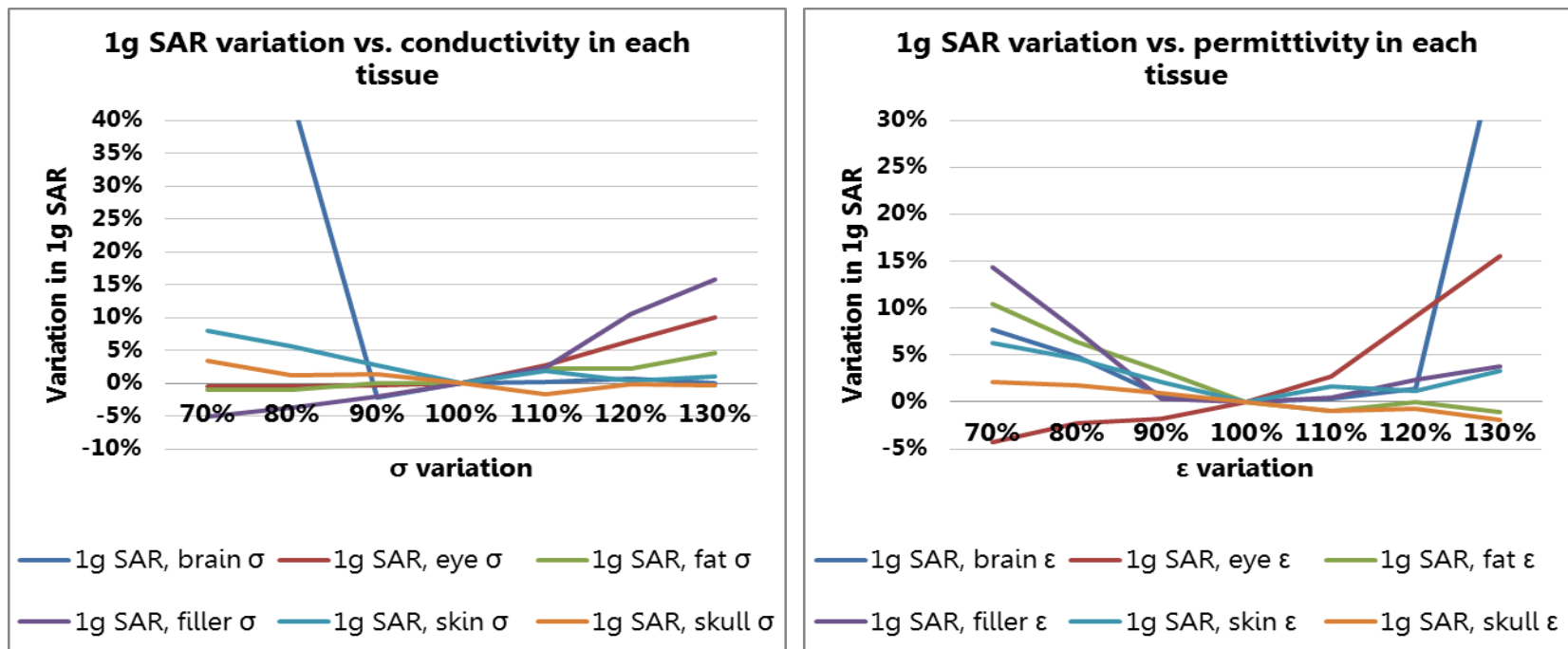


Figure 36: 1g peak spatial SAR variation with dielectric properties of all tissues

Table 18: 1g peak spatial SAR variation with dielectric properties of all tissues

1g SAR (W/kg)	70%	80%	90%	Original	110%	120%	130%	Range	1g SAR (W/kg)	70%	80%	90%	Original	110%	120%	130%	Range
1g SAR, brain σ	89%*	43%*	-2%	0%	0%	1%	0%	3%**	1g SAR, brain ε	8%	5%	1%	0%	0%	1%	39%*	8%**
1g SAR, eye σ	-1%	-1%	0%	0%	3%	7%	10%	11%	1g SAR, eye ε	-4%	-2%	-2%	0%	3%	9%	16%	20%
1g SAR, fat σ	-1%	-1%	0%	0%	2%	2%	5%	6%	1g SAR, fat ε	10%	6%	3%	0%	-1%	0%	-1%	12%
1g SAR, filler σ	-5%	-4%	-2%	0%	2%	10%	16%	21%	1g SAR, filler ε	14%	8%	0%	0%	0%	2%	4%	14%
1g SAR, skin σ	8%	6%	3%	0%	2%	0%	1%	8%	1g SAR, skin ε	6%	5%	2%	0%	2%	1%	3%	6%
1g SAR, skull σ	3%	1%	1%	0%	-2%	0%	0%	5%	1g SAR, skull ε	2%	2%	1%	0%	-1%	-1%	-2%	4%

* These results are explained in the text, and should be ignored

**Excluding artefact results

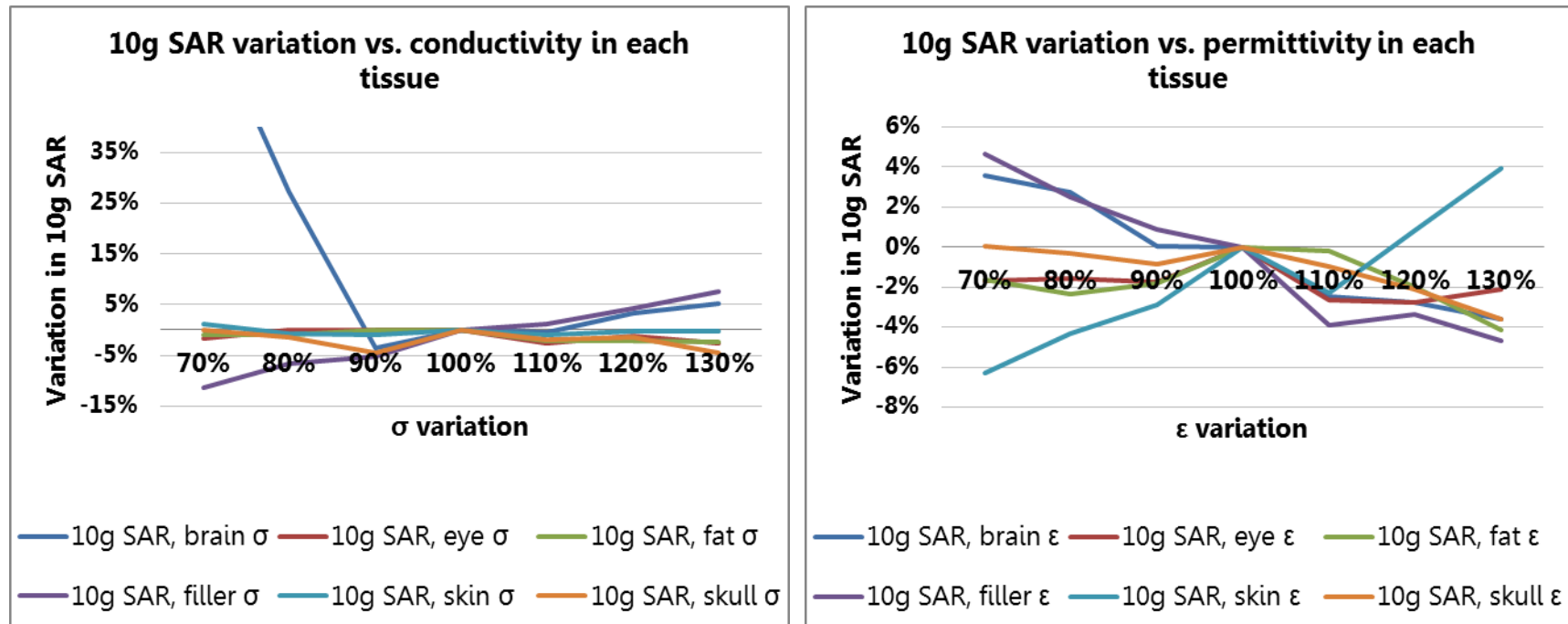


Figure 37: 10g peak spatial SAR variation with dielectric properties of all tissues

Table 19: 10g peak spatial SAR variation with dielectric properties of all tissues

10g SAR (W/kg)	70%	80%	90%	Original	110%	120%	130%	Range	10g SAR (W/kg)	70%	80%	90%	Original	110%	120%	130%	Range
10g SAR, brain σ	65%*	27%*	-4%	0%	0%	3%	5%	9%**	10g SAR, brain ϵ	4%	3%	0%	0%	-2%	-3%	-4%	7%
10g SAR, eye σ	-2%	0%	0%	0%	-3%	-1%	-3%	3%	10g SAR, eye ϵ	-2%	-2%	-2%	0%	-3%	-3%	-2%	3%
10g SAR, fat σ	-1%	-1%	0%	0%	-2%	-2%	-2%	2%	10g SAR, fat ϵ	-2%	-2%	-2%	0%	0%	-2%	-4%	4%
10g SAR, filler σ	-11%	-7%	-5%	0%	1%	4%	8%	19%	10g SAR, filler ϵ	5%	2%	1%	0%	-4%	-3%	-5%	9%
10g SAR, skin σ	1%	-1%	-1%	0%	-1%	0%	0%	2%	10g SAR, skin ϵ	-6%	-4%	-3%	0%	-2%	1%	4%	10%
10g SAR, skull σ	0%	-1%	-4%	0%	-2%	-1%	-4%	4%	10g SAR, skull ϵ	0%	0%	-1%	0%	-1%	-2%	-4%	4%

* These results are explained in the text, and should be ignored

**Excluding artefact results

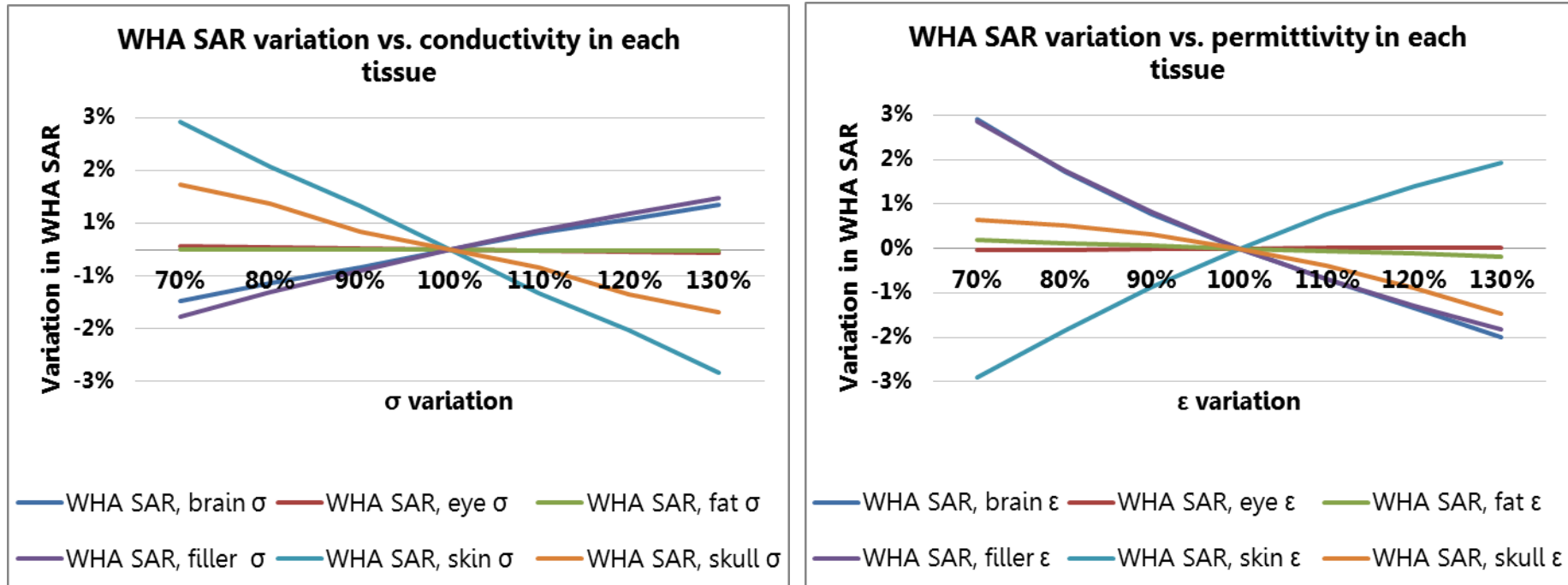


Figure 38: WHA SAR variation with dielectric properties in all tissues

Table 20: WHA SAR variation with dielectric properties in all tissues

WHA SAR	70%	80%	90%	Original	110%	120%	130%	Range	WHA SAR	70%	80%	90%	Original	110%	120%	130%	Range
WHA, brain σ	-1%	-1%	0%	0%	0%	1%	1%	2%	WHA, brain ϵ	3%	2%	1%	0%	-1%	-1%	-2%	5%
WHA, eye σ	0%	0%	0%	0%	0%	0%	0%	0%	WHA, eye ϵ	0%	0%	0%	0%	0%	0%	0%	0%
WHA, fat σ	0%	0%	0%	0%	0%	0%	0%	0%	WHA, fat ϵ	0%	0%	0%	0%	0%	0%	0%	0%
WHA, filler σ	-1%	-1%	0%	0%	0%	1%	1%	2%	WHA, filler ϵ	3%	2%	1%	0%	-1%	-1%	-2%	5%
WHA, skin σ	2%	2%	1%	0%	-1%	-2%	-2%	5%	WHA, skin ϵ	-3%	-2%	-1%	0%	1%	1%	2%	5%
WHA, skull σ	1%	1%	0%	0%	0%	-1%	-1%	2%	WHA, skull ϵ	1%	1%	0%	0%	0%	-1%	-1%	2%

3.6.8 What tissues' dielectric properties affect SAR in the brain?

In Figure 39 and Table 21 below, SAR in the brain tissue bears a simple relationship to changes in dielectric properties of most tissues for the range used here of $\pm 30\%$ σ and ϵ . Little variation is effected on SAR. For example, variations in eye and fat properties have no effect on brain SAR, nor does skull permittivity.

SAR in the brain tissue is unaffected by, i.e. 5% variation or less is seen (figures in brackets denote the range of SAR increase):

- fat dielectric properties, σ or ϵ (0%)
- eye dielectric properties, σ or ϵ (0%)
- average filler ϵ (2%)
- skull ϵ (1%)

Brain SAR increases with:

- increasing brain σ (10%)
- increasing skin ϵ (6%)

Brain SAR decreases with:

- increasing skin σ (13%)
- increasing skull σ (8%)
- increasing filler tissue σ (6%)
- increasing brain ϵ (6%)
 - a highly lossy skin layer acts as a protective barrier for the more delicate brain tissue
 - the skull cavity is formed of two tissues, brain ($\sigma = 0.77$) and filler ($\sigma = 0.97$); as the brain's conductivity increases to equal that of the filler tissue, it absorbs more energy, due to impedance matching between the two tissues

The **worst case brain SAR** is seen at lowest skin conductivity (skin $\sigma = 0.61$), highest brain conductivity ($\sigma = 1.00$), high skin permittivity ($\epsilon = 53.83$) and low brain permittivity ($\epsilon = 32.06$).

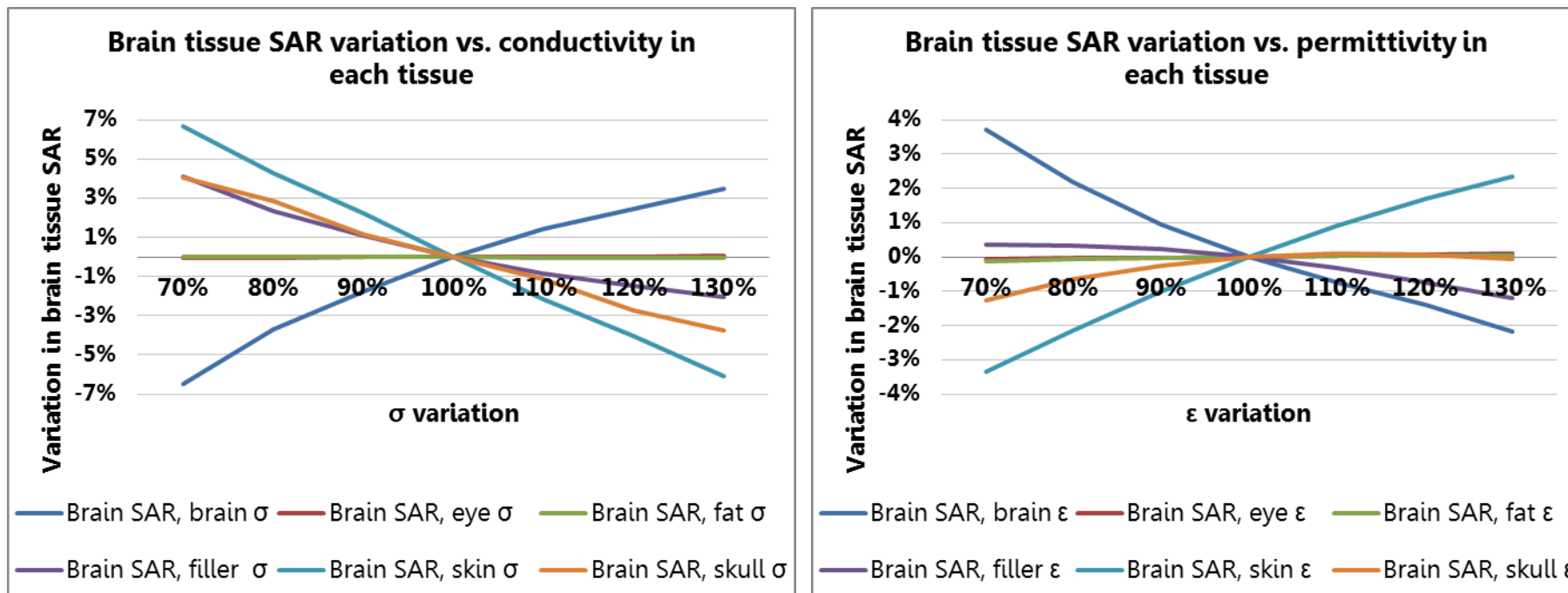


Figure 39: SAR variations in the brain tissue with dielectric properties in all tissues

Table 21: SAR variations in the brain tissue with dielectric properties in all tissues

Brain SAR	70%	80%	90%	100%	110%	120%	130%	Range	Brain SAR	70%	80%	90%	100%	110%	120%	130%	Range
Brain SAR, brain σ	-6%	-4%	-2%	0%	1%	2%	3%	10%	Brain SAR, brain ϵ	4%	2%	1%	0%	-1%	-1%	-2%	6%
Brain SAR, eye σ	0%	0%	0%	0%	0%	0%	0%	0%	Brain SAR, eye ϵ	0%	0%	0%	0%	0%	0%	0%	0%
Brain SAR, fat σ	0%	0%	0%	0%	0%	0%	0%	0%	Brain SAR, fat ϵ	0%	0%	0%	0%	0%	0%	0%	0%
Brain SAR, filler σ	4%	2%	1%	0%	-1%	-1%	-2%	6%	Brain SAR, filler ϵ	0%	0%	0%	0%	0%	-1%	-1%	2%
Brain SAR, skin σ	7%	4%	2%	0%	-2%	-4%	-6%	13%	Brain SAR, skin ϵ	-3%	-2%	-1%	0%	1%	2%	2%	6%
Brain SAR, skull σ	4%	3%	1%	0%	-1%	-3%	-4%	8%	Brain SAR, skull ϵ	-1%	-1%	0%	0%	0%	0%	0%	1%

3.6.9 What tissues' dielectric properties affect SAR in the eye?

Overall, tissue permittivities have a greater effect on eye SAR than conductivities. In Figure 40 and Table 22 below greatest increases of eye SAR are, unsurprisingly, effected by increases of the eye tissue's conductivity and permittivity. That is, the eye tissue becomes more absorbing with increases in σ and ϵ , though the relationships are non-linear.

SAR in the eyes is unaffected by, i.e. 5% or less change seen (figures in brackets denote the range of SAR change):

- changes in brain σ (1%) or ϵ (4%)
- changes in fat σ (4%)
- changes in filler ϵ (3%)
- changes in skull σ (3%)

SAR in the eyes increases with:

- increased eye σ (28%), increasing eye ϵ (28%)
- increasing fat ϵ (9%)
- increased filler tissue σ (6%)

SAR in the eyes decreases with:

- increasing skin σ (8%)
- increasing skin ϵ (10%)
- increasing skull ϵ (12%)

These trends can be explained thus:

- as the outer skin and skull layers become more absorbing with increasing conductivity and permittivity, less energy is deposited in the eyes
- the large tissues inside GH – brain and filler tissues – don't affect the eye SAR much, however a small increase in eye SAR is seen with increased filler conductivity (6%); looking at Figure 34, as the EM wave enters the head, it encounters, in order: skin – skull – filler – fat – eye. It would make sense, therefore,

that the absorbing characteristics of the filler tissue would affect eye SAR more than the brain tissue, which is several centimetres away

- some increased absorption in the fat tissue is expected to cause increased absorption in the eyeballs as more energy is collected in the area around the eyes. However, the SAR changes seen are proportionate with the relatively small size of the tissue

The worst case scenario for high SAR in the eyes is seen at the highest eye conductivity ($\sigma = 2.13 \text{ S/m}$) and highest eye permittivity ($\epsilon = 89.57$).

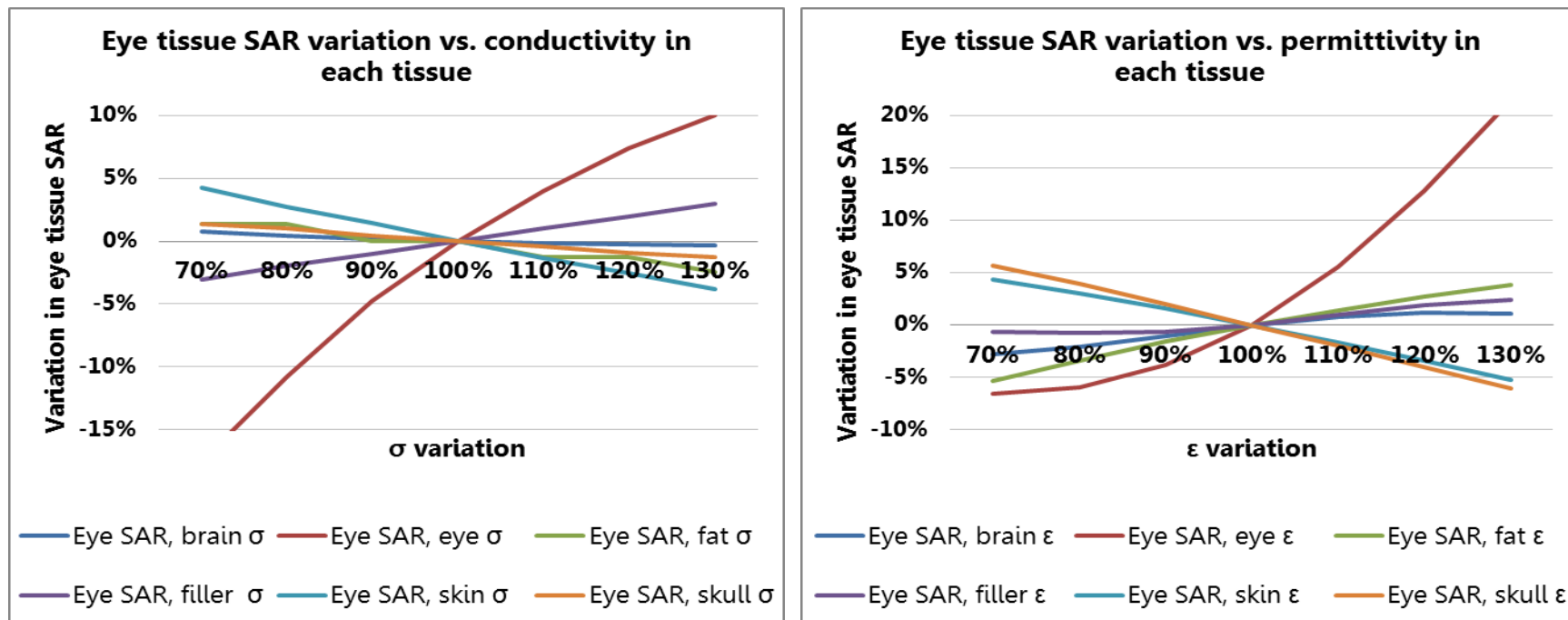


Figure 40: SAR variations in the eye tissue with dielectric properties in all tissues

Table 22: SAR variations in the eye tissue with dielectric properties in all tissues

Eye SAR	70%	80%	90%	100%	110%	120%	130%	Range	Eye SAR	70%	80%	90%	100%	110%	120%	130%	Range
Eye SAR, brain σ	1%	0%	0%	0%	0%	0%	0%	1%	Eye SAR, brain ϵ	-3%	-2%	-1%	0%	1%	1%	1%	4%
Eye SAR, eye σ	-18%	-11%	-5%	0%	4%	7%	10%	28%	Eye SAR, eye ϵ	-7%	-6%	-4%	0%	6%	13%	21%	28%
Eye SAR, fat σ	1%	1%	0%	0%	-1%	-1%	-2%	4%	Eye SAR, fat ϵ	-5%	-3%	-2%	0%	1%	3%	4%	9%
Eye SAR, filler σ	-3%	-2%	-1%	0%	1%	2%	3%	6%	Eye SAR, filler ϵ	-1%	-1%	-1%	0%	1%	2%	2%	3%
Eye SAR, skin σ	4%	3%	1%	0%	-1%	-3%	-4%	8%	Eye SAR, skin ϵ	4%	3%	2%	0%	-2%	-3%	-5%	10%
Eye SAR, skull σ	1%	1%	0%	0%	0%	-1%	-1%	3%	Eye SAR, skull ϵ	6%	4%	2%	0%	-2%	-4%	-6%	12%

3.6.10 What tissues' dielectric properties affect SAR in fat?

Marked changes in fat SAR are seen in Figure 41 and Table 23 with changes in fat tissue dielectric properties. Fat SAR is also seen to greatly increase with eye ϵ and filler tissue σ , with all other dielectric property variations associated with 5-14% SAR variation. The non-linear increase is likely due to location of the highest SAR changing (Table 27) from ear to eye to the artefact point.

SAR in the fat tissue is unchanged by (figures in brackets denote the range of SAR change):

- changes in brain σ (0%) or ϵ (1%)
- changes in skin ϵ (3%)

Fat SAR increases with:

- increasing eye ϵ (30%)
- increasing fat σ (47%)
- increasing filler σ (14%)

Fat SAR decreases with:

- increasing fat ϵ (49%)
- increasing eye σ (10%)
- increasing skin σ (11%)
- increasing skull σ (5%), skull ϵ (7%)

All the relationships above are either monotonous over the scales used here. Fat SAR also decreases non-linearly with increasing average-head tissue ϵ (8%).

These trends may be explained thus:

- as with eyes, dielectric property variations in the adjacent tissues have more effect than non-contiguous tissues; for example, increased average head tissue σ is associated with an increase in fat SAR, but variations in brain dielectric properties cause minimal changes

- interestingly, changes in eye dielectric properties show large changes in fat SAR, but the converse is not true – fat σ is not related to eye SAR, though increasing fat ϵ is associated with increased eye SAR in this model
- as the outer skin and skull tissues become more lossy, less absorption is seen in the fat tissue

The **worst case scenario for high SAR in the fat tissue** is low fat conductivity ($\sigma = 0.04$ S/m), high fat permittivity ($\epsilon = 7.02$), and high eye permittivity ($\epsilon = 89.57$).

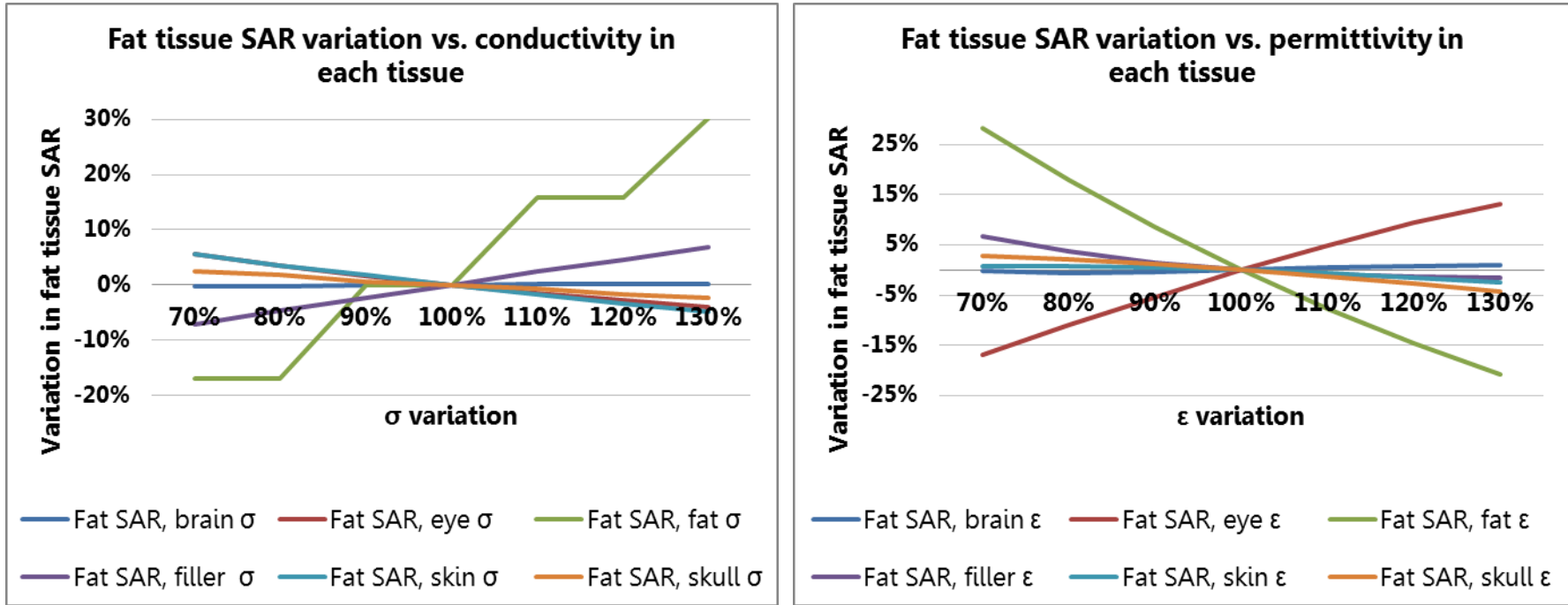


Figure 41: SAR variations in the fat tissue with dielectric properties in all tissues

Table 23: SAR variations in the fat tissue with dielectric properties in all tissues

Fat SAR	70%	80%	90%	100%	110%	120%	130%	Range	Fat SAR	70%	80%	90%	100%	110%	120%	130%	Range
Fat SAR, brain σ	0%	0%	0%	0%	0%	0%	0%	0%	Fat SAR, brain ϵ	0%	-1%	0%	0%	0%	1%	1%	1%
Fat SAR, eye σ	6%	4%	2%	0%	-1%	-3%	-4%	10%	Fat SAR, eye ϵ	-17%	-11%	-5%	0%	5%	9%	13%	30%
Fat SAR, fat σ	-17%	-17%	0%	0%	16%	16%	30%	47%	Fat SAR, fat ϵ	28%	18%	9%	0%	-8%	-15%	-21%	49%
Fat SAR, filler σ	-7%	-5%	-2%	0%	2%	4%	7%	14%	Fat SAR, filler ϵ	7%	4%	2%	0%	-1%	-1%	-2%	8%
Fat SAR, skin σ	6%	4%	2%	0%	-2%	-3%	-5%	11%	Fat SAR, skin ϵ	1%	1%	0%	0%	-1%	-1%	-2%	3%
Fat SAR, skull σ	2%	2%	1%	0%	-1%	-2%	-2%	5%	Fat SAR, skull ϵ	3%	2%	1%	0%	-1%	-3%	-4%	7%

3.6.11 What tissues' dielectric properties affect SAR in the filler tissue?

Figure 42 and Table 24 below shows that the SAR in the filler tissue is not greatly affected by dielectric property variations of the range used here – most SAR changes seen are in the order of about 5-10%. SAR variations associated with increasing ϵ and σ of filler tissue are opposite to those associated with skin tissue dielectric properties, and of comparable size. Dielectric property variations of smaller tissue volumes, such as eye and fat, create little or no change in filler tissue SAR using the GH model.

SAR in the filler tissue is unaffected by:

- changes in eye σ or ϵ ($\geq 1\%$)
- changes in fat σ or ϵ ($\geq 1\%$)
- changes in brain ϵ (2%)
- changes in skull ϵ (1%)

Filler SAR increases with (figures in brackets denote the range of SAR change):

- increasing filler σ (8%)
- increasing skin ϵ (5%)

Filler SAR decreases with:

- increasing skin σ (13%)
- increasing skull σ (8%)
- increasing brain σ (8%)
- increasing filler ϵ (5%)

These trends may be explained thus:

- as outer layers become less conductive and absorb less, RF energy penetrates deeper into the head; this effect is most obvious at low skin conductivity, which is the point of highest filler SAR (13% increase)
- as brain σ increases, it approaches and matches filler σ , and the entire skull cavity has the same conductivity

The **worst case scenario for high filler tissue SAR** is predicted by this model to be at lowest skin conductivity ($\sigma = 0.61$ S/m) and lowest filler permittivity ($\epsilon = 29.05$).

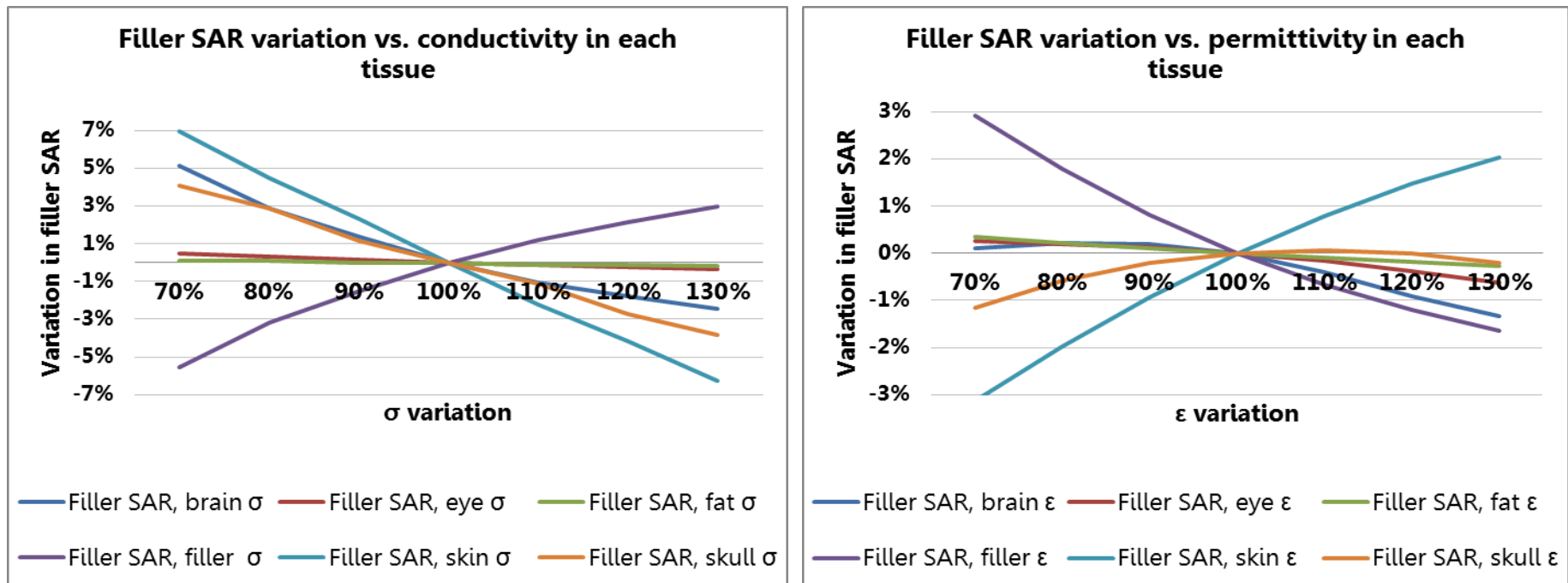


Figure 42: SAR variations in the filler (average head) tissue with dielectric properties in all tissues

Table 24: SAR variations in the filler (average head) tissue with dielectric properties in all tissues

Filler SAR	70%	80%	90%	100%	110%	120%	130%	Range	Filler SAR	70%	80%	90%	100%	110%	120%	130%	Range
Filler SAR, brain σ	5%	3%	1%	0%	-1%	-2%	-2%	8%	Filler SAR, brain ϵ	0%	0%	0%	0%	0%	-1%	-1%	2%
Filler SAR, eye σ	0%	0%	0%	0%	0%	0%	0%	1%	Filler SAR, eye ϵ	0%	0%	0%	0%	0%	0%	-1%	1%
Filler SAR, fat σ	0%	0%	0%	0%	0%	0%	0%	0%	Filler SAR, fat ϵ	0%	0%	0%	0%	0%	0%	0%	1%
Filler SAR, filler σ	-6%	-3%	-1%	0%	1%	2%	3%	8%	Filler SAR, filler ϵ	3%	2%	1%	0%	-1%	-1%	-2%	5%
Filler SAR, skin σ	7%	4%	2%	0%	-2%	-4%	-6%	13%	Filler SAR, skin ϵ	-3%	-2%	-1%	0%	1%	2%	2%	5%
Filler SAR, skull σ	4%	3%	1%	0%	-1%	-3%	-4%	8%	Filler SAR, skull ϵ	-1%	-1%	0%	0%	0%	0%	0%	1%

3.6.12 What tissues' dielectric properties affect SAR in the skin?

High skin conductivity is seen to significantly increase SAR in the skin in Figure 43 and Table 25 below. As discussed above in Section 8.2, it is reasoned *a priori* that the surface layer plays a significant role in energy absorption of the head. Note the ear, which is the closest GH dielectric to the source, consists of skin tissue, so the highest SAR likely occurs there, as any EM exposure deeper in the head has been already attenuated by the outer tissues. A few other interesting patterns are seen here: skin SAR drops when the skull layer is more conductive; as the inner volumes of the head increase in conductivity, skin SAR increases; as those volumes increase in permittivity, the skin SAR drops.

SAR in the skin tissue is unaffected by:

- changes in eye σ or ϵ (0%)
- changes in fat σ or ϵ ($\geq 1\%$)
- changes in skin ϵ (2%)

Skin SAR increases with (figures in brackets denote the range of SAR change):

- increasing skin σ (47%)
- increasing brain σ (5%)
- increasing filler σ (7%)

Skin SAR decreases with:

- increasing skull σ (5%) and ϵ (10%)
- increasing brain ϵ (8%)
- increasing filler ϵ (9%)

These trends may be thus explained:

- a highly lossy skin layer, i.e. one with a higher water content, absorbs a lot of energy, protecting the rest of the head tissues
- deconstructive interference of the EMF at the superposition of different dielectric layers is likely responsible for the patterns described above

The **worst case scenario for high SAR in the skin** is predicted by this model to be at highest skin conductivity ($\sigma = 0.61$).

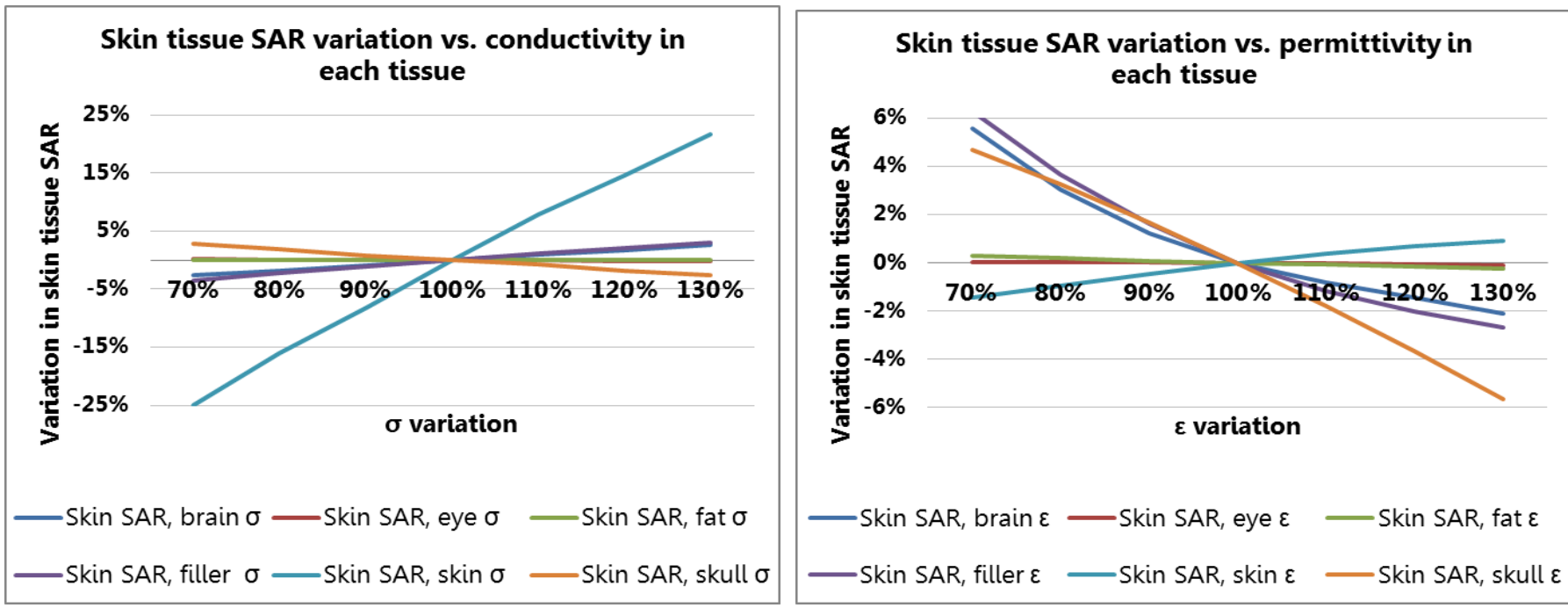


Figure 43: SAR variations in the skin tissue with dielectric properties in all tissues

Table 25: SAR variations in the skin tissue with dielectric properties in all tissues

Skin SAR	70%	80%	90%	100%	110%	120%	130%	Range	Skin SAR	70%	80%	90%	100%	110%	120%	130%	Range
Skin SAR, brain σ	-3%	-2%	-1%	0%	1%	2%	3%	5%	Skin SAR, brain ϵ	6%	3%	1%	0%	-1%	-1%	-2%	8%
Skin SAR, eye σ	0%	0%	0%	0%	0%	0%	0%	0%	Skin SAR, eye ϵ	0%	0%	0%	0%	0%	0%	0%	0%
Skin SAR, fat σ	0%	0%	0%	0%	0%	0%	0%	0%	Skin SAR, fat ϵ	0%	0%	0%	0%	0%	0%	0%	1%
Skin SAR, filler σ	-4%	-2%	-1%	0%	1%	2%	3%	7%	Skin SAR, filler ϵ	6%	4%	2%	0%	-1%	-2%	-3%	9%
Skin SAR, skin σ	-25%	-16%	-8%	0%	8%	15%	22%	47%	Skin SAR, skin ϵ	-1%	-1%	0%	0%	0%	1%	1%	2%
Skin SAR, skull σ	3%	2%	1%	0%	-1%	-2%	-3%	5%	Skin SAR, skull ϵ	5%	3%	2%	0%	-2%	-4%	-6%	10%

3.6.13 What tissues' dielectric properties affect SAR in the skull?

Increasing skull σ in Figure 44 and Table 26 below is seen to increase SAR in the skull, while the opposite is true of skull permittivity. The reverse trend is seen with respect to skin dielectric properties and skull SAR; high skin absorbance is correlated with lower SAR in the next tissue layer. Other tissues' σ and ϵ show a lesser or no effect on skull SAR, often with a complex relationship.

Skull SAR is unaffected by:

- changes in eye and fat ϵ and σ
- increasing filler σ , increasing brain σ (SAR changes by 3-4% at the range of σ used here, though a relationship does exist, which may cause high skull SAR at extremely high values of brain and filler σ values)

Skull SAR increases monotonously with (figures in brackets denote the range of SAR change):

- increasing skull σ (51%)
- increasing skin ϵ (5%)

Skull SAR decreases with:

- increasing skin σ (13%) and skin ϵ (5%)
- increasing filler ϵ (13%)
- increasing brain ϵ (13%)

These trends may be explained by:

- a protective effect is evident here, where higher conductivity in the outer layer of the skull causes lower SAR deeper within the head figure
- higher permittivity in the inner layers is associated with lower skull SAR and skin SAR, likely due to constructive or deconstructive interference at the boundaries between multiple dielectrics
- complex relationship between skull σ and skull SAR are likely due to the changing location of the highest SAR, from the ear to further inside the head; it is likely that

there are two SAR peaks on either side of the skull tissue (inside and outside), and the point of actual maximum varies somewhat as skull σ increases

The worst case scenario for high skull SAR is at high skull conductivity ($\sigma = 0.31$ S/m) and low skull permittivity ($\epsilon = 11.62$).

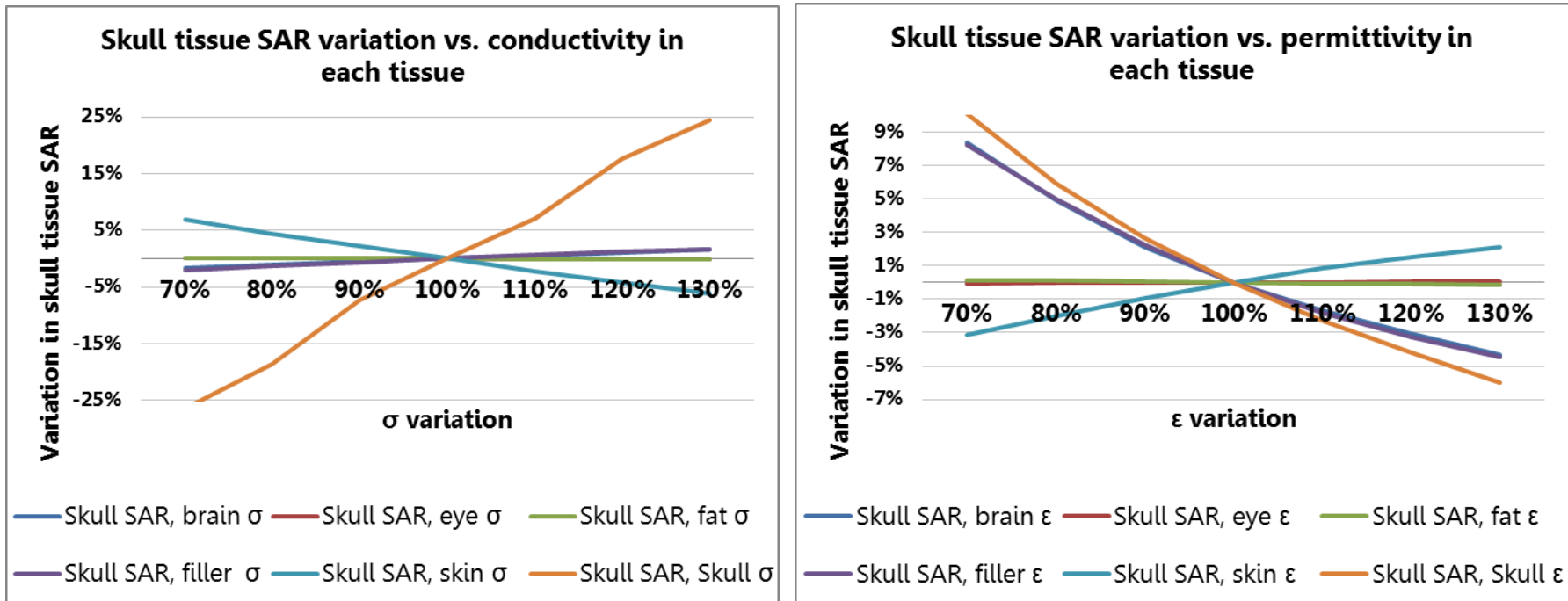


Figure 44: SAR variations in the skull tissue with dielectric properties in all tissues

Table 26: SAR variations in the skull tissue with dielectric properties in all tissues

Skull SAR	70%	80%	90%	100%	110%	120%	130%	Range	Skull SAR	70%	80%	90%	100%	110%	120%	130%	Range
Skull, brain σ	-2%	-1%	-1%	0%	1%	1%	2%	3%	Skull, brain ϵ	8%	5%	2%	0%	-2%	-3%	-4%	13%
Skull, eye σ	0%	0%	0%	0%	0%	0%	0%	0%	Skull, eye ϵ	0%	0%	0%	0%	0%	0%	0%	0%
Skull, fat σ	0%	0%	0%	0%	0%	0%	0%	0%	Skull, fat ϵ	0%	0%	0%	0%	0%	0%	0%	0%
Skull, filler σ	-2%	-1%	-1%	0%	1%	1%	2%	4%	Skull, filler ϵ	8%	5%	2%	0%	-2%	-3%	-4%	13%
Skull, skin σ	7%	4%	2%	0%	-2%	-4%	-6%	13%	Skull, skin ϵ	-3%	-2%	-1%	0%	1%	2%	2%	5%
Skull, skull σ	-26%	-19%	-7%	0%	7%	18%	24%	51%	Skull, skull ϵ	10%	6%	3%	0%	-2%	-4%	-6%	16%

3.6.14 General trends

Tissues in this model may be loosely grouped into three types: outer protective layers (skin and skull); large-volume cavity fillers (brain, filler); and low-volume (eyes, fat). Some interesting trends are seen across those groupings when dielectric properties of tissues are varied.

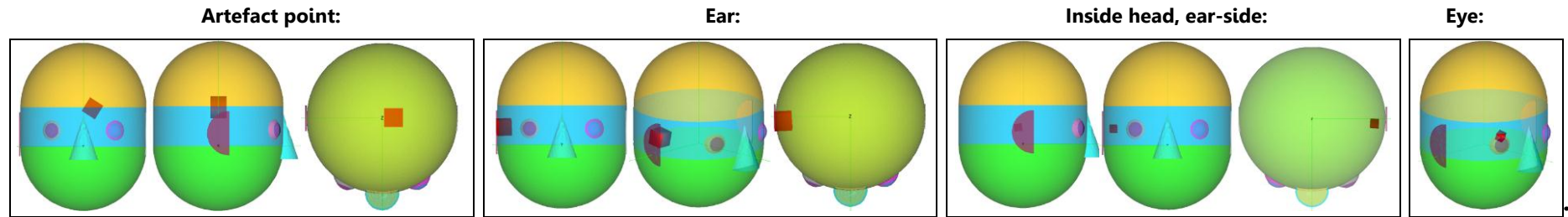
- as expected, the highest SAR in any given tissue is predicted by this model to occur when the conductivity of that tissue is highest
- altering the conductivity of the cavity-filler tissues alters their SAR by 3%; of the small tissues, 10-30%; of the outer layers, about 23%
- dielectric variations in small-volume tissues (eye, fat) do not affect the SAR in any other tissue, or the WHA SAR; 1g SAR varies by 20% over a ± 30 range of σ and ϵ of eye and fat tissues, however when increasing the averaging to 10g of contiguous tissue, the effect of those variations drop to about 3%
- altering the ϵ of either of the cavity-filler tissues over a $\pm 30\%$ range is associated with a 2% increase in SAR in the other cavity-filler tissue
- skull ϵ does not significantly affect SAR in either head or filler tissue, but increased skin ϵ is associated with a 5% increase in the SAR of both those tissues
- increased filler σ is associated with increased SAR in the skin, but decreased SAR in the skull
- small-volume tissues are unaffected by dielectric property variations in the brain, likely due to significant distal separation in this model
- increased skull ϵ lowers the SAR in both small-volume tissues (12% variation in eye SAR, 7% in fat SAR)
- increased skin σ lowers SAR of both eye and fat tissues by 8% and 11% respectively
- increasing filler σ is associated with increased SAR in both the eye and the fat tissues (by 6% and 14% respectively)
- a 30% increase in eye and fat SAR is associated with increased eye ϵ
- changes in fat σ do not affect eye SAR in the range tested here, but eye σ does decrease fat SAR by 10%

Unexpected highs and lows are seen at various permutations of tissue variations; these are likely due to the complex dielectric makeup of the head, even in such a simplified model as the Geometry Head. Constructive and deconstructive interference occurs at tissue boundaries, creating reflections and attenuations of the EM signal.

Table 27: Location of 1g and 10g peak spatial SARs. Images show examples of 1g and 10g locations as described in the table; exact location vary

Conductivity								Permittivity							
Brain	70%	80%	90%	100%	110%	120%	130%	Brain	70%	80%	90%	100%	110%	120%	130%
1g	Artefact point*	Artefact point*	Eye	Eye	Eye	Eye	Inside head	1g	Inside head	Inside head	Inside head	Eye	Eye	Eye	Artefact point*
10g	Artefact point*	Artefact point*	Ear	Ear	Ear	Ear	Ear	10g	Ear	Ear	Ear	Ear	Ear	Ear	Ear
Eye	70%	80%	90%	100%	110%	120%	130%	Eye	70%	80%	90%	100%	110%	120%	130%
1g	Inside head	Inside head	Inside head	Eye	Eye	Eye	Eye	1g	Inside head	Inside head	Eye	Eye	Eye	Eye	Eye
10g	Inside head	Inside head	Inside head	Inside head	Inside head	Inside head	Inside head	10g	Inside head	Inside head	Inside head	Inside head	Inside head	Inside head	Inside head
Fat	70%	80%	90%	100%	110%	120%	130%	Fat	70%	80%	90%	100%	110%	120%	130%
1g	Inside head	Inside head	Eye	Eye	Eye	Eye	Eye	1g	Eye	Eye	Eye	Eye	Inside head	Inside head	Inside head
10g	Ear	Ear	Inside head	Ear	Inside head	Inside head	Inside head	10g	Ear	Ear	Ear	Ear	Ear	Ear	Ear
Head	70%	80%	90%	100%	110%	120%	130%	Head	70%	80%	90%	100%	110%	120%	130%
1g	Eye	Eye	Eye	Eye	Ear	Ear	Ear	1g	Inside head	Inside head	Inside head	Eye	Eye	Eye	Eye
10g	Ear	Ear	Ear	Ear	Ear	Ear	Ear	10g	Inside head	Inside head	Inside head	Ear	Inside head	Inside head	Inside head
Skin	70%	80%	90%	100%	110%	120%	130%	Skin	0%	80%	90%	100%	110%	120%	130%
1g	Inside head	Inside head	Inside head	Eye	Eye	Eye	Eye	1g	Eye	Eye	Eye	Eye	Inside head	Inside head	Inside head
10g	Inside head	Inside head	Inside head	Ear	Ear	Ear	Ear	10g	Ear	Ear	Ear	Ear	Ear	Ear	Ear
Skull	70%	80%	90%	100%	110%	120%	130%	Skull	70%	80%	90%	100%	110%	120%	130%
1g	Eye	Eye	Eye	Eye	Eye	Eye	Eye	1g	Eye	Eye	Eye	Eye	Eye	Eye	Ear side
10g	Inside head	Inside head	Inside head	Inside head	Inside head	Inside head	Inside head	10g	Inside head	Inside head	Inside head	Inside head	Inside head	Inside head	Inside head

* These results are explained in the text, and should be ignored



3.6.15 When the dielectric properties of a single tissue vary, what happens to the rest of the tissues in the GH model?

Figure 45 shows the raw SAR values in each tissue in the GH model, as the σ and ϵ of an individual tissue are altered to ± 30 of the initial value. The SAR values have been scaled to a power density of the plane wave of 10 W/m^2 . The minima, maxima and range of SARs in each tissue are shown in Table 29.

The highest SAR values are found in the skin tissue (0.160 - 0.260 W/kg), followed in order by eye (0.098 - 0.144 W/kg); filler, WHA and brain in a close range (0.080 - 0.103 W/kg); fat (0.038 - 0.062); and skull (0.020 - 0.034).

The skin tissue also shows the highest variability in SAR with a range of 0.100 W/kg, more than double the next highest (eye SAR, 0.046 W/kg). As noted in Section 3.6.8 above, the highest variability in any tissue's SAR occurs when the dielectric properties of that tissue are altered. SAR values in the rest of the tissues stay more or less the same under those conditions.

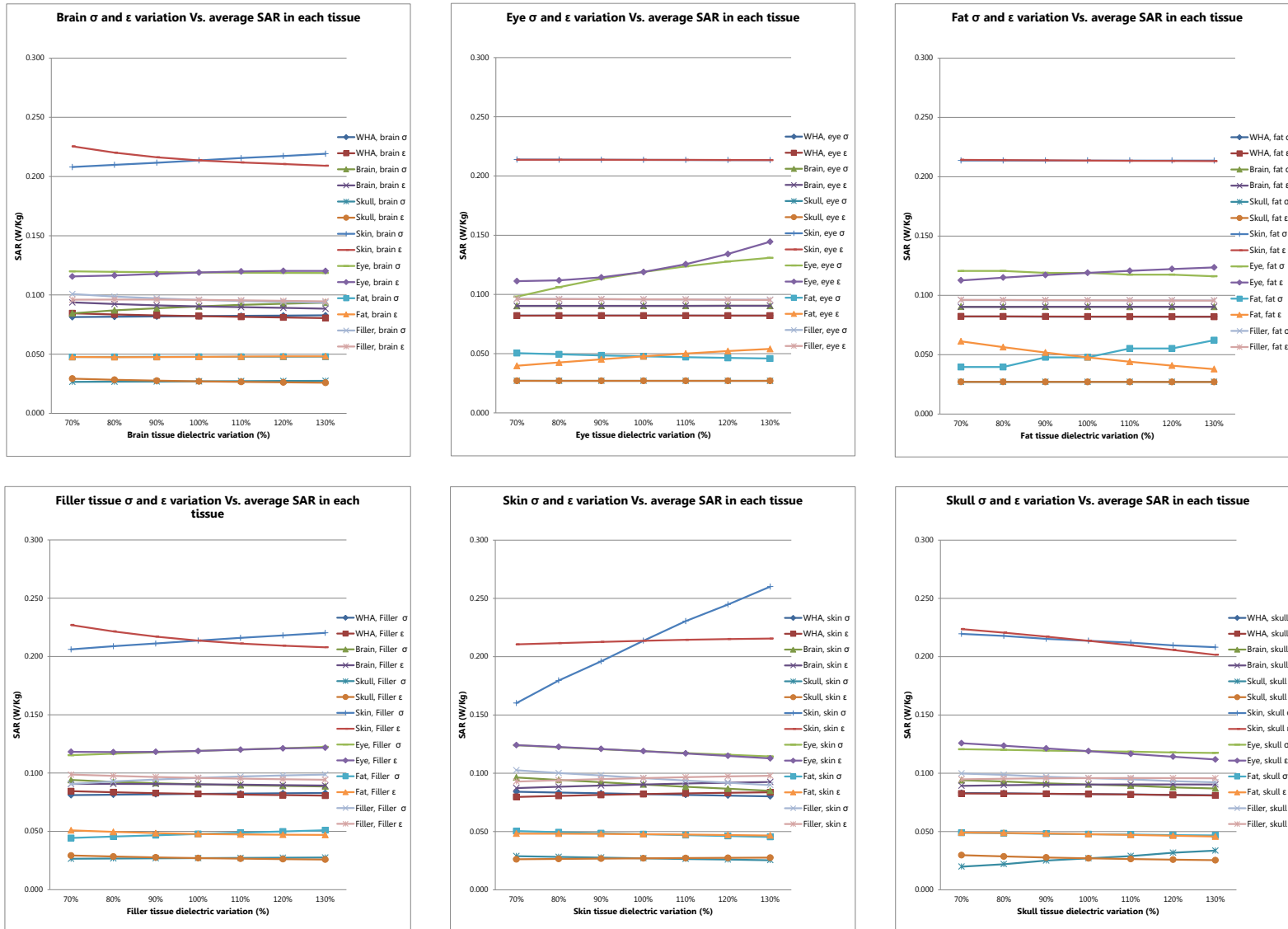


Figure 45: SAR changes in each tissue as the conductivity and permeability of one tissue are altered; values are detailed in Table 28

Table 28: SAR changes in each tissue as the conductivity and permeability of one tissue are altered; these results are graphed in Figure 45

Brain σ and ϵ		SAR (W/kg)						
Conductivity	70%	80%	90%	100%	110%	120%	130%	Range
WHA, brain σ	0.081	0.082	0.082	0.082	0.082	0.083	0.083	0.002
Brain, brain σ	0.085	0.087	0.089	0.090	0.092	0.093	0.093	0.009
Skull, brain σ	0.027	0.027	0.027	0.027	0.027	0.027	0.027	0.001
Skin, brain σ	0.208	0.210	0.212	0.214	0.216	0.217	0.219	0.011
Eye, brain σ	0.120	0.119	0.119	0.119	0.119	0.119	0.119	0.001
Fat, brain σ	0.048	0.048	0.048	0.048	0.048	0.048	0.048	0.000
Filler, brain σ	0.101	0.099	0.097	0.096	0.095	0.094	0.094	0.007
Permittivity	70%	80%	90%	100%	110%	120%	130%	Range
WHA, brain ϵ	0.084	0.084	0.083	0.082	0.082	0.081	0.080	0.004
Brain, brain ϵ	0.094	0.092	0.091	0.090	0.090	0.089	0.088	0.005
Skull, brain ϵ	0.029	0.028	0.028	0.027	0.027	0.026	0.026	0.003
Skin, brain ϵ	0.225	0.220	0.216	0.214	0.212	0.211	0.209	0.016
Eye, brain ϵ	0.116	0.116	0.118	0.119	0.120	0.120	0.120	0.005
Fat, brain ϵ	0.048	0.047	0.048	0.048	0.048	0.048	0.048	0.001
Filler, brain ϵ	0.096	0.096	0.096	0.096	0.095	0.095	0.095	0.001

Eye σ and ϵ		SAR (W/kg)						
Conductivity	70%	80%	90%	100%	110%	120%	130%	Range
WHA, eye σ	0.082	0.082	0.082	0.082	0.082	0.082	0.082	0.000
Brain, eye σ	0.090	0.090	0.090	0.090	0.090	0.090	0.090	0.000
Skull, eye σ	0.027	0.027	0.027	0.027	0.027	0.027	0.027	0.000
Skin, eye σ	0.214	0.214	0.214	0.214	0.214	0.213	0.213	0.000
Eye, eye σ	0.098	0.106	0.113	0.119	0.124	0.128	0.131	0.033
Fat, eye σ	0.050	0.049	0.049	0.048	0.047	0.046	0.046	0.005
Filler, eye σ	0.096	0.096	0.096	0.096	0.096	0.096	0.096	0.001
Permittivity	70%	80%	90%	100%	110%	120%	130%	Range
WHA, eye ϵ	0.082	0.082	0.082	0.082	0.082	0.082	0.082	0.000
Brain, eye ϵ	0.090	0.090	0.090	0.090	0.090	0.090	0.090	0.000
Skull, eye ϵ	0.027	0.027	0.027	0.027	0.027	0.027	0.027	0.000
Skin, eye ϵ	0.214	0.214	0.214	0.214	0.214	0.214	0.213	0.000
Eye, eye ϵ	0.111	0.112	0.114	0.119	0.126	0.134	0.144	0.033
Fat, eye ϵ	0.040	0.043	0.045	0.048	0.050	0.052	0.054	0.014
Filler, eye ϵ	0.096	0.096	0.096	0.096	0.096	0.096	0.095	0.001

Fat σ and ϵ		SAR (W/kg)						
Conductivity	70%	80%	90%	100%	110%	120%	130%	Range
WHA, fat σ	0.082	0.082	0.082	0.082	0.082	0.082	0.082	0.000
Brain, fat σ	0.090	0.090	0.090	0.090	0.090	0.090	0.090	0.000
Skull, fat σ	0.027	0.027	0.027	0.027	0.027	0.027	0.027	0.000
Skin, fat σ	0.214	0.214	0.214	0.214	0.214	0.214	0.214	0.000
Eye, fat σ	0.121	0.121	0.119	0.119	0.117	0.117	0.116	0.005
Fat, fat σ	0.040	0.040	0.048	0.048	0.055	0.055	0.062	0.023
Filler, fat σ	0.096	0.096	0.096	0.096	0.096	0.096	0.096	0.000
Permittivity	70%	80%	90%	100%	110%	120%	130%	Range
WHA, fat ϵ	0.082	0.082	0.082	0.082	0.082	0.082	0.082	0.000
Brain, fat ϵ	0.090	0.090	0.090	0.090	0.090	0.090	0.090	0.000
Skull, fat ϵ	0.027	0.027	0.027	0.027	0.027	0.027	0.027	0.000
Skin, fat ϵ	0.214	0.214	0.214	0.214	0.213	0.213	0.213	0.001
Eye, fat ϵ	0.113	0.115	0.117	0.119	0.121	0.122	0.124	0.011
Fat, fat ϵ	0.061	0.056	0.052	0.048	0.044	0.041	0.038	0.023
Filler, fat ϵ	0.096	0.096	0.096	0.096	0.096	0.096	0.096	0.001

Filler σ and ϵ		SAR (W/kg)						
Conductivity	70%	80%	90%	100%	110%	120%	130%	Range
WHA, Filler σ	0.081	0.081	0.082	0.082	0.082	0.083	0.083	0.002
Brain, Filler σ	0.094	0.092	0.091	0.090	0.090	0.089	0.089	0.006
Skull, Filler σ	0.026	0.027	0.027	0.027	0.027	0.027	0.028	0.001
Skin, Filler σ	0.206	0.209	0.211	0.214	0.216	0.218	0.220	0.014
Eye, Filler σ	0.115	0.117	0.118	0.119	0.120	0.121	0.122	0.007
Fat, Filler σ	0.044	0.046	0.047	0.048	0.049	0.050	0.051	0.007
Filler, Filler σ	0.091	0.093	0.094	0.096	0.097	0.098	0.099	0.008
Permittivity	70%	80%	90%	100%	110%	120%	130%	Range
WHA, Filler ϵ	0.084	0.084	0.083	0.082	0.082	0.081	0.081	0.004
Brain, Filler ϵ	0.091	0.091	0.091	0.090	0.090	0.090	0.089	0.001
Skull, Filler ϵ	0.029	0.028	0.028	0.027	0.027	0.026	0.026	0.003
Skin, Filler ϵ	0.227	0.221	0.217	0.214	0.211	0.209	0.208	0.019
Eye, Filler ϵ	0.118	0.118	0.118	0.119	0.120	0.121	0.122	0.004
Fat, Filler ϵ	0.051	0.050	0.048	0.048	0.047	0.047	0.047	0.004
Filler, Filler ϵ	0.099	0.098	0.097	0.096	0.095	0.095	0.094	0.004

Skin σ and ϵ		SAR (W/kg)						
Conductivity	70%	80%	90%	100%	110%	120%	130%	Range
WHA, skin σ	0.084	0.083	0.083	0.082	0.081	0.081	0.080	0.004
Brain, skin σ	0.096	0.094	0.092	0.090	0.088	0.087	0.085	0.012
Skull, skin σ	0.029	0.028	0.028	0.027	0.026	0.026	0.025	0.004
Skin, skin σ	0.160	0.180	0.196	0.214	0.230	0.245	0.260	0.100
Eye, skin σ	0.124	0.122	0.121	0.119	0.117	0.116	0.114	0.010
Fat, skin σ	0.050	0.049	0.049	0.048	0.047	0.046	0.045	0.005
Filler, skin σ	0.103	0.100	0.098	0.096	0.094	0.092	0.090	0.013
Permittivity	70%	80%	90%	100%	110%	120%	130%	Range
WHA, skin ϵ	0.080	0.081	0.081	0.082	0.083	0.083	0.084	0.004
Brain, skin ϵ	0.087	0.088	0.089	0.090	0.091	0.092	0.092	0.005
Skull, skin ϵ	0.026	0.027	0.027	0.027	0.027	0.027	0.028	0.001
Skin, skin ϵ	0.211	0.212	0.213	0.214	0.214	0.215	0.216	0.005
Eye, skin ϵ	0.124	0.123	0.121	0.119	0.117	0.115	0.113	0.011
Fat, skin ϵ	0.048	0.048	0.048	0.048	0.047	0.047	0.047	0.002
Filler, skin ϵ	0.093	0.094	0.095	0.096	0.097	0.097	0.098	0.005

Skull σ and ϵ		SAR (W/kg)						
Conductivity	70%	80%	90%	100%	110%	120%	130%	Range
WHA, skull σ	0.083	0.083	0.082	0.082	0.082	0.081	0.081	0.002
Brain, skull σ	0.094	0.093	0.091	0.090	0.089	0.088	0.087	0.007
Skull, skull σ	0.020	0.022	0.025	0.027	0.029	0.032	0.034	0.014
Skin, skull σ	0.220	0.218	0.215	0.214	0.212	0.210	0.208	0.011
Eye, skull σ	0.121	0.120	0.119	0.119	0.119	0.118	0.117	0.003
Fat, skull σ	0.049	0.049	0.048	0.048	0.047	0.047	0.047	0.002
Filler, skull σ	0.100	0.099	0.097	0.096	0.095	0.093	0.092	0.008
Permittivity	70%	80%	90%	100%	110%	120%	130%	Range
WHA, skull ϵ	0.083	0.083	0.082	0.082	0.082	0.081	0.081	0.002
Brain, skull ϵ	0.089	0.090	0.090	0.090	0.090	0.090	0.090	0.001
Skull, skull ϵ	0.030	0.029	0.028	0.027	0.026	0.026	0.025	0.004
Skin, skull ϵ	0.224	0.221	0.217	0.214	0.210	0.206	0.202	0.022
Eye, skull ϵ	0.126	0.124	0.121	0.119	0.117	0.114	0.112	0.014
Fat, skull ϵ	0.049	0.049	0.048	0.048	0.047	0.046	0.046	0.003
Filler, skull ϵ	0.095	0.095	0.096	0.096	0.096	0.096	0.096	0.001

Table 29: minimum, maximum and range of SAR in each tissue, as the σ and ϵ of individual tissues is altered to $\pm 30\%$

Tissue	Minimum SAR (W/kg)	Maximum SAR (W/kg)	Range SAR (W/kg)
WHA	0.080	0.084	0.005
Brain	0.085	0.096	0.012
Eye	0.098	0.144	0.046
Fat	0.038	0.062	0.024
Filler	0.090	0.103	0.013
Skin	0.160	0.260	0.100
Skull	0.020	0.034	0.014

3.6.16 Summary

The conductivity and permittivity of tissues in the head, varied in a 60% range, are predicted by the Geometry Head model to affect SAR in individual tissues by up to about $\pm 25\%$ and affect 1g and 10g SAR by at most 5%. These results agree with previous work by Keshvari, Christ and others (Christ, Klingenbock et al. 2006; Keshvari, Keshvari et al. 2006). In line with others' work, results of this study further suggest that dielectric properties of tissues nearest the source, and closest to the surface play a greater part in SAR. More detail is provided below.

3.6.17 SAR in the brain

SAR in the brain varies by 10% or less due to most σ and ϵ variations in different tissues; it is not affected by eye or fat dielectric properties at all. Increasing skin conductivity over a 60% range is associated with a 13% decrease in brain SAR. The relationships between brain SAR and tissues' σ and ϵ are for the most part monotonous, so important to note.

Changing the brain's dielectric properties by $\pm 30\%$ has little effect on SAR of different tissues, except those of skin and brain. Using the Geometry Head model, the highest WHA SAR is seen when the brain conductivity is lowest ($\sigma = 0.54$ S/m) and the permittivity is highest ($\epsilon = 59.54$).

3.6.18 SAR in the eye

SAR in the eye tissue is greatly affected by the dielectric properties of the eyes, though in a complex manner, increasing by 28% over a $\pm 30\%$ range in σ and ϵ . Dielectric property variations in other tissues create eye SAR changes in the order of 6-12%, with the greatest decreases in SAR seen with increasing ϵ of the two outer layers, skin and skull.

3.6.19 SAR in the fat

Most SAR variations in the fat tissue are in the order of 5-14%. Large changes in the order of about 50% are associated with changes in the fat tissue dielectric properties, and with eye permittivity (30%). As with the eyes, dielectric properties of tissues adjacent to the fat have a greater effect on fat SAR. Changes in eye dielectric properties show large changes in fat SAR, but the converse is not true – fat σ is not

related to eye SAR, though increasing fat ϵ is associated with increased eye SAR in this model.

3.6.20 SAR in the filler

Filler SAR is only seen to increase with increasing filler conductivity (by 8% over a 60% range of σ), and increasing skin permittivity (by 5% over the same range). All other dielectric property changes either lower the filler SAR or don't affect it, suggesting a protective skin effect. Dielectric property variations in this model mostly show a simple relationship to filler SAR. Dielectric properties of small-volume tissues, i.e. eyes and fat, do not affect filler SAR.

3.6.21 SAR in the skin

At the ranges of dielectric properties used here, it was found that a highly conductive skin layer absorbs 47% more energy than a low conductivity one, providing excellent protection to tissues deeper inside the head. Higher skin SAR is also seen, to a much lesser extent, to be associated with increasing conductivity of the large-volume inner tissues, brain and filler. A skull layer with higher ϵ or σ , directly beneath the skin in this model, will lower the SAR in the skin. SAR predictions using GH show that as, expected, a strong relationship exists between skin conductivity and absorption.

3.6.22 SAR in the skull

This model predicts high skull SAR at the highest values of skull conductivity, i.e. when the skull forms a lossy layer: a 51% increase of SAR in the skull is seen over a $\pm 30\%$ σ change. Higher permittivity in the inner, large-volume tissues (brain and filler) is associated with a 13% skull SAR decrease.

3.6.23 Overall re-distribution of SAR with dielectric property variation

The averaging mass is an important factor in assessing RF energy absorption. As SAR is averaged over larger volumes, from 1g to 10g to whole tissues, distribution is seen to be more regular. It is clear that regions of high SAR in this model occur in four specific locations: at the ear, eye, or brain region closest to the source; and at a point in the centre of the model, where an artefact exists.

This study shows that the SAR value in the head does not necessarily increase markedly with significant increases in dielectric parameters. Furthermore, the

interaction of RF energy with biological tissues such as the human head is an extremely complex biophysical phenomenon. *A priori* reasoning, such as examining of the SAR equation, may suggest that SAR bears a direct correlation to fundamental physical parameters such as tissue dielectric properties. However, far-reaching conclusions cannot be theorised for such a complex system without in-depth analysis.

Chapter 4: Further discussion

For in-depth discussion regarding validation of the Geometry Head model, and testing of individual parameters, please see Chapter 3. This section provides a summary of results, and discussion and assessment of the methodology and results of this project. Benefits of this work are also explored.

4.1 Summary and further discussion of results

Recall that all variables tested here are for adults, not children.

4.1.1 What anatomic variations affect SAR?

- Dielectric properties:
 - conductivity and permittivity of tissues in the head, varied to $\pm 30\%$ from the widely accepted values, are predicted by the Geometry Head model to affect SAR in individual tissues by up to about $\pm 25\%$
 - dielectric properties of the 6 tissue types in this model affect 1g, 10g and whole head average SAR by up to $\pm 5\%$
 - complex relationships exist between dielectric properties of the tissues and location of maximum SAR and SAR distribution, which cannot be anticipated without modelling
- Overall size of the head:
 - as head size increase, the whole head average SAR decreases; smallest head modelled here of 90% the original size of the GH model showed 11% increase in WHA SAR
 - location and value of 1g and 10g peak spatial SAR vary with increased head size, with variations of up to $\pm 15\%$ over the range tested here, with unexpected peaks in sensitive eye tissue (119% SAR increase at 95% head size model), though eye SAR values are comparatively low

4.1.2 What tested variables do not significantly affect SAR?

- cranial thickness:
 - at the range of human anatomic variation of 3.7 to 10.8 mm (5th to 95th percentiles) is not predicted to significantly affect SAR by this model
- skin thickness:
 - at the range of human anatomic variation of 0.03 to 1.86 mm (5th to 95th percentiles) has a negligible effect on SAR in this model; however, when skin thickness is increased to 5 mm, which is well outside the normal range for the face and head but is normal for other regions of the body, WHA and 10g SAR decrease by 5% and 11% respectively; where the skin thickness is increased to 10 mm, WHA drops by 27% and 10g SAR by 34%

4.1.3 Where does high SAR occur?

SAR values in different tissues

Using a plane wave exposure, the highest SAR values are found in the skin tissue, with 1g and 10g cubes often encompassing the ear ipsilateral to the plane wave (the ear is modelled as skin tissue). When a dipole exposure is used, 1g and 10g SARs are found deeper inside the head, ipsilateral to the antenna feed point.

After skin, the tissue with the next highest SAR levels is the eye, followed in order by filler tissue, brain, fat, and skull. SAR values in filler and brain tissues are similar.

Regions of high SAR

Three regions of the head are predicted by this model to experience high SAR, all of them ipsilateral to the source: the ear, the eye and inside the head, often at the brain or filler tissue medially from the ear.

4.1.4 What anatomic variations create the worst case SAR scenario?

Factors that increase SAR in the skin and eyes provide worst-case scenarios. Factors that affect SAR in the brain tissue are also counted, as this a particularly sensitive tissue.

High skin conductivity is predicted by this model to show highest SAR in the skin, but also lowest SAR in the brain, providing a protective effect. The brain SAR increase was 13% at low skin σ , as opposed to

Factors that increase skin, eye and brain SAR;

- as overall head size is varied in a range of -5 to +30%, the WHA is seen to linearly decrease with increased head size; smallest **head size of 90%** that was able to be modelled (without artefact results) is predicted to cause a 11% increase in WHA SAR and a 119% increase in SAR in the eye
- **high skin conductivity** (highest tested here was $\sigma = 0.61$ S/m) is associated with high skin SAR (increase of 47% in SAR over a 60% increase in σ)
- **high eye conductivity** (highest tested here was $\sigma = 2.13$ S/m) and high eye permittivity (highest tested $\epsilon = 89.57$) are predicted by this model to cause high eye SAR (increasing by 28% over a 60% range in σ and ϵ)

As discussed in Chapter 1, SAM was designed to provide conservative SAR estimates for all users; various studies indicate that a homogeneous, larger-sized adult male head absorbs more SAR than a woman's or child's head (Petersen 2007). Shapes of SAM parts - head, for example - cannot be altered, nor sub-parts such as 'brain', the way GH can. The only things you can alter in SAM are the dielectric properties of the model, and only en masse. Taking advantage of today's powerful computing powers, Geometry Head can provide a worst-case model with barely more effort than using SAM, and far more fidelity to real life situations.

4.2 Results in context

Table 30 to Table 32 below show results of GH model when compared with other models commonly used for RF research and compliance.

The skin thickness, skull thickness and overall head sizes of GH are comparable with other commonly used models. The results show that in most cases, resultant SAR in GH is somewhere between the homogeneous models used for compliance and the heterogeneous models, suggesting that GH provides accurate SAR predictions.

Interestingly, the Geometry Head SAR values when testing cranial thickness were found to be lower than those of the homogenous head and Norman, and quite similar to those of Visible Human.

Table 30: Cranial thickness results and consequent SAR results in GH versus other models

Model name	Model type	Cranial thickness (mm)	Whole head average SAR (W/Kg)	10g Ave SAR (W/Kg)
SAM	Homog	-	0.043	0.27
Geometry Head	Semi-homog	4	0.036	0.12
		6	0.036	0.13
		11	0.035	0.13
VH	Hetero	3 - 16	0.034	0.15
Norman		2 - 13	0.043	0.19

Table 31: Skin thickness and consequent SAR results in GH versus other models

Model name	Model type	Skin thickness (mm)	1g SAR (W/Kg)	10g SAR (W/Kg)
SAM	Homog	-	0.66	0.27
Geometry Head	Semi-homog	1	0.37	0.27
		2	0.36	0.29
		5	0.35	0.25
		10	0.34	0.19
Visible Human	Hetero	1 - 2	0.59	0.15
Norman		1 - 2	0.73	0.19

Skin thicknesses of human anatomic range of 1 and 2 mm at 0.31 and 0.30 W/kg respectively, are comparable with those of other computational models. GH SAR results are lower than those of the SAM (0.27 W/kg), and higher than those of the heterogeneous models (0.15 W/kg for VH and 0.19 for NORMAN). Being homogeneous, the SAM model does not have a separate skin tissue. Skin thickness of VH and Norman models is dependent on mesh size - 1.5 mm and 2 mm respectively, however some areas contain no skin voxels (skin thickness of zero).

Table 32: Dimensions of GH and commonly used models (heads only)

Model name	Model type	Height x Breadth (mm)	1g SAR (W/Kg)	10g SAR (W/Kg)
SAM	Homog	228 x 190	0.66	0.27
GH	Semi-homog	230 x 176	0.36	0.29
GH 90%		207 x 158	0.32	0.25
GH 130%		299 x 229	0.36	0.26
VH	Hetero	226 x 236	0.59	0.15
Norman		296 x 238	0.73	0.19

Dimensions of the GH model are comparable to other commonly used models, as seen in Table 32. The largest GH head modelled here (130% size of the original) is of a quite similar size to Norman. SAR results of GH are about half those of both SAM and the highly heterogeneous models.

The dielectric property results of this study agree with previous work such as performed by Keshvari (Keshvari, Keshvari et al. 2006), Christ (Christ and Kuster 2005); Bashayreh (Bashayreh, Omar et al. 2010) and Cerri (Cerri, De Leo et al. 1997) that suggests that dielectric properties of tissues affect SAR by $\pm 10\%$ or less.

4.3 Validity of results

The map is not the territory; it is important to remember that a model is only as good as its input parameters. If the parameters chosen to represent reality were not appropriate, the model's predictions are meaningless.

Effort was made to use best practice methodology in modelling the human head according to features known or reasoned to be contributing factors for energy absorption of RF, without sacrificing ease of use. This model is intended to provide a point of diminishing returns in complexity, where adding more complexity would not add much more accuracy of results.

4.3.1 What other factors could be included in the model?

It is difficult to answer this question without including more parameters in the model and testing their effects on SAR. The relationship between SAR and anatomic variations are complex, and cannot be determined by *a priori* reasoning. For example, although skin absorbs the most SAR, the thickness and dielectric properties of this tissue at the ranges of human variation (0.05 – 2 mm, though only 1 and 2 mm values were tested) has little effect on SAR distribution; variations in skin dielectric properties affect whole head SAR very little, but cause increases in individual tissue SAR distributions. It is likely that including more tissue layers between the skull and the skin, of alternating high- and low-conductivity such as muscle and fat respectively, would produce different energy absorption patterns. The GH model is available for general use and such amendments are easy to implement.

Tissues inside the skull are mostly of similar dielectric properties. As such, it is unlikely that including them in this model would add much accuracy. Another anatomic variation that may affect SAR which is not currently incorporated into GH is an ear canal. This would be easy to implement (possibly as a conic air gap) and not prohibitively difficult to measure in humans for personal adjustments of the model.

Another advantage of this model is the relative ease with which complexity (such as added layers and features) may be added. This, however, is outside the scope of this project.

4.3.2 Uncertainty

4.3.2.1 *Computational modelling*

Software rounding errors using today's powerful machines are minimal.

Computational techniques are now regarded as equally effective to measured results in the area of RF dosimetry, where they techniques allow the study of complex system and natural phenomena that would be too costly, time consuming, dangerous, and often impossible to study directly by experimentation. Significant progress has resulted from rapid and powerful advances in computer algorithms and architecture, enabling computational scientists and engineers to solve, with relative accuracy, large-scale problems that were once thought intractable. Little to no uncertainty is introduced via numerical solving approximation. A literature search was undertaken to quantify accuracy of FEKO code against canonical models, none was found. Information from the software manufacturers suggests this has been thoroughly tested with satisfactory results.

The reduced tissue set is a mixed blessing. On the one hand, it is an approximation of reality, which introduces uncertainty. On the other, using fewer tissues reduces uncertainty.

The artefact described in Chapter 3 (see Section 3.5 for a thorough discussion) causes an unrealistically high SAR region at the 'brain'-'filler' interface, and some SAR results have been discarded during parameter testing due to that. It is unlikely that the overall SAR patterns are much distorted by internal reflections from the artefact, as all other regions of high SAR in GH correspond with predictions of existing models.

Dielectric properties, relative sizes and morphologies of tissues were chosen to approximate reality as much as possible given available knowledge based on extensive literature review. Few anthropometric studies provide detailed descriptions of anthropomorphic standardisation methods, much less statistical analysis of measurement reliability assessments. If superior information is found, parameters of Geometry Head can be easily adjusted to better represent reality.

4.3.2.2 *Physical modelling*

The DASY4 system, and the testing apparatus setup at the Ericsson Research Laboratories, Sweden, are designed for, and are almost exclusively, used for

compliance testing. Work involved using entirely non-standard phantoms, which severely hampered the explorations that could be performed. It was not possible, for example, to test SAR in tissues other than the 'brain'.

However, all tests were undertaken in a laboratory that routinely performs compliance-quality SAR testing using refined techniques, calibrated equipment and with support from highly qualified and experienced staff. Results can therefore be assumed to be of the same high quality as any other measured work reported on in literature.

Uncertainty of physical measurements can be broken down into the several categories described below.

SAR assessment uncertainty is related to evaluating the peak spatial-average SAR value of the SAR distribution produced by for the specific exposure condition with the specified setup configuration. These include measurement and calibration tolerances in the instrumentation, uncertainties in the algorithms used to process the data, and other equipment related variations and tolerances.

Uncertainties introduced by the DASY4 system have been well quantified by its manufacturers at under $\pm 25\%$ (Speag 2008), see Appendix D for a full uncertainty budget. The highest source of uncertainty in DASY ($\pm 9.6\%$) is the hemispherical isotropy; the next highest is probe calibration, with an uncertainty value of $\pm 5.9\%$. Care was taken to meet the minimal software and hardware requirements for low DASY uncertainty. For example, the minimum size of measurement grid used was of $7 \times 7 \times 7$ points with 5 mm resolution, whereby the uncertainty of the extrapolation routines is less than $\pm 1\%$ for 1g and 10g SAR cubes.

Source uncertainty due to variations of operating parameters such as drift of output power due to changes in battery voltages, operating frequency, signal modulation, antenna performance, and other device performance tolerances, can produce significant variations in the measured SAR (IEEE 2003). Experiments were performed using a test system designed to comply with the $\pm 30\%$ variability in SAR results as specified by measurement standards (IEEE 2003).

Test position uncertainty due to deviations of source positioning uncertainties may have been introduced here. Efforts were made to ensure dipole was positioned flush with the phantom and within 1 mm of the Ear Reference Point, however even small variations in position can produce significant changes in SAR distributions (IEEE 2003). It is suspected that the low SAR values seen in the heterogeneous adult model with 'eyes' are due to relatively high separation of the dipole from the phantom, which affected the RF coupling. These results are included for observation but are discounted.

Phantom uncertainty describes the variations in SAR introduced by differences in the dielectric parameters of the tissue-equivalent liquid used during the measurement and the target parameters specified by the protocol.

Potential human errors in constructing the models, for example existence of air bubbles in equivalent tissue liquids, were kept to a minimum, but cannot be discounted. It is estimated that human error contributed no more than 20% to the uncertainty factor. Due to the difficulty of measuring dielectric properties of high-viscosity tissue-equivalent liquids, likely due to inhomogeneity of supersaturated solutions, variation of up to 15% was considered acceptable (measurement standards recommend no more than $\pm 5\%$ variation). This would have affected the calculation of SAR by the DASY software, and the matching of computational to physical parameters and consequent GH SAR predictions by 15%. As Gabriel et al. noted in a paper discussing uncertainty analysis of tissue simulating liquids (Gabriel and Peyman 2006), in practice, for most tissue types the random inhomogeneity is by far the greatest source of error.

Variations between dimensions of anatomies in physical and computational models were kept to within $\pm 10\%$ as much as possible. Exact reproductions of the physical models (or real human heads) are not possible due to the approximation of using geometrical shapes; for example, heads are not spheroids, and noses are not conic.

4.3.3 Limitations of the model

4.3.3.1 Limited tissue set

The tissue set of GH model may be expanded, and this is encouraged by the author. For example, adding several layers of tissue between the skin and the skull layers

would be a relatively simple exercise. The model as it stands has 6 tissues and all the features considered *a priori* as relevant to SAR analysis. As seen in Section 3.2, it is possible to turn GH into a homogeneous model (as is possible for all multi-tissue models, but altering the dielectric properties of all tissues to the same values).

A drawback of the low granularity of this model when compared to the highly heterogeneous ones is a reduced ability to distinguish which exact tissue within the head is experiencing higher SAR. Using VH or NORMAN, for example, it is possible to see absorption patterns in up to 42 separate tissues. On the other hand, the benefit of relatively low complexity is the ability to get a 'quick and dirty' estimation of a single individual's SAR, without the expense and time of high-resolution medical imaging. If the individual's SAR is within the safety limits, no further explorations need be undertaken.

4.3.3.2 *Artefact*

A known artefact exists in this model which creates unrealistically high SAR predictions inside the model. This is discussed in full in Section 3.5. Some results have been ignored, however overall SAR patterns are clearly discernible using this model.

4.3.3.3 *Thermoregulation*

As discussed in Section 1.1, the SAR metric serves as an analogue to temperature change, which is the only measurable effect of low level RF exposure. Like all other human models used for RF dosimetry, the GH model takes into account different tissues' water content and dielectric properties, but does not account for blood perfusion or the thermoregulatory effects of a living mammalian organism. It cannot estimate thermal change, only energy absorption patterns.

4.4 Critical analysis of methods

4.4.1 Computational modelling

4.4.1.1 *Modelling package*

FEKO was seen to be a suitable modelling package for this model. Parametrically adjustable anatomic variations were able to be incorporated into the model with relative ease, a critical requirement. In earlier versions of the software, edge cases were found, where certain variable combinations could not be solved. This ceased to be a problem in the current version (v6.21). The software allows determination of relevant SAR metrics such as whole head average, 1g and 10g SAR, SAR plots within the entire model, and point SAR.

4.4.1.2 *Model construction*

The GH model works well for its intended purpose: it is successfully parametrically adjustable for all tissue variations explored in this work. For example, adjusting the interpupillary breadth moves the eyes laterally around the circumference of the head, rather than in a single dimension on the frontal plane; the skin thickness on the nose remains constant regardless of skin thickness or position on the nose, modelled as a conic section; adjusting the dimension of any one tissue creates automatic proportional adjustments in all other dimensions to keep the model's integrity. The entire model can also be easily adjusted to incorporate more or fewer tissues and features.

4.4.1.3 *Parameters incorporated into the model*

Features incorporated into the model such as eyes, brains, skull, skin and ear all showed some contribution towards SAR magnitude and distribution, suggesting they were correctly chosen. The use of the adult Caucasian head for initial base-level variables provided comparability with how results of this work fit within the context of existing scientific exploration in the field.

4.4.2 Physical modelling

4.4.2.1 *Model construction*

Parameters incorporated into the model are seen in Section 3.2 to alter SAR metrics, indicating successful testing. Best efforts were made to work within practical resource limitations to create faithful yet simplified representations of human anatomy, with sound reasoning for all decisions made. Considerable research was made into how

best to physically model human anatomy for RF compliance. Before embarking on the phantom creation task, several maxillofacial and forensic facial reconstruction experts were consulted for advice and a moulding course was undertaken.

4.4.2.2 Model testing

A world class standards compliant measurement and exposure system and protocols were used, with support from experienced staff. Measurements taken were of a high standard.

4.5 Benefits and uses of this work

4.5.1 Parametric model

To the best of the author's knowledge, Geometry Head is the only existing human head model suitable for SAR compliance studies that allows easy adjustment of anatomic features. It serves as a highly sophisticated version of the layered sphere models used in studies, with far more scope for systematically determining relationships between individual anatomic parameters and SAR. This unique feature provides the ability to further test what relationships exist between anatomic features and energy absorption from exposure due to use of non-ionising radiation sources in popular use such as wireless communications devices.

4.5.2 Ethnic populations

The large trove of data collection regarding anatomic variations in cranial and skin thicknesses of different ethnic populations can be used to create models of different ethnic groups to ascertain whether some are not covered by the current safety limits.

4.5.3 Other frequencies

This model can very easily be adapted for testing SAR at other non-ionising frequencies by adjusting a single variable in the software.

4.5.4 Implications for safety standards

Safety limits take into account the inexactness of measurement. If it is assumed that SAR measurements have a high level of uncertainty, then the SAR limits need to be stringent; if the SAR estimation techniques can be assumed to have low uncertainty, the limits may be relaxed.

With the advent of high-powered computers and high-fidelity numerical solving techniques, computational modelling of humans for SAR estimation can often be considered as accurate as physical modelling. The new RF standard for exposure around base stations (IEC 2011) allows just that.

Existing human models used for SAR have various drawbacks. Geometry Head takes advantage of new computing power by providing less overestimation of SAR than the homogeneous phantoms currently used for compliance testing. It also has the advantage over highly homogeneous model, with its ability for quick and easy

adjustment of parameters such as relative size and location of anatomic features, and dielectric properties, to provide a close estimation of any individual's head for SAR testing.

Given that, it is not unreasonable to suggest that the use of higher fidelity models such as Geometry Head could lead to more lenient RF safety standards.

Chapter 5: Conclusions

The project described here has made some inroads into determining how certain anatomic variations in human populations impact energy absorption due to exposure to radiofrequency sources at 900 MHz. The question of whether some combinations of anatomic populations place some people in danger of exposure above the safety limits has been explored here using a novel computational model of the human head, along with extensive data collection regarding what variation exists in the skin thickness and cranial thickness of adults. The range of variability in those parameters have been described for subpopulations of different sexes, ages and ethnicities, and combined to give statistical data for overall human distributions. Though cranial & skin thickness do not affect SAR significantly at the range of human variation (5th to 95th percentile), results of SAR tests while varying dielectric properties and head tests indicate that these tissues can significantly affect maximum SAR, both location and magnitude. The tissues chosen for inclusion in the model are in fact tissues that affect SAR. As Christ et al. and Keshvari et al. (Christ, Klingenbock et al. 2006; Keshvari, Keshvari et al. 2006) have noted, the reflections and absorptions at dielectric boundaries with a combination of high – low – high – low conductivities creates worst-case SAR scenarios. In a complex structure like the human head, the effects of composition, morphology, and relative location of these layers on SAR distribution cannot be anticipated with *a priori* reasoning. Physical validation of this model suggests results obtained provide a reasonable estimate of absorption in human heads.

To assess the outcomes of this thesis the research questions defined in Section 1.3 are answered below.

5.1.1 What parameters of human anatomy contribute to absorption of energy due to RF exposure?

Results suggest that presence of skin, skull, brain, eye and fat tissues affect SAR distribution in ways that cannot be anticipated without modelling. Direct relationship is observed between decreasing head size and increased SAR, by head size and dielectric properties.

5.1.2 What variability exists in the relevant anatomic variations?

An extensive literature survey has provided a range of variability of cranial thickness and skin thickness on the head and face in adults.

5th, 50th and 95th percentiles of skin thickness in adult humans are 0.03 mm, 0.84 mm and 1.86 mm respectively. Summary results in Table XXX are split for sex (female and male), age groups (20-29, 30-39, 40-49, 50-59, 60+ years old), and ethnicity (Caucasian, African-American, unknown/unspecified) sub-populations

5th, 50th and 95th percentiles of skull thickness in adult humans were found to be 3.70 mm, 6.43 mm and 10.80 mm respectively. Summary results in Table XXX are split for sub-populations of sex (female and male), age groups (20-29, 30-39, 40-49, 50-59, 60+ years old), and ethnicity (African, African-American, Australian Aboriginal, Caucasian, Bedouin, Chinese, Japanese, unknown/unspecified).

Variations in data gathering methods and results pertaining to variability in dielectric properties of tissues rendered this a futile search; a range of $\pm 30\%$ was used to test effects of this parameter instead, as well as the parameter of adult head size.

5.1.3 What is the relationship between these anatomic parameters and SAR?

At the ranges of normal variation, skin and skull thickness do not significantly affect SAR, however their inclusion in the model is vital for accurate SAR estimations.

WHA SAR is predicted to increase with decreasing head size using this model. For the smallest viable head size modelled here, 90% the original size of the GH model, an 11% increase in WHA SAR was observed. A 119% increase eye tissue SAR is observed at the next largest head size of 95%, though SAR in the eye is low relative to other tissues. Location and value of 1g and 10g peak spatial SAR vary with increased head size, with variations of up $\pm 15\%$ over the range tested here.

Conductivity and permittivity of tissues in the head, varied to $\pm 30\%$ from the widely accepted values, are predicted by the Geometry Head model to affect SAR in individual tissues by up to about $\pm 25\%$. Dielectric properties of the 6 tissue types in this model affect 1g, 10g and whole head average SAR by up to $\pm 5\%$. Complex

relationships exist between dielectric properties of the tissues and location of maximum SAR and SAR distribution, which cannot be anticipated without modelling

5.1.4 What do these results imply for the safety standards for RF exposure?

Using today's high computing power and software capabilities, where computational estimation of SAR is as accurate as physical measurement, a more accurate model such as Geometry Head can be used to predict with higher granularity the SAR maxima and distributions in human heads, without resorting to simplified homogeneous models. This kind of parametric model can also serve to discern whether safety limits are too conservative.

While it's much simpler today than 20 years ago to create highly representative models of any person's anatomy using imaging technology and scanning algorithms, the process is still costly and resource intensive. It also fails to provide information regarding effect of population-wide anatomic variability, with many studies indicating individual differences show as much variability within a population as when compared with other populations. Epidemiological testing as provided by GH may provide the ability to determine whether the current safety standards protect all populations and individuals.

5.1.5 Given that existing models do not allow easy exploration of effect of anatomic parameters on SAR, can a new model be created without this limitation?

This question arose as a result of attempting to answer the previous research questions using pre-existing models. The Geometry Head model was custom built to allow investigation into some of the research questions presented above, and has shown to be successful at providing answers. Factors that are known or have been *a priori* reasoned to affect SAR have been included in the model, and have been made parametric and easily adjustable. The model, created using a commercially available software package, is accessible upon request. A battery of anatomic variation tests as well as physical validation work have been used to verify the model's efficacy and accuracy.

5.2 Recommendations for future research

The Geometry Head model is available for further research upon request.

5.2.1 Further explorations with the model as it stands

The Geometry Head model could benefit from some further testing of parameters, and perhaps some improvements. For example, efforts could be made to minimise the artefact in the model best described in Section 3.5 which causes unrealistically high SAR predictions at certain tissue variations.

This model can also very easily be adapted for testing SAR at other non-ionising frequencies, or at the tail ends of anatomic variation distributions, by adjusting a single variable in the software.

Further testing of how results of this model compare with existing ones could be done by editing the model variables to match those of existing heterogeneous models.

GH can also be used for SAR testing of epidemiological population variations and the implications of these results for safety standards. Anatomic variation data of several tissue properties, provided in this thesis, can be used for performing sensitivity studies to determine what combinations of anatomic variations result in exposures above the safety standard recommendations.

Another suggested use for this model is re-examining the scientific basis for current appropriateness of safety standards. Using this high accuracy model with low variability between measured and modelled results, it is possible to garner evidence for either raising or lowering exposure levels considered safe for all human populations.

5.2.2 Augmenting the model

Children's exposure to RF is currently of high public concern; augmenting GH for investigating relationships between SAR and children would be of value. Other tissues can be added to the model to test their contribution to SAR, for example fat and muscle layers between the skin and skull. Tissue layers can also be removed to simplify the model, if it is determined that their contribution to SAR results are sufficiently minor.

References

- Abdalla, A. and A. Teoh (2005). "A multi layered model of human head irradiated by electromagnetic plane wave of 100mhz-300ghz." Int. J. Sci. Res. **15**.
- Adeloye, A., K. R. Kattan, et al. (1975). "Thickness of the normal skull in the american blacks and whites." Am J Phys Anthropol. **43**(1): 23-30.
- Alanen, E., T. Lahtinen, et al. (1998). "Measurement of dielectric properties of subcutaneous fat with open-ended coaxial sensors." Phys Med Biol **43**(3): 475-485.
- Anderson, V. (2003). "Comparisons of peak SAR levels in concentric sphere head models of children and adults for irradiation by dipole at 900 MHz." Phys Med Biol **48**: 3263-3275.
- Anderson, V. and K. Joyner (1995). "Specific absorption rate levels measured in a phantom head exposed to radio frequency transmissions from analog hand-held mobile phones." Bioelectromagnetics **16**: 60-69.
- ARPANSA. (2002). "Radiation protection standard for maximum exposure levels to radiofrequency fields - 3khz to 300ghz (rps-3)."
- Baer, M. J. (1956). "Dimensional changes in the human head and face in the third decade of life." Am J Phys Anthropol **14**(4): 557-575.
- Bao, J.-Z., S.-T. Lu, et al. (1997). "Complex dielectric measurements and analysis of brain tissues in the radio and microwave frequencies." IEEE Transactions on Microwave Theory and Techniques **45**(10): 1730-1741.
- Bashayreh, Q. M., A. A. Omar, et al. (2010). The effect of RF radiation on human health using stratified human head model. Radar Conference, 2010 IEEE.
- Bassen, H. I. and T. M. Babij (1990). Experimental techniques and instrumentation. Biological effects and medical applications of electromagnetic energy. Ghandi, O. P. Englewood Cliffs, New Jersey, Prentice Hall: 141-173.
- Beard, B. and W. Kainz (2004). "Review and standardization of cell phone exposure calculations using the sam phantom and anatomically correct head models." BioMedical Engineering Online **3**(1): 34.
- Beard, B. B., W. Kainz, et al. (2006). "Comparisons of computed mobile phone induced SAR in the sam phantom to that in anatomically correct models of the human head." Electromagnetic Compatibility, IEEE Transactions on **48**(2): 397-407.
- Behari, J. and S. Singh (1981). "Bioelectric characteristics of unstressed in vivo bone." Med Biol Eng Comput **19**(1): 49-54.

- Bit-Babik, G., A. W. Guy, et al. (2005). "Simulation of exposure and SAR estimation for adult and child heads exposed to radiofrequency energy from portable communication devices." Radiation Research **163**: 580-590.
- Black, M. (1969). "A modified radiographic method for measuring skin thickness." Br J Dermatol **81**(661): 661-666.
- Bliznak, J. and T. Staple (1975). "Roentgenographic measurement of skin thickness in normal individuals." Diagnostic Radiology **116**: 55-60.
- Bo, W. (2007). Comparative study of numerically computed spatial peak SAR values in uniformly scaled sam head models exposed to mobile phone radiation. Electromagnetic Compatibility, 2007. EMC 2007. International Symposium on.
- Brown, P. (1992). "Recent human evolution in east asia and australiasia." Phil Trans Soc Lond B **337**: 235-242.
- Brown, T., Pinkerton, et al. (1979). "Thickness of the cranial vault in australian aboriginals." Arch & Phys Anthropol in Oceania **14**(1): 54-71.
- CENELEC. (2006). "EN 62209-1:2006 basic standard for the measurement of specific absorption rate related to human exposure to electromagnetic fields from mobile phones (300 MHz–3 GHz)."
- Cerri, G., R. De Leo, et al. (1997). "Evaluation of electromagnetic power deposition in a spherical multilayer head in the near field of a linear antenna." Wireless Networks **3**: 499-510.
- Chakkalakal, D. A., M. W. Johnson, et al. (1980). "Dielectric properties of fluid-saturated bone." IEEE Trans Biomed Eng **27**(2): 95-100.
- Christ, A., N. Chavannes, et al. (2005). "A numerical and experimental comparison of human head phantoms for compliance testing of mobile telephone equipment." Bioelectromagnetics **26**: 125-137.
- Christ, A., M.-C. Gosselin, et al. (2010). "Age-dependent tissue-specific exposure of cell phone users." Phys Med Biol **55**(7): 1767.
- Christ, A., W. Kainz, et al. (2010). "The virtual family—development of surface-based anatomical models of two adults and two children for dosimetric simulations." Phys Med Biol **55**(2): N23.
- Christ, A., A. Klingenbock, et al. (2006). "The dependence of electromagnetic far-field absorption on body tissue composition in the frequency range from 300 MHz to 6 GHz." Microwave Theory and Techniques, IEEE Transactions on **54**(5): 2188-2195.
- Christ, A. and N. Kuster (2005). "Differences in RF energy absorption in the heads of adults and children." Bioelectromagnetics **7**(Supplement): s31-s44.

- Churchill, E. M., John T. (1976). "Sampling and data gathering strategies for future USAF anthropometry."
- Cole, K. S. and R. M. Cole (1941). "Dispersion and absorption in dielectrics. I alternating current characteristics." J. Chem. Phys. **9**: 341.
- Dahan, S., J. M. Lagarde, et al. (2004). "Treatment of neck lines and forehead rhytids with a nonablative 1540-nm Er:Glass laser: A controlled clinical study combined with the measurement of the thickness and the mechanical properties of the skin." Dermatol Surg **30**(6): 872-879; discussion 879-880.
- De Salles, A. A., G. Bulla, et al. (2006). "Electromagnetic absorption in the head of adults and children due to mobile phone operation close to the head." Electromagnetic Biology and Medicine **25**(4): 349-360.
- Dimbylow, P. J. (1997). "FDTD calculations of the whole-body averaged SAR in an anatomically realistic voxel model of the human body from 1 MHz to 1 GHz." Phys Med Biol **42**(3): 479-490.
- Dimbylow, P. J. (2005). "Development of the female voxel phantom, NAOMI, and its application to calculations of induced current densities and electric fields from applied low frequency magnetic and electric fields." Phys Med Biol **50**: 1047-1070.
- Diridollou, S., M. P. Vienne, et al. (1999). "Efficacy of topical 0.05% retinaldehyde in skin aging by ultrasound and rheological techniques." Dermatology **199 Suppl 1**: 37-41.
- Drossos, A., V. Santomaa, et al. (2000). "The dependence of electromagnetic energy absorption upon human head tissue composition in the frequency range of 300-3000mhz." IEEE Transactions on Microwave Theory and Techniques **48**(11): 1988-1995.
- Durney, C. and D. A. Christensen (1999). Basic introduction to bioelectromagnetics, CRC Press.
- Durney, C., M. Iskander, et al. (1979). "An empirical formular for broad-band SAR calculations of perlate spheroidal models of humand and animals." IEEE Transactions on Microwave Theory and Techniques **mtt-27**(8): 758-763.
- Ebraheim, N. A., J. Lu, et al. (1996). "An anatomic study of the thickness of the occipital bone. Implications for occipitocervical instrumentation." Spine **21**(15): 1725-1729; discussion 1729-1730.
- El-Domyati, M., S. Attia, et al. (2002). "Intrinsic aging vs. Photoaging: A comparative histopathological, immunohistochemical, and ultrastructural study of skin." Exp Dermatol **11**(5): 398-405.
- Elahi, M., L. Lessard, et al. (1997). "Ultrasound in the assessment of cranial bone thickness." J. Craniofac. Surgery **8**(3): 213-221.
- EMSS. (2009). "FEKO." 6.21. from <http://www.feko.info/>.

- Eshel, Y., S. Witman, et al. (1995). "Correlation between skull thickness asymmetry and scalp potential estimated by a numerical model of the head." IEEE transactions on biomedical engineering **42**(3): 242-249.
- Evans, R., E. V. Cowdry, et al. (1943). "Ageing of human skin. I. Influence of dermal shrinkage on appearance of the epidermis in young and old fixed tissues." The Anatomical Record **86**(4): 545-565.
- Farkas, L. (1994). Anthropometry of the head and face. New York, Raven Press.
- Farkas, L. G., M. J. Katic, et al. (2005). "International anthropometric study of facial morphology in various ethnic groups/races." J Craniofac Surg **16**(4): 615-646.
- FCC, F. C. C. "FCC website on tissue dielectrics." Retrieved Last accessed 2009, from <http://www.fcc.gov/fcc-bin/dielec.sh>.
- Foster, K. and H. Schwan (1989). "Dielectric properties of tissues and biological materials: A critical review." Crit Rev Biomed Eng **17**(1): 25-104.
- Foster, K. R., J. L. Schepps, et al. (1980). "Microwave dielectric relaxation in muscle. A second look." Biophys J **29**(2): 271-281.
- Fujiwara, O. and K. Takai (1997). "Electrical properties of skin and SAR calculation in a realistic human model for microwave exposure." Electrical Engineering in Japan **120**(4): 75-80.
- Gabriel, C. (1996). "Compilation of the dielectric properties of body tissues at RF and microwave frequencies." Report No. AL/OE-TR-1996-0037, from citeulike-article-id:3907853
- Gabriel, C. (2007). "Tissue equivalent material for hand phantoms." Phys Med Biol **52**(14): 4205-4210.
- Gabriel, C., S. Gabriel, et al. (1996). "The dielectric properties of biological tissues: I. Literature survey." Phys Med Biol **41**: 2231-2249.
- Gabriel, C. and A. Peyman (2006). "Dielectric measurement: Error analysis and assessment of uncertainty." Phys Med Biol **751**(23): 6033-6046.
- Gabriel, S., R. W. Lau, et al. (1996). "The dielectric properties of biological tissues: Ii. Measurements in the frequency range 10 Hz to 20 GHz." Phys Med Biol **41**: 2251-2269.
- Gabriel, S., R. W. Lau, et al. (1996). "The dielectric properties of biological tissues: Iii. Parametric models for the dielectric spectrum of tissues." Physics in Medicine & Biology **41**(11): 2271-2293.
- Gandhi, O. P. (1980). "State of knowledge for electromagnetic absorbed dose in man and animals." Proceedings of the IEEE **68**(24-32).

- Gandhi, O. P., L. Gianluca, et al. (1996). "Electromagnetic absorption in the human head and neck for mobile telephones at 835 and 1900 MHz." IEEE Transactions on Microwave Theory and Techniques **44**(10): 1884-1897.
- Gandhi, O. P. and G. Kang (2002). "Some present problems and a proposed experimental phantom for SAR compliance testing of cellular telephones at 835 and 1900 MHz." Phys Med Biol **47**(9): 1501-1518.
- Garfin, S. R., M. J. Botte, et al. (1985). "Osteology of the skull as it affects halo pin placement." Spine **10**(8): 696-698.
- Getz, B. (1961). "Skull thickness in the frontal and parietal regions. (a roentgenological examination)." Acta Morphol Neerl Scand **3**: 221-228.
- Grant, J. P., R. N. Clarke, et al. (1988). "In vivo dielectric properties of human skin from 50 MHz to 2.0 GHz." Phys Med Biol **33**(5): 607-612.
- Gray, H. (1918). Gray's anatomy of the human body. London, Churchill Livingstone.
- Grob, D., B. Jeanneret, et al. (1991). "Atlanto-axial fusion with transarticular screw fixation." J Bone Joint Surg Br **73**(6): 972-976.
- Guy, A. W. (1968). "Analyses of electromagnetic fields induced in biological tissues by thermographic studies on equivalent phantom models." Microwave Theory and Techniques, IEEE Transactions on **19**(2): 205-214.
- Guy, A. W. (1971). "Analyses of electromagnetic fields induced in biological tissues by thermographic studies on equivalent phantom models." IEEE Trans. Microwave Theory Tech. (Special Issue on Biological Effects of Microwaves) **MTT-19**: 205.
- Habash, R. W. (2002). Electromagnetic fields and radiation: Human bioeffects and safety. New York, Marcel Dekker, Inc.
- Habash, R. W., L. M. Brodsky, et al. (2003). "Health risks of electromagnetic fields. Part ii: Evaluation and assessment of radio frequency radiation." Crit Rev Biomed Eng **31**(3): 197-254.
- Habash, R. W. Y., J. M. Elwood, et al. (2009). "Recent advances in research on radiofrequency fields and health: 2004–2007." Journal of Toxicology and Environmental Health, Part B: Critical Reviews **12**(4): 250 - 288.
- Hadjem, A., D. Lautru, et al. (2005). "Study of specific absorption rate (SAR) induced in two child head models and in adult heads using mobile phones." IEEE Transactions on Microwave Theory and Techniques **53**(1): 4-11.
- Hartsgrove, G. (1982). "New formulas for tissue equivalent materials used in electromagnetic absorption studies."
- Heyvaert and Martens (1998). "Accuracy study of FDTD calculations of a dipole antenna irradiating a lossy sphere." IEEE MTT-S digest: 767-770.

- Hombach, V., K. Meier, et al. (1996). "The dependence of EM energy absorption upon human head modeling at 900 MHz." Microwave Theory and Techniques, IEEE Transactions on **44**(10): 1865-1873.
- Hori, H., G. Moretti, et al. (1972). "The thickness of human scalp: Normal and bald." J. Invest. Derm. **58**(6): 396-399.
- Hwang, K., J. Kim, et al. (1997). "Thickness map of parietal bone in korean adults." J Craniofac Surg **8**(3): 208-212.
- ICNIRP (1998). "Guidelines for limiting exposure to time-varying electric, magnetic, and electromagnetic fields (up to 300 GHz)." Health Physics **74**(4): 494-522.
- IEC. (2011). "IEC 62232 ed. 1: Determination of RF field strength and SAR in the vicinity of radiocommunication base stations for the purpose of evaluating human exposure."
- IEEE. (1999). "C95.1-1999: IEEE standard for safety levels with respect to human exposure to radio frequency electromagnetic fields, 3 kHz to 300 GHz." from <http://ieeexplore.ieee.org/servlet/opac?punumber=614>.
- IEEE. (2003). "P1528-2003: IEEE recommended practice for determining the peak spatial-average specific absorption rate (SAR) in the human head from wireless communications devices: Measurement techniques."
- IEEE. (2005). "C95.1-2005: IEEE standard for safety levels with respect to human exposure to radio frequency electromagnetic fields, 3 kHz to 300 GHz." from <http://ieeexplore.ieee.org/servlet/opac?punumber=10830>.
- IEEE. (2005). "IEEE p1528/d1.2: Recommended practice for determining the peak spatial-average specific absorption rate (SAR) in the human head from wireless communications devices: Measurement techniques."
- Ingerslev, C. H. and B. Solow (1975). "Sex differences in craniofacial morphology." Acta Odontol Scand **33**(2): 85-94.
- Institute, S. S. (1998). "SSI/DRB TP-D01-031 phantom design requirements".
- Ishida, H. and Y. Dodo (1990). "Cranial thickness of modern and neolithic populations in japan." Hum Biol **62**(3): 389-401.
- Israel, H. (1973). "Age factor and the pattern of change in craniofacial structures." Am J Phys Anthropol **39**(1): 111-128.
- Kainz, W., A. Christ, et al. (2005). "Dosimetric comparison of the specific anthropomorphic mannequin (sam) to 14 anatomical head models using a novel definition for the mobile phone positioning." Phys Med Biol **50**(14): 3423.
- Kang, G. and O. P. Gandhi (2004). "Effect of dielectric properties on the peak 1-and 10-g SAR for 802.11 a/b/g frequencies 2.45 and 5.15 to 5.85 GHz." IEEE Trans Electromagnetic Compatibility **46**(2): 268-274.

- Keshvari, J., R. Keshvari, et al. (2006). "The effect of increase in dielectric values on specific absorption rate (SAR) in eye and head tissues following 900, 1800 and 2450 MHz radio frequency (RF) exposure." Phys Med Biol **51**(6): 1463-1477.
- Keshvari, J. and S. Lang (2005). "Comparison of radio frequency energy absorption in ear and eye region of children and adults at 900, 1800 and 2450 MHz." Phys Med Biol **50**(18): 4355-4369.
- Khalafalla, A. S., L. Turner, et al. (1971). "An electrical model to simulate skin dielectric dispersion." Comput Biomed Res **4**(4): 359-373.
- Kim, C., S. Choi, et al. (2008). "Hdk-man: A whole-body voxel model based on high-resolution color slice images of a korean adult male cadaver." Phys Med Biol **53**: 4093-4106.
- Kligman, A. M. (1969). "Early destructive effect of sunlight on human skin." Jama **210**(13): 2377-2380.
- Kraszewski, A., M. A. Stuchly, et al. (1982). "In vivo and in vitro dielectric properties of animal tissues at radio frequencies." Bioelectromagnetics **3**(4): 421-432.
- Kraus, J. D. (1992). Electromagnetics. New York, Mcgraw-Hill.
- Kuster, N. and Q. Balzano (1992). "Energy absorption mechanism by biological bodies in the near field of dipole antennas above 300 MHz." Vehicular Technology, IEEE Transactions on **41**(1): 17-23.
- Lagendijk, J. J. W. and P. Nilsson (1985). "Hyperthermia dough: A fat and bone equivalent phantom to test microwave/radiofrequency hyperthermia heating systems." Phys Med Biol **30**(7): 709.
- Law, S. (1993). "Thickness and resistivity variations over the upper surface of the human skull." brain Topography **6**(2): 99-107.
- Lazebnik, M., E. L. Madsen, et al. (2005). "Tissue-mimicking phantom materials for narrowband and ultrawideband microwave applications." Phys Med Biol **50**(18): 4245-4258.
- Lee, A. K., H. D. Choi, et al. (2007). "Study on sars in head models with different shapes by age using sam model for mobile phone exposure at 835 MHz." IEEE Trans EMC **49**(2).
- Lee, A. K., H. D. Choi, et al. (2002). "Human head size and SAR characteristics for handset exposure." ETRI J. **24**(2): 176-179.
- Li, L. W., M. S. Leong, et al. (2000). "Specific absorption rates in human head due to handset antennas: A comparative study using FDTD." JAMA **14**(7): 987-1000.
- Lynnerup, N. (2001). "Cranial thickness in relation to age, sex and general body build in a danish forensic sample." Forensic Sci. Intl **117**: 45-51.

- Martínez-Búrdalo, M., A. Martín, et al. (2004). "Comparison of FDTD-calculated specific absorption rate in adults and children when using a mobile phone at 900 and 1800 MHz." Phys Med Biol **49**(2): 345.
- Maximow, A. and W. Bloom (1943). A textbook of histology.
- McIntosh, R. L. and V. Anderson (2011). "SAR versus var, and the size and shape that provide the most appropriate RF exposure metric in the range of 0.5–6 GHz." Bioelectromagnetics.
- McIntosh, R. L., R. J. McKenzie, et al. (2001). Validation study of SAR measurement and modelling using the phantom at the telstra research laboratories. URSI Wireless Applications of Radio Science Workshop (WARS 02), Sydney, Australia.
- Meema, H. E., R. H. Sheppard, et al. (1964). "Roentgenographic visualization and measurement of skin thickness and its diagnostic application in acromegaly." Radiology **82**: 411-417.
- Meier, K., V. Hombach, et al. (1997). "The dependence of electromagnetic energy absorption upon human-head modeling at 1800 MHz." IEEE Transactions on Microwave Theory and Techniques **45**(11): 2058-2062.
- Miyauchi, S. and Y. Miki (1983). "Normal human skin echogram." Arch Dermatol Res **275**(5): 345-349.
- Montagna, W. (1962). The structure and function of skin. Providence, Rhode Island, Academic Press.
- Nagaoka, T., S. Watanabe, et al. (2004). "Development of realistic high-resolution whole-body voxel models of Japanese adult males and females of average height and weight, and application of models to radio-frequency electromagnetic-field dosimetry." Phys Med Biol **49**(1): 1.
- Nikita, K. S., G. S. U. Stamatakos, N.K., et al. (2000). "Analysis of the interaction between a layered spherical human head model and a finite-length dipole." IEEE transactions on microwave theory **84**(11): 2003-2013.
- Okoniewski, M. and M. A. Stuchly (1996). "A study of the handset antenna and human body interaction." IEEE Transactions on Microwave Theory and Techniques **44**(10 part 2): 1855 - 1864
- Olivier, G. (1975). "Biometry of the human occipital bone." J Anat **120**(Pt 3): 507-518.
- Pensler, J. and J. G. McCarthy (1985). "The calvarial donor site: An anatomic study in cadavers." Plast Reconstr Surg **75**(5): 648-651.
- Petersen, R. (2007). Radiofrequency/microwave safety standards. RF dosimetry handbook. Chadwick, P. J., http://www.emfdosimetry.org/petersen/Radiofrequency_Safety_Standards.html.

- Pethig, R. (1987). "Dielectric properties of body tissues." Clin Phys Physiol Meas **8 Suppl A**: 5-12.
- Peyman, A., C. Gabriel, et al. (2009). "Variation of the dielectric properties of tissues with age: The effect on the values of SAR in children when exposed to walkie-talkie devices." Phys Med Biol **54**(2): 227.
- Peyman, A., A. A. Rezazadeh, et al. (2001). "Changes in the dielectric properties of rat tissue as a function of age at microwave frequencies." Phys Med Biol **46**: 1617-1629.
- Raicu, V., N. Kitagawa, et al. (2000). "A quantitative approach to the dielectric properties of the skin." Phys Med Biol **45**(2): L1-4.
- Remcom, I. (2006). "xFDTD." v6.0. from <http://www.remcom.com>.
- Roach, P. W. E. (2009). "Radio frequency radiation dosimetry handbook."
- Ross, K. A. Lee, et al. (1976). "Skull thickness of black and white races." S Afr Med J **50**(16): 635-638.
- Ross, A., R. Jantz, et al. (1998). "Cranial thickness in american females and males." Journal of Forensic Sciences **43**(2): 267-272.
- Sadiku, M. N. O. (1989). "A simple introduction to finite element analysis of electromagnetic problems." Education, IEEE Transactions on **32**(2): 85-93.
- Schonborn, F., M. Burkhardt, et al. (1998). "Difference in energy absorption between heads of adults and children in the near field of sources." Health Phys **74**(2): 160-168.
- Schwan, H. P. (1981). Dielectric properties of biological tissues and biophysical mechanism of electromagnetic field interaction. ACS Symposium Series 157 American Chemical Society - Biological Effects of Nonionizing Radiations. Washington D. C, Illinger, K. H.
- Schwan, H. P. and K. R. Foster (1980). "RF-field interactions with biological systems - electrical properties and biophysical mechanisms." proc IEEE **68**(1): 104-113.
- Schwartz, J. L. and G. a. R. Mealing (1985). "Dielectric properties of frog tissues in vivo and in vitro." Phys Med Biol **30**(2): 117.
- Siervogel, R. M., A. F. Roche, et al. (1982). "Subcutaneous fat distribution in males and females from 1 to 39 years of age." Am J Clin Nutr **36**(1): 162-171.
- Simms, D. and Neely (1989). "Thickness of the lateral surface of the temporal bone in children." ann otol rhinol laryngol **98**: 726-731.
- Smith, P., Y. Wax, et al. (1985). "Diachronic variation in cranial thickness of near eastern populations." Am J Phys Anthropol **67**(2): 127-133.
- Southwood, W. F. (1955). "The thickness of the skin." Plast Reconstr Surg **15**(5): 423-429.
- Speag. (2008). "Dasy4 v4.7 system handbook."
- Speag (2008). <http://www.Speag.Com/products/semcad/applications/mobile-phone-simulations/dasy4-5-measurement-data-interface/>.

- Spitzer, V., M. J. Ackerman, et al. (1996). "The visible human male: A technical report." JAMIA **3**: 118-130.
- Stauffer, P. R., F. Rossetto, et al. (2003). "Phantom and animal tissues for modelling the electrical properties of human liver." Int J Hyperthermia **19**(1): 89-101.
- Stephan, C. N. (2002). "Position of superciliare in relation to the lateral iris: Testing a suggested facial approximation guideline." Forensic Sci Int **130**(1): 29-33.
- Stephan, C. N. (2003). "Anthropological facial 'reconstruction--recognizing the fallacies, 'unembracing' the errors, and realizing method limits." Sci Justice **43**(4): 193-200.
- Swan, L. K. and C. N. Stephan (2005). "Estimating eyeball protrusion from body height, interpupillary distance, and inter-orbital distance in adults." J Forensic Sci **50**(4): 774-776.
- Takema, Y., Y. Yorimoto, et al. (1994). "Age-related changes in the elastic properties and thickness of human facial skin." Br J Dermatol **131**(5): 641-648.
- Tan, C. Y., B. Statham, et al. (1982). "Skin thickness measurement by pulsed ultrasound: Its reproducibility, validation and variability." Br J Dermatol **106**(6): 657-667.
- Thurai, Goodridge, et al. (1984). "Variation with age of the electric properties of mouse brain cerebrum." Phys Med Biol **29**(9): 1133-1136.
- Thurai, Steel, et al. (1985). "Dielectric properties of developing rabbit brain at 37c." Bioelectromagnetics **6**: 235-242.
- Todd (1924). "Thickness of the male white cranium." The Anatomical Record **27**(5): 245-256.
- Upham, E. and W. Landauer (1935). "The relation of thickness of cutis and subcutis to hair slope in human skin." The Anatomical Record **61**(3): 359-366.
- Wang, J. and O. Fujiwara (2003). "Comparison and evaluation of electromagnetic absorption characteristics in realistic human head models of adult and children for 900-MHz mobile telephones." Microwave Theory and Techniques, IEEE Transactions on **51**(3): 966-971.
- Wang, J., O. Fujiwara, et al. (2006). "FDTD calculation of whole-body average SAR in adult and child models for frequencies from 30 MHz to 3 GHz." Phys Med Biol **51**(17): 4119.
- Wang, J., O. Fujiwara, et al. (2006). "Approximation of aging effect on dielectric tissue properties for SAR assessment of mobile telephones." Electromagnetic Compatibility, IEEE Transactions on **48**(2): 408-413.
- Watanabe, S., S. Mochizuki, et al. (2001). Specific absorption rate in head phantoms of different shape and size for a cell telephone use. Asia-Pacific Radio Science Conference. Tokyo, Japan.

- Weber, G. and J. Kim (1999). "Thickness distribution of the occipital bone--a new approach based on ct-data of modern humans and oh 9 (h. Ergaster)." Coll Antropol. **23**: 333-343.
- Whitton, J. and Everall (1973). "The thickness of the epidermis." British Journal of Dermatology **89**: 467-476.
- Wiat, J., A. Hadjem, et al. (2007). RF exposure assessment in children head: Present questions and future challenges. Electromagnetics in Advanced Applications, 2007. ICEAA 2007. International Conference on.
- Wiat, J., A. Hadjem, et al. (2008). "Analysis of RF exposure in the head tissues of children and adults." Phys Med Biol **53**(13): 3681-3695.
- Wu, T., T. Liwen, et al. (2011). "Chinese adult anatomical models and the application in evaluation of RF exposures." Phys Med Biol **56**(7): 2075.
- Zvyagin, V. N. (1975). "The study of cranial vault thickness in sutural regions in males and females." Vopr. Anthropol. **49**: 108-115.

Appendix A – Purchasing information for materials used in this study

Barnes Moulding & Casting Supplies

40-42 Swan St, Richmond VIC 3121

Ph: (03) 9428 5511

Moulding materials

- Pinkysil fast-set silicon
- Artist's clay
- Sundry mixing materials (rubber gloves, stirrers, plastic cups)

Skulls Unlimited International, Inc.

10313 South Sunnyslane

Oklahoma City OK 73160 USA

<http://www.skullsunlimited.com>

Ph: +1 405 794 9300

Plastic skulls

Human Male African / Negroid Skull

Catalogue #: WBC-110 (formerly WBC-154)

http://www.skullsunlimited.com/record_variant.php?id=3563

5-year-old Human Caucasian Child Skull - No Alterations

Catalogue #: WBC-190 (formerly WBC-312)

http://www.skullsunlimited.com/record_variant.php?id=3805

Appendix B – Creating shell phantoms

Two fibreglass shell phantoms were created at the ACRBR (Australian Centre for Radiofrequency Bioeffects Research) RF Laboratory at Swinburne University, Melbourne, Australia, and shipped to Ericsson Research Laboratories, Sweden for SAR testing. The following protocol was used for making both phantoms.

1. 2 mm thick 'sheets' of artist's clay were rolled using a pasta roller; clay was softened using a space heater, hair dryer or by kneading with hands
2. For eyes, two clay balls were rolled by hand, of 50 mm and 30 mm diameter for adult and child heads respectively
3. 'eyes' were measured using callipers and positioned in centre of orbital cavities
4. orbital cavities were covered with a sheet of clay such that 'eyes' did not move freely (Figure 46)
5. clay was used to block and build up nasal cavity
6. a 'nose' was constructed to anatomically accurate proportions; dimensions were appropriate to the age and ethnicity of the skull



Figure 46: Artist's clay rolled into 2 mm thicknesses using a pasta roller was used for creating head casts for fibreglass shell phantoms

7. entire structure was carefully covered in three layers of rolled clay; care was taken not to overlap edges of layers

8. four to six clay sheets were added onto cheeks to pad out the facial cavity on the maxima and mandible
9. for the child skull, a heavier padding was applied around the zygomatic arch, mandibular shelf and cheek cavity, in accordance with children's facial anatomy
10. the face was used as a cast (positive image) in the construction of a latex mould (negative image):
 - a. the 'face' was held nose-down a few centimetres above a board, while a 'shelf' of artist's clay was built several centimetres around the it (see Figure 47)
 - b. the space between the shelf and the 'face' was filled with the fast-setting liquid silicon sold under the trade name Pinkysil ©; the 'face' was light enough to float a few centimetres in the silicon so did not need to be held in place

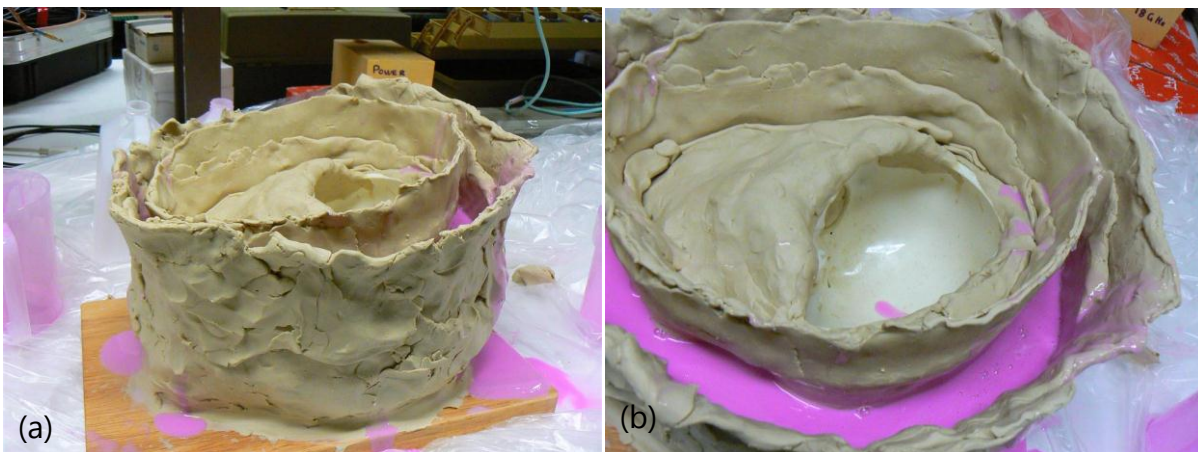


Figure 47: (a) side and (b) top view of the process of making a negative impression of the 'face' using fast set liquid silicon and a 'shelf' of artist's clay

11. once the mould was set, the clay 'wall' and the 'face' were carefully removed
12. fibreglass sheets were layered inside the mould and painted with epoxy resin (Figure 48)

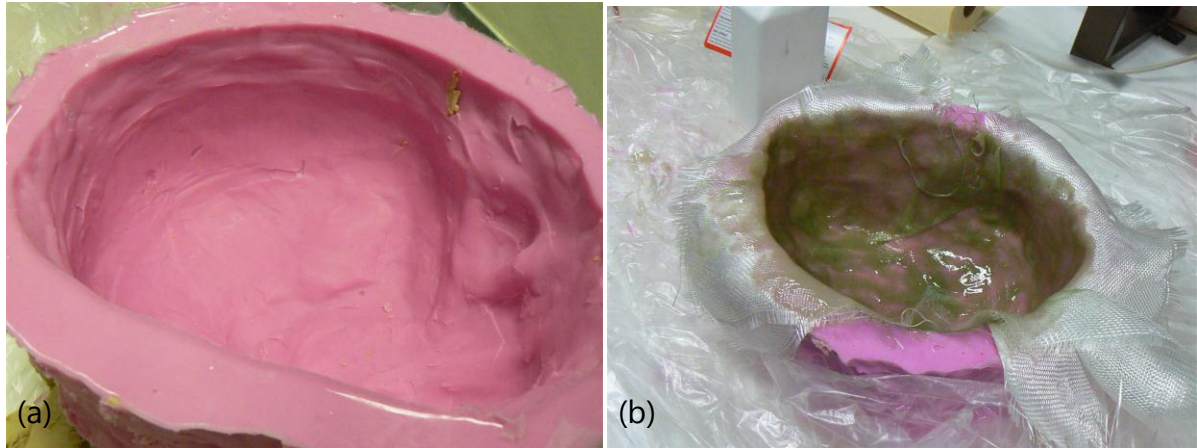


Figure 48: (a) completed silicon mould and (b) fibreglass sheets pressed into a latex mould and painted with resin

13. once dried, the resin and fibreglass shells were carefully removed from the latex mould (Figure 49)
14. before testing, shells were reinforced with further fibreglass sheets and resin as they were found to leak; this increased the separation of the 'head' from the dipole

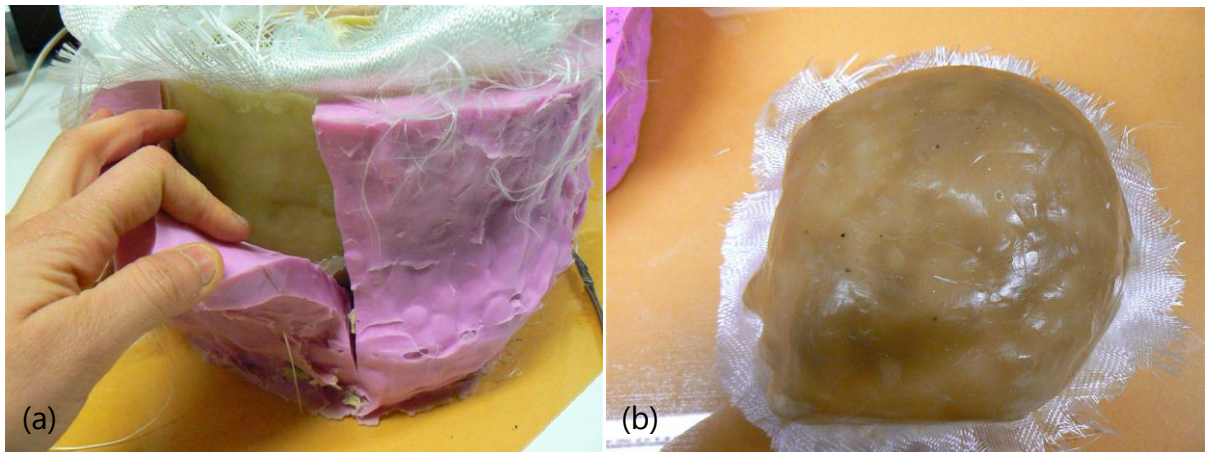


Figure 49: (a) the flexible latex mould was carefully loosened from the fibreglass shell (b) underside view of a fibreglass shell

15. each shell phantom was supported on a 700 * 700 * 20 mm wooden board, with a hole just large enough for the shell to fit through (Figure 50) cut using a jigsaw

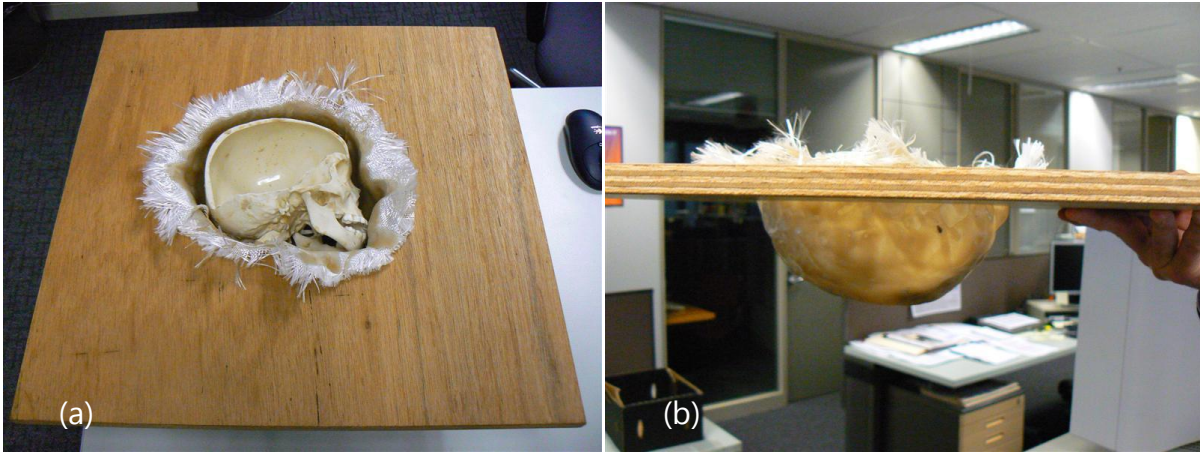


Figure 50: shell phantoms inside board supports, (a) top view with skull inside phantom and (b) side view

16. boards were used to hold phantoms in place during testing (Figure 51)



Figure 51: phantom and wooden frame with DASY4 system

Appendix C – Tissue-simulating liquid recipes

Hartsgrove liquids were used for most tissue-simulating liquids for the physical validation part of this project. Equations used to calculate requisite quantities of salt, sugar, and water, were provided by Telstra Research Laboratories, and are based on line of best fit derivations using extensive experimental data. Quantities used to create 'tissues' are also provided.

'Average head' and 'average brain' tissues were made according to the protocol provided below. All other tissues were created using Hartsgrove methods. Salt and sugar were purchased at a supermarket. All other ingredient information is as above.

Table XXXIII: Recipes for ingredients used in heterogeneous models

Skull A heterogeneous without eyes			
	Skin	Fat	Muscle
Sugar (g)	298.38	320	222.67
Salt (g)	2.06	0 [□]	4.1
Water (ml)	203.49	105.58	256.51
HEC (g)	20	20	20
Preservative (g)	1	1	1
Dielectric values	$\epsilon = 36.7, \sigma = 0.75$	$\epsilon = 6.8, \sigma = 1.0$	$\epsilon = 50.0, \sigma = 0.95$

[□] the recipe called for a negative value of salt

Skull A heterogeneous with eyes[‡]				
	Skin	Fat	Muscle	Eye
Sugar (g)	298.38	482	1336.03	35.17
Salt (g)	2.06	0	24.60	8.29
Water (ml)	203.49	154.37	1593.03	145.09
HEC (g)	20	30	120	20
Preservative (g)	1	1	1	1
Dielectric values	$\epsilon = 36.7, \sigma = 0.75$	$\epsilon = 23.6, \sigma = 0.51$	$\epsilon = 52.6, \sigma = 0.98$	$\epsilon = 42.8, \sigma = 1.25$

Skull B heterogeneous[‡]				
	Skin	Fat	Muscle	Eye
Sugar (g)	298.38	482	1336.03	35.17
Salt (g)	2.06	0	24.60	8.29
Water (ml)	203.49	154.37	1593.03	145.09
HEC (g)	20	30	120	20
Preservative (g)	1	1	1	1
Dielectric values	$\epsilon = 36.7, \sigma = 0.75$	$\epsilon = 17.5, \sigma = 0.38$	$\epsilon = 52.6, \sigma = 0.98$	$\epsilon = 42.8, \sigma = 1.24$

[‡] the same batches of tissue liquids were used for both of these models; dielectric properties of 'fat' tissue drifted significantly over time

Table XXXIV: Suggested recipes for achieving target dielectric parameters (adapted from Appendix C, P1528-2003: IEEE Recommended Practice for Determining the Peak Spatial-Average Specific Absorption Rate (SAR) in the Human Head from Wireless Communications Devices: Measurement Techniques)

Frequency (MHz)	300		450		835		900			1450		1800			1900		1950		2000		2100		2450		3000	
Recipe #	1	1	3	1	1	2	3	1	1	2	2	3	1	2	4	1	1	2	2	3	2	2	3	2		
Ingredients (% by weight)																										
1,2-Propanediol						64.81																				
Bactericide	0.19	0.19	0.50	0.10	0.10		0.50					0.50												0.50		
Diacetin			48.90				49.20					49.43												49.75		
DGBE								45.41	47.00	13.84	44.92		44.94	13.84	45.00	50.00	50.00	7.99	7.99					7.99		
HEC	0.98	0.98		1.00	1.00																					
NaCl	5.95	3.95	1.70	1.45	1.48	0.79	1.10	0.67	0.36	0.35	0.18	0.64	0.18	0.35							0.16	0.16			0.16	
Sucrose	55.32	56.32		57.00	56.50																					
Triton X-100											30.45				30.45						19.97	19.97			19.97	
Water	37.56	38.56	48.90	40.45	40.92	34.40	49.20	53.80	52.64	55.36	54.90	49.43	54.90	55.36	55.00	50.00	50.00	71.88	71.88	49.75	71.88			71.88		
Measured dielectric parameters																										
ϵ_r'	46.00	43.4	44.3	41.6	41.2	41.8	42.7	40.9	39.3	41	40.4	39.2	39.9	41	40.1	37	36.8	41.1	40.3	39.2	37.9					
σ (S/m)	0.86	0.85	0.9	0.9	0.98	0.97	0.99	1.21	1.39	1.38	1.4	1.4	1.42	1.38	1.41	1.4	1.51	1.55	1.88	1.82	2.46					
Temp. (°C)	22	22	20	22	22	22	20	22	22	21	22	20	21	21	20	22	22	20	20	20	20					
Target dielectric parameters (Table 2)																										
ϵ_r'	45.30	43.50	41.5	41.50			40.5	40.0								39.80		39.2		38.5						
σ (S/m)	0.87	0.87	0.9	0.97			1.2	1.4								1.49		1.8		2.4						
NOTE—Multiple columns for any single frequency are optional recipes. Recipe #, reference: 1 (Kanda et al. [B85]), 2 (Vigneras [B143]), 3 (Peyman and Gabriel [B119]), 4 (Fukunaga et al. [B50]).																										

^aThe formulas containing Triton X-100 and corresponding measured parameters are under review and verification.

Appendix D – DASY 4 uncertainty budget

Table XXXV: DASY4 worst-case uncertainty budget for DASY4 assessed according to IEEE 1528. The budget is valid for the frequency range 300 MHz - 3 GHz and represents a worst-case analysis. For specific tests and configurations, the uncertainty could be considerable smaller (adapted from DASY4 User Manual)

Error Description	Uncertainty value	Prob. Dist.	Div.	(c_i) 1g	(c_i) 10g	Std. Unc. (1g)	Std. Unc. (10g)	(v_i) v_{eff}
Measurement System								
Probe Calibration	±5.9 %	N	1	1	1	±5.9 %	±5.9 %	∞
Axial Isotropy	±4.7 %	R	$\sqrt{3}$	0.7	0.7	±1.9 %	±1.9 %	∞
Hemispherical Isotropy	±9.6 %	R	$\sqrt{3}$	0.7	0.7	±3.9 %	±3.9 %	∞
Boundary Effects	±1.0 %	R	$\sqrt{3}$	1	1	±0.6 %	±0.6 %	∞
Linearity	±4.7 %	R	$\sqrt{3}$	1	1	±2.7 %	±2.7 %	∞
System Detection Limits	±1.0 %	R	$\sqrt{3}$	1	1	±0.6 %	±0.6 %	∞
Readout Electronics	±0.3 %	N	1	1	1	±0.3 %	±0.3 %	∞
Response Time	±0.8 %	R	$\sqrt{3}$	1	1	±0.5 %	±0.5 %	∞
Integration Time	±2.6 %	R	$\sqrt{3}$	1	1	±1.5 %	±1.5 %	∞
RF Ambient Noise	±3.0 %	R	$\sqrt{3}$	1	1	±1.7 %	±1.7 %	∞
RF Ambient Reflections	±3.0 %	R	$\sqrt{3}$	1	1	±1.7 %	±1.7 %	∞
Probe Positioner	±0.4 %	R	$\sqrt{3}$	1	1	±0.2 %	±0.2 %	∞
Probe Positioning	±2.9 %	R	$\sqrt{3}$	1	1	±1.7 %	±1.7 %	∞
Max. SAR Eval.	±1.0 %	R	$\sqrt{3}$	1	1	±0.6 %	±0.6 %	∞
Test Sample Related								
Device Positioning	±2.9 %	N	1	1	1	±2.9 %	±2.9 %	145
Device Holder	±3.6 %	N	1	1	1	±3.6 %	±3.6 %	5
Power Drift	±5.0 %	R	$\sqrt{3}$	1	1	±2.9 %	±2.9 %	∞
Phantom and Setup								
Phantom Uncertainty	±4.0 %	R	$\sqrt{3}$	1	1	±2.3 %	±2.3 %	∞
Liquid Conductivity (target)	±5.0 %	R	$\sqrt{3}$	0.64	0.43	±1.8 %	±1.2 %	∞
Liquid Conductivity (meas.)	±2.5 %	N	1	0.64	0.43	±1.6 %	±1.1 %	∞
Liquid Permittivity (target)	±5.0 %	R	$\sqrt{3}$	0.6	0.49	±1.7 %	±1.4 %	∞
Liquid Permittivity (meas.)	±2.5 %	N	1	0.6	0.49	±1.5 %	±1.2 %	∞
Combined Std. Uncertainty						±10.9 %	±10.7 %	387
Expanded STD Uncertainty						±21.9 %	±21.4 %	

Appendix E – Previous relevant publications

Book chapters

Sauren, M., McKenzie, R. J. McIntosh, R. L. (2008) 'Effects of skin dielectric properties on radiofrequency exposure compliance using an alternative human head model', Volume 29 Studies in Applied Electromagnetics and Mechanics, Edited by: A. Krawczyk, R. Kubacki, S. Wiak and C. Lemos Antunes, June 2008, ISBN: 978-1-58603-860-1

Journal papers and conference papers published as full papers

Sauren, M., McKenzie, R. J. McIntosh, R. L., (2007) 'Effects of skin dielectric properties on radiofrequency exposure compliance using an alternative human head model', 2nd international Conference on Electromagnetic Fields, Health And Environment, EHE'07 September 10 – 12, 2007, Wroclaw, Polands

Sauren, M., McKenzie, R. J. McIntosh, R. L. (2006), 'Determining the Influence of Adult Skin Thickness on Compliance with Radiofrequency Exposure Limits', World Congress on Medical Physics and Biomedical Engineering 2006 (WC2006), Aug 27 - Sep 1, 2006, Seoul, Korea.

Sauren, M., McKenzie, R. J., Cosic I. (2005) 'Determining The Influence Of Population Variation On Compliance With Radiofrequency Exposure Limits: Proposed Study', Conf Proc IEEE Eng Med Biol Soc. 2005;3(1):2962-2965

Conference abstracts (peer-reviewed)

Sauren, M., McKenzie, R. J. McIntosh, R. L., (2007) 'Effects of skin dielectric properties on radiofrequency exposure compliance using an alternative human head model', 2nd international Conference on Electromagnetic Fields, Health And Environment, EHE'07, September 10 – 12, 2007, Wroclaw, Poland

Sauren, M., McKenzie, R. J. McIntosh, R. L., (2007) 'Effects of Dielectric Properties on Radiofrequency Exposure Compliance Using an Alternative Human Head Model', Progress In Electromagnetics Research Symposium (PIERS), August 27–30, 2007, Prague, Czech Republic

Industry conference presentations

Sauren, M., McKenzie, R. J. McIntosh, R. L. (2008), 'Head size and its effect on SAR – tests using Geometry Man', 33rd Australasian Radiation Protection Society (ARPS) Conference, Canberra, Australia

Sauren, M., McKenzie, R. J. McIntosh, R. L. (2007), 'Validating Geometry Man: physical validation study of a human head model' 33rd Australasian Radiation Protection Society (ARPS) Conference, 21-24 Canberra, Australia

Sauren, M., McKenzie, R. J. McIntosh, R. L. (2006), 'Determining The Influence Of Adult Skin Thickness On Compliance With Radiofrequency Exposure Limits', 32nd Australasian Radiation Protection Society (ARPS) Conference, 26-29 Nov, 2006 Sydney, Australia

Sauren, M., McKenzie, R. J. McIntosh, R. L. (2006), 'Determining the influence of adult cranial thickness on compliance with radiofrequency exposure limits', Bioelectromagnetics Society 28th Annual Meeting, Cancun, Mexico

Sauren, M., McKenzie, R. J. McIntosh, R. L. (2005), 'Determining the influence of adult skin thickness on compliance with radiofrequency exposure limit', 31st Australasian Radiation Protection Society (ARPS) Conference, Sydney, Australia, Nov 26-29 2006.

Sauren, M., McKenzie, R. J. McIntosh, R. L. (2005), 'Determining the influence of population variance on compliance with radiofrequency exposure', 30th Annual Conference of the Australian Radiation Protection Society and World Health Conference, Melbourne, Nov, 2005.